P-06-02

Oskarshamn site investigation

Mineralogical, chemical and redox features of red-staining adjacent to fractures – Results from drill core KLX04

Henrik Drake, Department of Geology, Earth Sciences Centre, Göteborg University

Eva-Lena Tullborg, Terralogica AB

January 2006

Svensk Kärnbränslehantering AB
Swedish Nuclear Fuel
and Waste Management Co
Box 5864
SE-102 40 Stockholm Sweden
Tel 08-459 84 00
+46 8 459 84 00
Fax 08-661 57 19
+46 8 661 57 19

ISSN 1651-4416
SKB P-06-02

Oskarshamn site investigation

Mineralogical, chemical and redox features of red-staining adjacent to fractures – Results from drill core KLX04

Henrik Drake, Department of Geology, Earth Sciences Centre, Göteborg University

Eva-Lena Tullborg, Terralogica AB

January 2006

Keywords: Laxemar, Red-staining, Oxidation, Hydrothermal wall rock alteration, Mineralogy, Whole rock chemistry, Mössbauer spectroscopy, SEM-EDS, Reducing capacity, Porosity, Density.

Abstract

The Swedish Nuclear Fuel and Waste Management Co (SKB) is currently investigating the Simpevarp/Laxemar area in the Oskarshamn region on the Swedish East Coast in order to find a suitable place for a radioactive waste repository. Drill core KLX04 from the Laxemar subarea has been sampled for detailed studies of red-staining in Ävrö granite adjacent to fractures. This is a very common feature in the Simpevarp/Laxemar area and is caused by hydrothermal alteration in combination with oxidation. Thin sections of twelve samples, comprising six red-stained samples, five samples of reference rock and one highly altered sample without red-staining, were investigated with petrographic microscope and SEM-EDS. Whole rock chemical analyses of major, minor and trace elements were performed using ICP-AES and ICP-QMS, in order to distinguish which elements that were depleted, enriched or unaffected during alteration. In order to make out the total Fe^{3+}/Fe_{tot}-ratio in the red-stained rock compared to the reference rock, Mössbauer spectroscopy was carried out. This indicates how much reducing capacity that remains in the red-stained rock. In addition, measurements of porosity and density were carried out. A comparison of the results from the present study with a similar study from the Simpevarp subarea /Drake and Tullborg 2006c/ is also presented.

The red-staining is mainly caused by minute inclusions of Fe^{3+}-rich minerals, mainly hematite. These are hosted in porous secondary K-feldspar and albite completely replacing primary plagioclase. Accompanying this alteration is replacement of magnetite by hematite and of biotite by chlorite, formation of secondary sericite, prehnite, titanite and epidote, and a general increase in porosity and micro-fractures and decrease in density. The red-staining is thought to occur at temperatures of c 280–400°C, based on e.g. indications from earlier studies on plagioclase alteration/replacement and the low-temperature paragenesis in general e.g. /Liou et al. 1983, Frey et al. 1991, Deer et al. 1992, Slaby 1992, Spear 1993, Lee and Parsons 1997, Bucher and Frey 2002, Wilamowski 2002/. Intense local red-staining caused by hematite and possibly also Fe-oxyhydroxide in micro-fractures is thought to be formed subsequently to the major red-staining event, presumably at lower temperatures. Primary quartz, K-feldspar and titanite remained rather fresh during alteration. The reference rock was occasionally altered as well, characterized by partial replacement of biotite by chlorite and of magnetite by hematite, which shows that the hydrothermal alteration often reaches further into the wall rock than the red-staining does.

The red-stained rock is enriched in e.g. K, Na, Mg, Rb, H_2O, and is slightly enriched in Fe and Mn. This enrichment is associated to formation of secondary adularia, albite, chlorite, prehnite and sericite. The red-stained rock is depleted in e.g. Ca, Sr, Cs, Al and Ga. This depletion is mainly due to break down of primary plagioclase and alteration of biotite. The total contents of e.g. Ti, Si, Y and REE:s are constant or are only slightly changed. Mössbauer analyses reveal that $Fe^{3+/}Fe_{tot}$-contents are actually only slightly changed in the red-stained rock compared to the reference rock in contrast to studies at Simpevarp /Drake and Tullborg 2006c/, where the red-stained rock was increased in Fe^{3+}. Average change is < 1%, and average $Fe^{3+/}Fe_{tot}$-contents are 42–43%. Enrichment of up to 4% and depletion of up to 7% of Fe^{3+}/Fe_{tot} are however found in the red-stained samples. The highest Fe^{3+}/Fe_{tot}-ratios are found in the samples with the highest amounts of epidote. The unexpected small change in Fe^{3+}/Fe_{tot} is mainly depending on the higher content of epidote in the reference rock, which might be due to heterogeneities of the rock, but also due to partial hematitization of magnetite.

Sammanfattning

Svensk Kärnbränslehantering AB (SKB) utför för närvarande platsundersökningar i Simpevarp/Laxemar området i Oskarshamns kommun på svenska östkusten, med syfte att hitta en lämplig plats för slutförvaring av utbränt kärnbränsle. Prover har tagits från borrkärna KLX04 från Laxemarområdet i syfte att undersöka rödfärgningen av Ävrö granit i anslutning till sprickor. Rödfärgning orsakad av hydrotermal omvandling i kombination med oxidering är en mycket vanlig företeelse i Simpevarp/Laxemar-området. Tunnslip från 12 prover, sex rödfärgade, fem referensprover och ett omvandlat men inte rödfärgat prov, har undersökts med petrografiskt mikroskop och SEM-EDS. Kemiska analyser, med hjälp av ICP-AES och ICP-QMS, har utförts för att undersöka vilka ämnen som anrikats, urlakats eller varit konstanta under hydrotermalomvandlingen och rödfärgningen. För att utröna skillnader i Fe^{3+}/Fe_{tot}-kvoten mellan de rödfärgade proverna och referensproverna har Mössbauer spektroskopi/spektrometrianalyser utförts. Detta ger indikation på hur mycket reducerande kapacitet som finns kvar i det rödfärgade berget. Mätningar av porositet och densitet har också utförts. En jämförelse av resultaten från denna studie och resultaten från en liknande studie från delområde Simpevarp /Drake and Tullborg 2006c/ presenteras också.

Rödfärgningen runt sprickor är främst orsakad av mikroskopiskt till submikroskopiskt små Fe^{3+}-rika mineral, huvudsakligen hematit, som sitter i porer i sekundär kalifältspat och albit, vilka har ersatt ursprunglig plagioklas. Hematitisering av magnetit, kloritisering av biotit, bildande av sekundär sericit, prehnit, titanit och epidot, generell ökning av porositeten samt antalet mikrosprickor inklusive minskad densitet är också karakteristiskt för det rödfärgade berget. Rödfärgningen har troligen skett vid temperaturer runt 280–400 °C, baserat på temperaturangivelser från tidigare studier av nedbrytning/omvandling av plagioklas och lågtemperaturparagenesen i övrigt /Liou et al. 1983, Frey et al. 1991, Deer et al. 1992, Slaby 1992, Spear 1993, Lee and Parsons 1997, Bucher and Frey 2002, Wilamowski 2002/. Intensiv lokal rödfärgning i mikrosprickor fyllda med hematit och möjligen Fe-oxyhydroxider, tolkas som ett senare fenomen, troligen bildat vid lägre temperaturer än den huvudsakliga rödfärgningen. Ursprunglig kvarts, kalifältspat och titanit har huvudsakligen inte påverkats av hydrotermalomvandlingen. Referensproverna innehåller ibland kloritiserad biotit och delvis hematitiserad magnetit, vilket visar att hydrotermalomvandlingen ofta sträcker sig längre ut i sidoberget än vad rödfärgningen gör.

Det rödfärgade berget är anrikat på t ex K, Na, Mg, Rb, H_2O och till viss del också på t ex Mn och Fe. Denna anrikning är relaterad till bildandet av sekundär adularia, albit, klorit, prehnit och sericit. Det rödfärgade berget är urlakat på t ex Ca, Sr, Cs, Al och Ga. Denna urlakning är huvudsakligen relaterad till nedbrytning av plagioklas och biotit. Den totala koncentrationen av t ex Si, Ti, Y och REE är konstant eller bara något förändrat under den hydrotermala omvandlingen. Mössbauer-analyser visar på förvånansvärd liten förändring av Fe^{3+}/Fe_{tot}-kvoten i de rödfärgade proverna jämfört med referensproverna, i motsatts till studier i Simpevarp /Drake and Tullborg 2006c/ där Fe^{3+}-innehållet var förhöjt i det rödfärgade berget. Medelförändringen är < 1 % och Fe^{3+}/Fe_{tot}-värdena är i medel 42–43 %, dock har anrikning med upp till 4 % och urlakning med upp till 7 % kunnat urskiljas i de rödfärgade proverna. Den oväntat låga förändringen i Fe^{3+}/Fe_{tot} beror huvudsakligen på en högre halt av epidot i referensproverna, möjligen beroende på heterogenitet i berget, samt att magnetit i referensproverna ofta är delvis hematitomvandlad. Fe^{3+}/Fe_{tot}-kvoten för oxider är dock generellt högre i de rödfärgade proverna. Högst Fe^{3+}/Fe_{tot}-kvot för oxider+silikater finns i de prover som har högst halt av epidot.

Contents

1 Introduction

The Swedish Nuclear Fuel and Waste Management Co (SKB) is currently carrying out site investigations in the Simpevarp/Laxemar area in the Oskarshamn region on the Swedish east coast. The site is situated in an area dominated by granitoids of the Transscandinavian Igneous Belt (TIB). Drill-core KLX04 from the Laxemar subarea (Figure 1-1) has been sampled for detailed studies of red-stained wall rock occurring adjacent to fractures. The red-staining is caused by hydrothermal alteration in combination with oxidation and is a very common feature in the Simpevarp/Laxemar area, and has been described in detail on the Simpevarp peninsula in drill cores KSH01 and KSH03 /Drake and Tullborg 2006c/ and briefly from e.g. drill cores KSH01 and KSH02 /Drake and Tullborg 2004, Mattsson and Thunehed 2004/ and from field observations /Wahlgren et al. 2004/. Earlier studies of red-stained rock from Äspö HRL, have been carried out by /Eliasson 1993, Mazurek et al. 1995, Tullborg 1995, Stosnach and Mengel 1998/.

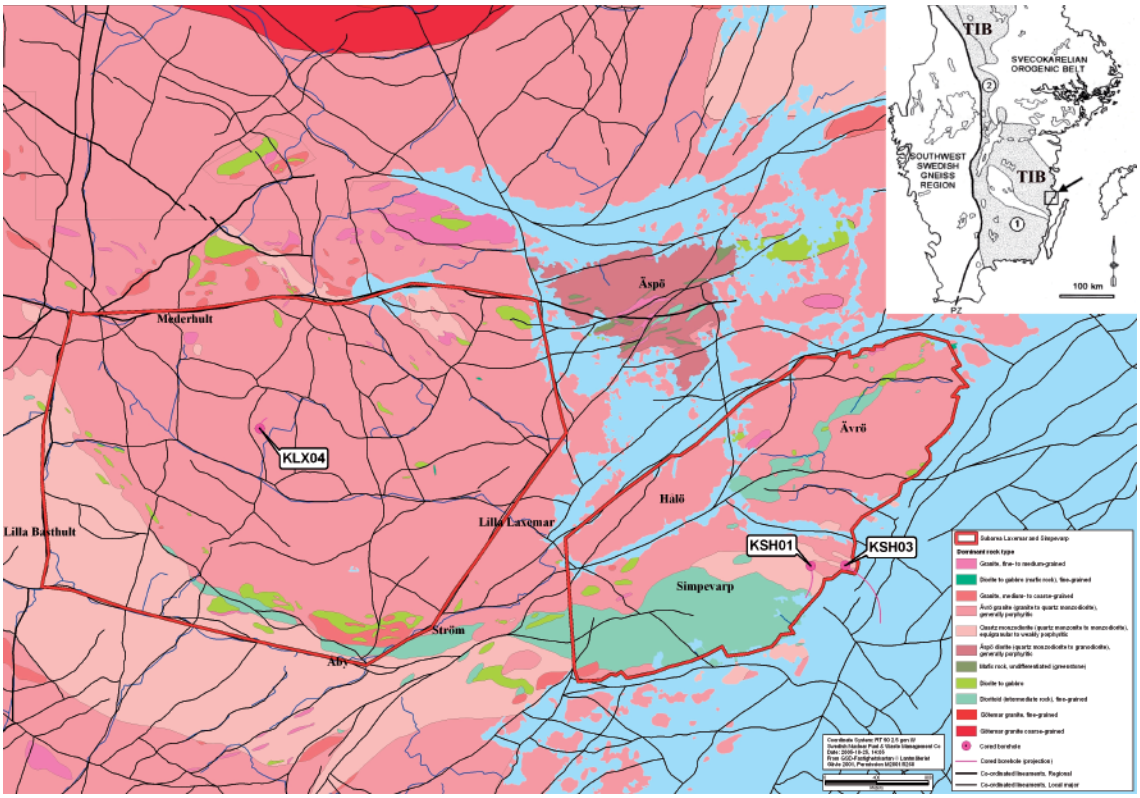

Figure 1-1. *Map showing the location of bore holes KLX04 (Laxemar subarea), KSH01A+B and KSH03A+B (Simpevarp subarea). The small map shows southern Sweden and the location of the study area (arrow) and TIB, /Kornfält et al. 1997/.*

A total number of five samples of granitic/granodioritic to quartz monzodioritic Ävrö granite were collected from the drill core. Each sample was divided into an "unaltered" reference rock and an altered red-stained rock. One additional sample of red-stained Ävrö granite and one sample of altered, somewhat porous granite without red-staining were also collected. Thin sections were prepared from each of these twelve samples. The thin sections were investigated and point-counted using petrographic microscope. Scanning electron microscope (SEM) equipped with an energy dispersive spectrometer (EDS) was used for high resolution investigation and analysis of the different minerals. Measurements of porosity and density have been carried out on all the samples.

Whole rock chemical analyses of major, minor and trace elements, using ICP-AES and ICP-QMS, were performed on each of the twelve samples in order to distinguish which elements were depleted, enriched or constant in the red-stained sample, compared to the reference rock, during alteration.

In order to make out the Fe^{3+}/Fe_{tot}-ratio in the red-stained rock compared to the reference rock, and in order to estimate how much reducing capacity that was lost in the red-stained rock, Mössbauer spectroscopy was carried out on all of the samples.

Although there are some contradicting results, a generalized model of the processes causing the red-staining can be suggested by comparison and evaluation of the thin section investigations, the chemical analyses, the results from Mössbauer spectroscopy and the results from the measurements of porosity and density.

The results from this study is compared to results from the investigations of red-stained wall rock from the Simpevarp peninsula /Drake and Tullborg 2006c/.

This report also includes a section on how the features of the oxidation and hydrothermal alteration affect a nuclear repository. This includes changes in reducing capacity, porosity, sorption, rock mechanics and thermal conductivity.

The work was carried out in accordance with activity plan SKB PS 400-04-018. In Table 1-1 controlling documents for performing this activity are listed. Both activity plan and method descriptions are SKB's internal controlling documents.

Table 1-1. Controlling documents for the performance of the activity.

Activity plan	**Number**	**Version**
Sprickmineralogiska undersökningar	AP PS 400-04-018	1.0
Method descriptions	**Number**	**Version**
Sprickmineralogi	SKB MD 144.000	1.0

2 Objective and scope

The aim of the study is to describe the mineralogical, chemical, physical (porosity and density) and redox features of the red-stained rock adjacent to fractures, compared to the relatively unaltered rock about a meter away. By combining results from several different analytical methods, such as microscopy, SEM-EDS, whole rock chemistry analyses, measurements of porosity and density and Mössbauer spectroscopy, the general features and processes causing the red-staining can be recognized. For instance microscopy shows the minerals that have been altered and/or replaced and shows also the secondary minerals formed during the alteration. Whole rock chemical analyses show what elements are depleted, enriched or constant during alteration. Changes in reducing capacity caused by the hydrothermal oxidation are of special interest in this study and are largely determined by Fe^{2+} available in the rock. Other elements contributing to the reducing capacity are S^{2-} (usually present as pyrite) and Mn^{2+} present in chlorite. Elements like U and V are also redox sensitive but present in very low concentrations. Mössbauer spectroscopy shows how much of the Fe^{2+} that is oxidized to Fe^{3+} and thereby how much reducing capacity that is left in the red-stained rock.

Another task of this report is to compare the features of the red-staining in the subareas of Laxemar and Simpevarp /Drake and Tullborg 2006c/.

The properties and features of the red-stained rock and the processes behind the red-staining provide useful information of a phenomenon that is widespread in all rock types in the area. Since the red-stained rock makes up such a high portion of the rocks in the area, especially in association with major deformation zones, it is important to understand these properties, features and principal processes in the planning of a nuclear waste repository. This report includes a section on how the features of the oxidation and hydrothermal alteration affect a nuclear repository. This includes changes in reducing capacity, porosity, sorption, rock mechanics and thermal conductivity.

3 Geological setting

The bedrock in the Simpevarp/Laxemar area north of Oskarshamn is dominated by Småland granitoids and dioritoids of the Transscandinavian Igneous Belt (TIB) e.g. /Gaal and Gorbatschev 1987, Kornfält and Wikman 1987, Kornfält et al. 1997, Wahlgren et al. 2004/. This belt is found between the older Svecofennian (c 1.9 Ga) crust to the east-north-east and the younger, Gothian rocks to the west e.g. /Larson and Berglund 1992/. The TIB granitoids and volcanics were formed during several pulses of magmatism between 1.85 and 1.66 Ga. They were formed at three major magmatic events, TIB 1 (1.81–1.77 Ga), TIB 2 (1.72–1.69 Ga) and TIB 3 (1.69–1.66 Ga) /Larson and Berglund 1992, Åhäll and Larson 2000/. The Småland granitoids in the Simpevarp/Laxemar/Äspö area belong to the TIB 1 and have been dated with U-Pb-dating to 1,804+/–4 Ma (zircon) /Kornfält et al. 1997/ and 1,802+/–4 Ma (zircon), 1,793+/–4 (titanite) and 1,800+/–4 Ma (titanite and zircon) /Wahlgren et al. 2004/. Other intrusions are e.g. Götemar /Kresten and Chyssler 1976, Åberg et al. 1984/ and Uthammar. These coarse-grained granites were emplaced at 1,452 +11/–9 Ma (Götemar) and 1,441 +5/–3 Ma (Uthammar) /Åhäll 2001/. Dating and determination of a paleomagnetic pole of the "Äspö diorite" from Äspö HRL, show that the rock has not been heated above 550–600°C since its crystallization /Maddock et al. 1993/.

The bedrock surface in the Laxemar subarea (cf Figure 1-1) is dominated by the Ävrö granite (80%) /Nilsson et al. 2004/. The Ävrö granite is a collective name for a suite of more or less porphyritic rocks that vary in composition from quartz monzodiorite to granite, including quartz dioritic and quartz monzonitic varieties. The Ävrö granite is reddish grey to greyish red, medium-grained with megacrysts of microcline that are usually 1–2 cm in size. A characteristic feature in the Ävrö granite is the occurrence of intermediate to mafic enclaves. The Ävrö granite has been observed to mix and mingle with the equigranular quartz monzodiorite and gradual contact relationships indicate that the two rock types formed more or less synchronously /Nilsson et al. 2004, Wahlgren et al. 2004/.

The rocks in the Laxemar subarea are generally well preserved. A week foliation is occasionally observed in the Ävrö granite and this foliation affects the matrix whereas the megacrysts of microcline show no or weak preferred orientation. Several local shear zones (mylonitic, ductile shear zones and brittle-ductile shear zones) have been mapped /Nilsson et al. 2004/. The width of these zones varies between a decimetre to several tens of metres. A characteristic phenomenon that affects all rock types in the Laxemar subarea is inhomogeneous red staining caused by oxidation in association with hydrothermal alteration /Nilsson et al. 2004/. Geological surface mapping of the adjacent Simpevarp subarea reveals that similar red-staining is present also in this area, although more common than in the Laxemar subarea /Wahlgren et al. 2004/.

The lithology in drill core KLX04 is dominated by "Ävrö granite", which is generally more granitic in the upper couple of hundred metres of the drill core and more quartz monzodioritic at higher depths.

In KLX04, red-staining caused by oxidation is most intensive in the sections 100–300 m, 320–327 m, 340–380 m, 405–420 m, 430–445 m, 580–600 m, 615–640 m, 760–765 m, 845–850 m and 875–985 m. Generally, these sections have higher fracture frequencies than the rest of the drill core.

3.1 Related fracture mineralogy and timing

Studies of the fracture mineralogy from drill cores KSH01, KAS04, KA1755A, KLX02 and ongoing studies of KSH03, KLX03, KLX04 and KLX06, show that the red-staining is present in the entire Äspö-Laxemar-Simpevarp area although more widespread and extensive adjacent to fractures in the Simpevarp area /Drake and Tullborg 2004, 2005, 2006b/. Furthermore, this red-staining of wall rock has been identified adjacent to fractures filled with minerals of generations 1–4 (Table 3-1), in particular by prehnite of generation 4 /Drake and Tullborg 2005/. In contrast, red-stained wall rock is generally not observed when pyrite of generation 3 (early hydrothermal pyrite) is present in the fracture filling. The fracture mineral generations have not been dated but the mylonites of generation 1 are inferred to be older than the Götemar granite (1,450 Ma cf above) e.g. /Tullborg 1997, Stanfors et al. 1999/. K-Ar datings of biotite and whole-rock samples from SE Sweden /Åberg 1978, 1988/ suggest that the mylonites are older than c 1.5 Ga. Generation 2 and 3 might be related to the intrusion of the Götemar granite and re-activation of mylonites /Tullborg 1997, Drake and Tullborg 2005/. It can thus be proposed that hydrothermal conditions that were favourable for oxidizing and red-staining of the wall rock have occurred during several episodes, possibly during a long period of time in the early geological record of the region. The red-staining took place at semi-ductile to brittle conditions. The most extensive red-staining and also the last red-staining event was related to wide spread prehnite crystallization in fractures. Based on datings of wall rock and fracture fillings /Maddock et al. 1993/ it can be proposed that the feldspar alteration in the altered wall rock is at least older than 1,100 Ma and probably c 1,400 Ma

Table 3-1. Schematic fracture filling model for drill cores KSH01A+B, KSH03A+B, KLX02, KLX03, KLX04, KLX05, KLX06, KAS04 and KA1755A modified from /Drake and Tullborg 2006b/.

1. **Quartz- and Epidote-rich mylonite**, occasionally including muscovite, titanite, Fe-Mg-chlorite, albite, (apatite), (calcite), (K-feldspar)
2. **Cataclasite**
   a. Early **epidote**-rich, with quartz, titanite, Fe-Mg-chlorite, (K-feldspar), (albite)
   b. Late **hematite**-rich, with epidote, K-feldspar, quartz, albite, chlorite
3. Euhedral **quartz, epidote, Fe/Mg chlorite, calcite**, pyrite, fluorite, muscovite, (K-feldspar)
4. Prehnite, (fluorite)
5. a. **Calcite**, (fluorite, hematite)
   b. **Dark red/brown filling – Adularia, Mg-chlorite** (also as ML-clay with Illite), hematite (quartz), (apatite); sometimes cataclastic.
   c. **Calcite, adularia, laumontite, Mg-chlorite, quartz, illite** (also as ML-clay with chlorite), hematite, (albite)
6. **Calcite, adularia, Fe-chlorite, hematite, fluorite, quartz, pyrite, barite, gypsum**, harmotome, REE-carbonate, apophyllite, illite/chlorite (ML-clay), corrensite, chalcopyrite, galena, sphalerite, Ti-oxide, U-silicate, laumontite, Cu-oxide, sylvite, (Fe-oxyhydroxide), (Mg-chlorite), (apatite), (wolframite)
7. **Calcite**, pyrite

4 Earlier studies

The features (mineralogy, chemistry, redox potential) of the red-stained rock adjacent to fractures have been studied in drill cores KSH01 and KSH03 at Simpevarp /Drake and Tullborg 2006c/. The study from Simpevarp included rocks of a broader range of compositions than in the present study. Comparisons of the results from Simpevarp and Laxemar (KLX04) are discussed in Section 7.7.

In drill cores KLX01, KLX03 and KLX04 from the Laxemar subarea, /Mattsson et al. 2005/ investigated geophysical and petrophysical properties of the rock. In drill core KSH02, Simpevarp, /Mattsson and Thunehed 2004/ investigated geophysical and petrophysical properties of hydrothermally red-stained dioritoid and compared these to the properties of unaltered fine-grained dioritoid.

Earlier studies of altered, predominantly red-stained rocks from Äspö HRL, have been carried out by e.g./Eliasson 1993, Mazurek et al. 1995, Tullborg 1995, Stosnach and Mengel 1998, Landström et al. 2001/. Although the dominant rock types differ somewhat between Äspö and Simpevarp, with a higher amount of fine-grained dioritoid and quartz monzodiorite at the Simpevarp peninsula and a higher amount of Ävrö granite at Äspö, the red-staining features are reported to be similar at both of the sites.

A number of studies on fracture minerals and altered wall rock conclude that the most significant red-staining of the rock occurs in association with hydrothermal alteration of plagioclase adjacent to fractures /Eliasson 1993, Mazurek et al. 1995, Tullborg 1995, Stosnach and Mengel 1998, Drake and Tullborg 2004, 2005, 2006b/. The plagioclase is originally grey but is red-stained adjacent to many fractures. Red-staining may also occur along grain boundaries and in micro-fractures /Eliasson 1993, Mazurek et al. 1995/. The red-staining is mainly caused by very fine-grained hematite and/or Fe-oxyhydroxide which are present as inclusions in the altered plagioclase /Eliasson 1993, Tullborg 1995, Drake and Tullborg 2004, 2006c/. These minute Fe^{3+}-rich minerals along with other fine-grained alteration products like sericite and an increased porosity, give the plagioclase crystals a clouded appearance. /Eliasson 1993/ estimates that the major red-staining event, caused by Fe-oxyhydroxide precipitation in the altered plagioclases took place at temperatures of about 150–250°C. /Landström et al. 2001/ showed that the hydrothermal alteration of the wall rock, indicated by the chloritization of biotite and alteration of plagioclase, not always coincide with the extension of the red-staining – the hydrothermal alteration often reaches further into the wall rock than the red-staining does.

Analyses of whole rock chemistry of red-stained wall rock have been compared to relatively fresh rock nearby /Eliasson 1993, Tullborg 1995, Stosnach and Mengel 1998, Landström et al. 2001/. From these studies it is shown that REE and several other trace elements remain fairly constant during the alteration. /Eliasson 1993, Landström et al. 2001/ report increases in Na, Cs and LOI and a decrease in Ca in the red-stained rock compared to the unaltered rock. /Eliasson 1993/ also reports increase in K, and constant values of Ti and Al. /Tullborg 1995/ reports increase in LOI, a slight loss in Na and K, while Ca was constant. /Stosnach and Mengel 1998/ reports increase in e.g. K, Ba, Sr and Rb and depletion of Ca, Si and Cs, in the red-stained rock while Al, Ti, Mg, Fe_{tot}, Na and P are fairly constant during alteration. Sr is fixed in secondary epidote during alteration, and Rb and K are fixed in sericite and K-feldspar.

/Tullborg 1995/ found that Fe_{tot} increases somewhat in the altered rock compared to the unaltered rock at Äspö and that the Fe^{2+}/Fe_{tot}-ratio is slightly lower in chlorite in the altered rock than in biotite in the unaltered rock. /Eliasson 1993/ found that the Fe^{3+}/Fe_{tot}-ratio increased in the red-stained rock compared to the unaltered rock, which reflects oxidation of magnetite and formation of hematite, and subordinate Fe-oxyhydroxides.

/Gebel et al. 1999/ investigated the distribution of trace elements on a grain size scale, in rocks from Äspö HRL. It was shown that titanite hosts nearly all bulk rock HREE (including Y), about 80% of the LREE, more than 70% of the Ti, 50% of the Th and about 40% of the U in granodioritic rocks at Äspö. Rb and Cs are mainly found in biotite and Ba is mainly found in K-feldspar. Biotite also contains about 50% of the Mn and Co. The REE-concentrations in biotite are very low. During the alteration process biotite reacts to chlorite, which seems to have significantly lower concentrations of Rb and Cs than the original biotite.

Petrophysical and geophysical investigations show an increase in porosity /Eliasson 1993, Mazurek et al. 1995, Landström et al. 2001, Mattsson and Thunehed 2004, Mattsson et al. 2005/ and a decrease in magnetization /Eliasson 1993, Mattsson and Thunehed 2004, Mattsson et al. 2005/, density /Eliasson 1993, Mazurek et al. 1995, Mattsson and Thunehed 2004, Mattsson et al. 2005/ and electrical resistivity /Mattsson and Thunehed 2004, Mattsson et al. 2005/ in the highly fractured and red-stained rock compared to the unaltered rock. These results indicate oxidation of magnetite and formation of secondary Fe^{3+}-bearing minerals and hydrous minerals in combination with increased secondary porosity in the secondary minerals and the altered primary minerals in the red-stained rock.

5 Equipment

The following equipment was used for sampling, sample preparation, microscopy, SEM-EDS and data processing.

- Scanning electron microscope (Hitachi S-3400N) with EDS (Oxford Instruments).
- Petrographic microscopes (Leica DMRXP and Leica DMLP).
- Microscope camera (Leica DFC 280).
- Digital camera (Konica Revio KD-420Z).
- Rock saws.
- Rock Labs swing mill.
- Point-counting equipment (Swift, Model F).
- Scanner (Epson 4180) and polaroid filters.
- Computer software (e.g. Corel Draw 11, Microsoft Word, Microsoft Excel, SolvCalc, NewPet, TriDraw).

All equipment listed above is property of Earth Sciences Centre, Göteborg University or is owned by the authors. For equipment used for whole rock chemistry analyses, porosity and density measurements and Mössbauer spectroscopy, see the “Execution”-section below.

6 Execution

6.1 Sampling

The drill core from the bore hole KLX04 were sampled for detailed study of the wall rock alteration. The drill core is approximately 1,000 m long and has a diameter of about 50 mm.

Samples were collected from the most extensively and homogenously red-stained parts of the rock. Sampling was generally focused to the parts of the drill cores which where homogenous and intensely red-stained and free from sealed minor fractures. In addition, the adjacent reference rock had to be free from fractures, homogeneous and fresh. The sampling was focused on red-stained samples of more than 30 cm in length in order to get as large and representative samples as possible. Reference samples of fresh, in this case not red-stained rock were collected up to a meter from the red-stained samples. Samples free from minor- and micro-fractures, as well as truly fresh reference rock adjacent to the red-stained rock, were however very difficult to find, since the red-stained parts of the drill core are focused to parts of high fracture frequency. The intensity of the red-staining varies between the samples. Table 6-1 shows rough estimations of the red-staining intensity, sample volume, presence of sealed micro-fractures, grain-size and presence of pertithe- and quartz phenocrysts, for each sample. The sampled sections are mapped as "Ävrö granite" in the detailed Boremap drill core mappings. The sample volumes collected in this study and the distance between the red-stained rock and the reference rock are larger, compared to the study of the red-staining at the Simpevarp subarea /Drake and Tullborg 2006c/, where all samples were concentrated to within 50 cm adjacent to single fractures. A reason for this is that the Ävrö granite is more heterogeneous, coarse-grained and porphyritic, with occasional mafic enclaves, than the rock types sampled at Simpevarp /Drake and Tullborg 2006c/. Sample volumes are 0.5 to 1.5 kg. The red-stained samples are generally mapped as "weakly oxidized" in the Boremap mapping, which means that the rock is extensively red coloured but not dark red. The rock is mechanically strong in these weakly oxidized sections, in contradiction to the sections mapped as strongly oxidized (sample 320R) where the rock strength is weaker and where the rock is more homogenously red coloured and more heavily altered.

The samples were divided into one red-stained sample (labeled "R") and one "unaltered" reference sample (labeled "G", Figure 6-1). However, no reference sample could be sampled close to sample 168A (altered without red-staining) and 170R. Sealed fractures and basic enclaves were removed by sawing and the samples were grinded to powder in a Rock labs swing mill at the Earth Sciences Centre in Göteborg, Sweden. A small rock chip of each sample was sawed for thin-section preparation. A five centimeter piece of each sample was sent for density and porosity analysis at the Swedish National Testing and Research Institute (SP).

Figure 6-1. *Photo of drill core samples 630R ("R"= red-stained rock) and 630G ("G"= reference rock) after they were sawed clean from fractures. Drill core diameter is about 50 mm.*

Table 6-1.

Sample name	Depth	Red-staining	Red-staining (mapping)	Sample volume	Microfractures
108G	108.65–109.30			xxx	
108R	108.65–109.30	xxx	Weak	xxx	xx
137G	137.15–137.39			xxx	xx
137R	138.21–138.54	xx	Weak	xxx	xx
153G	153.73–153.96			xxx	x
153R	154.92–155.09	xxx	Weak	xx	xx
168A	168.60–168.91	x	Sauss(medium)	xxx	xxx
170R	170.34–170.75	xxx	Weak	xxx	xx
320G	320.63–320.96			xxx	x
320R	322.25–322.59	xxx	Strong	xxx	xxx
630G	630.33–630.76			xxx	x
630R	630.95–631.20	xxx	Weak	xxx	xx

x= faint/small/few, xx=medium, xxx=intense/big/numerous, "G"=Reference sample, "R"=Red-stained sample, "A"=Altered without red-staining, "Sauss"=Saussuritization

6.2 Thin section

Polished, 30 µm thick, thin-sections were prepared from each of the twelve samples. The thin-sections were impregnated with blue ink, so that micro-fractures, voids and highly porous parts of the rock could be more easily traced.

The thin sections were examined using petrographic microscope and scanning electron microscope (SEM-EDS). SEM-images were acquired using a Hitachi S-3400N scanning electron microscope at the Earth Sciences Centre, Göteborg University. Point-counting was performed with petrographic microscope, with 10 times magnification. Oxides were identified and point-counted using the reflective light mode on the microscope.

Point-counting was carried out in order to obtain general information of the whole rock and to obtain modal mineral composition in the red-stained rock compared to the reference rock. The results from the point-counting are combined with the results from the chemical analyses. The SEM-EDS investigations provide e.g. high resolution pictures and analyses of fine-grained minerals in the thin sections.

The SEM-EDS microanalyses were carried out on an Oxford Instruments Energy Dispersive System mounted on a Hitachi S-3400N scanning electron microscope at the Earth Sciences Centre, Göteborg University, Sweden. Polished thin-sections were coated with carbon for electron conductivity. The acceleration voltage was 20 kV, the working distance 10 mm and the specimen current was about 1nA. The instrument was calibrated at least twice every hour using a cobalt standard linked to simple oxide and mineral standards, to confirm that the drift was acceptable. X-ray spectrometric corrections were made by an on-line computer system. These quantitative analyses give reliable mineral compositions but Fe^{2+} and Fe^{3+} are not distinguished and the H_2O content is not calculated. Detection limit is 0.1 oxide %. Note that the SEM-EDS analyses used in this report show the Fe_{tot}-content as "FeO" (78% Fe) in contrast to the chemical analyses which gives the Fe content as Fe_2O_3 (70% Fe).

6.3 Chemical analyses

Each sample was analysed for major, minor and trace element contents by Analytica AB. The following is valid for Co, Cu, Ni, S and Zn: Digestion was done by microwave heating in closed teflon vessels with HNO_3/H_2O 1:1. The following is valid for the other elements: 0.125 g sample is fused with 0.375 g $LiBO_2$ and dissolved in dilute HNO_3. LOI (Loss on ignition) is carried out at 1,000°C. Concentrations of the elements are determined by ICP-AES and ICP-QMS. Analyses are carried out according to EPA methods (modified) 200.7 (ICP-AES) and 200.8 (ICP-QMS). Fluorine was measured with an ion selective electrode.

6.4 Mössbauer spectroscopy

Written by Prof. Hans Annersten, Uppsala University.

Rock powder from each of the twelve samples were analysed by Prof. Hans Annersten, Uppsala University, with a Mössbauer spectrometer.

Mössbauer spectroscopy is the resonant absorption of γ-rays. It is a highly selective analytical method that has especially been developed for the study of Fe in solid material e.g. minerals. The Mössbauer effect is a nuclear resonance effect that involves the recoil free emission of γ−rays from a radioactive source, in the case of iron, ^{57}Co that decays to the stable ^{57}Fe with an energy of 14.7 keV. ^{57}Fe in the sample (absorber) absorb this low energetic γ-ray. Natural iron contains 2% of this stable isotope. In order to achieve the right energy for recoilless resonant absorption of the γ-quanta, the Doppler effect modulates the emitted energy by accelerating the source towards the absorber sample. The Mössbauer spectrometer is therefore built by a source (^{57}Co diffused into Rh matrix) sitting on a vibrator that successively increase the acceleration to achieve resonant absorption in the iron containing absorber sample (powder or single crystals) and a detector measuring the transmitted radiation. Vibrator and detector are coupled through a computer and a spectrum where each channel shows the transmission as a function of velocity or energy. Resonant absorption will show up as absorption dips in the spectrum.

Absorption peaks are usually seen as doublets with two symmetric lines because there are two transitions from the ground state +/–1/2 = > +/–1/2 and +/–1/2 = > +/–3/2 in the exited state in ^{57}Fe. The splitting of the doublet is a measure of the crystal field and is characteristic for each mineral, yielding crystallographic information. In the case of magnetic materials e.g. Fe_3O_4 and Fe_2O_3, the different magnetic spins give rise to a six-line absorption pattern.

In all experiments the chemical difference between the source and the absorber will result in a centroid shift of the absorption pattern. The value of the centroid shift gives information on the electron density around the nucleus and the d^5 and d^6 electron configuration of Fe^{3+} and Fe^{2+} make is possible to separate the two types of iron in the sample and hence determining the oxidation degree.

In summary the Mössbauer effect will allow determination of the type of coordination of iron in the mineral, the valence state of iron and the magnetic properties of iron. Mössbauer spectroscopy will to some extent also act as a fingerprint method for identifying solids in a multi-phase sample where only the iron containing phases of course will be observed.

Normally 20–50 mg sample, depending on the iron content, is needed for a Mössbauer analysis but samples smaller than 5 mg can be analysed. In the present study of powder samples absorbers from rocks were analysed 20–40 mg sample were pressed into Cu-holders between low absorbing Mylar films and mounted in the magic angle 54.7° to avoid textural effects from the flaky phyllosilicates. This result in symmetric absorption doublets and will make the fitting of strong overlapping absorption line more easy. Measuring time for each sample took 1–3 days depending on the iron content. Each spectra, 512 channels each, was analysed in computer and fitted using a least square fitting program that give the Mössbauer parameters centroid shift, quadrupole splitting, magnetic hyperfine field and intensity. Velocity scale of the spectrometer is calibrated against metallic iron.

Centroid shifts for ferrous iron are around 1.12 mm/s and for ferric iron between 0.35–0.45 mm/s. Quadrupole splitting are generally much higher for ferrous iron, 2.60 mm/s while splitting from ferric iron is between 0.60–1.0 mm/s. However ferric iron quadrupole splitting in epidote group minerals are the highest measured for ferric iron in silicates, 2.0 mm/s. This is an important diagnostic feature for identifying epidote in rock samples by use of Mössbauer spectroscopy. Magnetite and hematite are identified from their large magnetic hyperfine field 48 and 51 T respective. Examples of Mössbauer spectra containing different iron phases are shown in Figures 6-2 and 6-3.

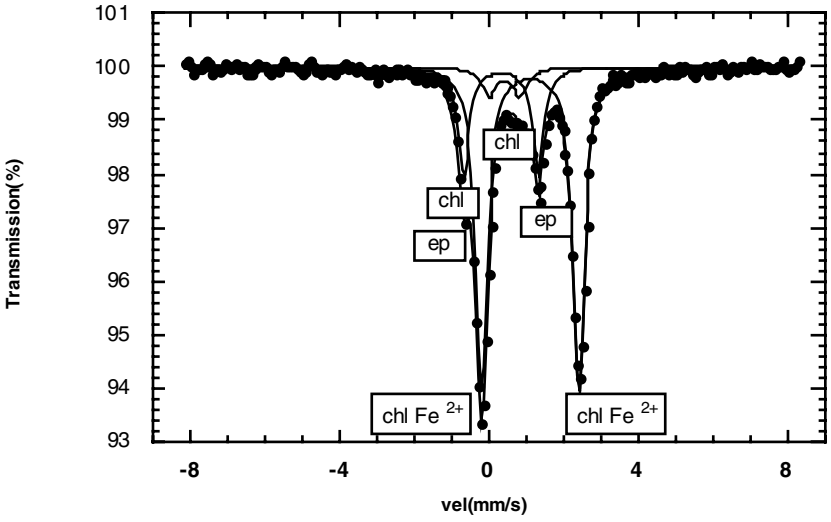

***Figure 6-2**. Sample containing Fe-Mg silicate (mainly chlorite) and epidote. "Chl" indicate doublet for ferric iron in chlorite.*

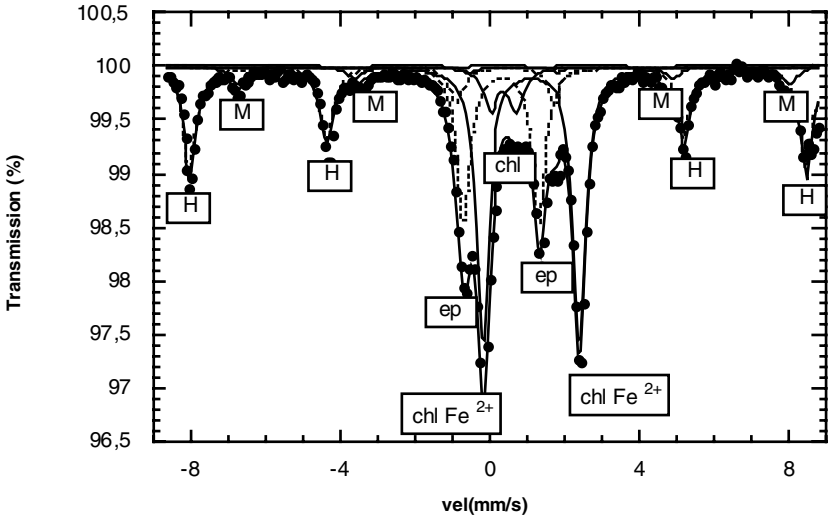

Figure 6-3. *Spectra of rock sample containing hematite (H), magnetite (M), epidote (ep), and Fe-Mg silicates (mainly chlorite [chl]). "Chl" indicate ferric iron in Fe-Mg silicates (mainly chlorite).*

Oxidation degree of the sample is calculated from the intensity ratios between the ferric iron and ferrous iron absorption pattern assuming similar recoil free fractions.

Detection limit for iron bound to magnetic oxides is 1% intensity and 3% for a meaningful fit. Iron bound into paramagnetic silicates has a detection limit of 3% of total intensity and 5% for a reasonable correct fit.

6.5 Porosity and density

Determination of the porosity and density for the 12 samples was made in accordance with SKB's method description SKB MD 160.002, (SKB internal controlling document). This includes determination of density in accordance to ISRM 1979 and EN 1936 in accordance to Activity plan AP PS 400-05-028 (internal controlling document of SKB). The department of Building Technology and Mechanics (BM) at the Swedish National Testing and Research Institute (SP) performed the test.

7 Results and discussion

7.1 Mineralogy

The thin sections were point-counted in order to compare the mineralogy between the reference rock and the red-stained rock (Table 7-1). However, the samples are highly heterogeneous with unevenly distributed phenocrysts of K-feldspar and more plagioclase rich parts, clusters of biotite (and hornblende) and opaque minerals etc. This heterogeneity is visible in the results from the modal analyses, which makes comparisons between thin sections from red-stained samples and reference samples imprecise. The point counting was carried out using an extended subdivision of the different mineral phases compared with what is usually applied for classification of rocks at the investigated sites /Wahlgren et al. 2004/ This was done in order to better describe the hydrothermal alteration.

SEM-EDS investigations reveal that minerals counted as “altered plagioclase” in the reference rock are partly replaced by sericite, albite, prehnite, epidote and K-feldspar but that a substantial portion of the original plagioclase is still present, counted as “plagioclase”. Points counted as “altered plagioclase” in the red-stained rock samples are as a rule completely replaced in a pseudomorphic manner by albite, K-feldspar and sericite mainly and subordinately by epidote and prehnite. The points counted as “plagioclase” in the red-stained samples are mostly fresh, secondary albite. The oxides are point-counted as “opaque” minerals, but are subdivided into magnetite, hematite, magnetite+hematite, and pyrite.

Chlorite, sometimes along with muscovite and prehnite, is often replacing biotite, and to a lesser degree amphibole. The chloritization of biotite is pseudomorphic and include crystallisation of fine-grained secondary titanite, which is present along with the chlorite. These titanite crystals and small remnants of the original biotite can often be traced in thin section but are often too small to be point-counted. Biotite, secondary titanite, prehnite, muscovite, K-feldspar, albite and epidote are underrepresented in the point-counting.

The thin sections are impregnated in order to reveal micro-porosity and micro-fractures. Those parts that are big enough to point-count are counted as “impregnated”. The impregnated parts are often too small to give a fair comparison between the red-stained and the reference rock. Examinations of the thin sections show that the porosity is generally more common in the red-stained rock than in the unaltered rock. These observations are in correspondence with the measurements of porosity in this study and earlier studies of porosity and micro-fracturing in altered granite from Äspö, using the more advanced ^{14}C- and ^{3}H-PMMA-techniques /Kelokaski et al. 2001/. Micro-fractures filled with fracture minerals may occur in the thin sections and are not counted.

Table 7-1. Modal composition, mineral content in%.

Sample	Pl	Alt.Pl	Kfs	Alt.Kfs	Qz	Op	Bt	Tit	Amf	Epi	Chl	Preh	Cc	Imp	No
108G	15.4	18.8	23.6	0.4	24.2	0.9	9.8	1.0	0.9	2.7	1.6	0.8	0.4	0.0	1,144
108R	0.3	41.6	21.4	0.7	25.8	0.4	0.0	0.8	0.0	1.5	4.4	1.5	1.0	0.1	1,187
137G	18.0	17.8	21.9	0.3	23.2	1.7	9.6	1.6	0.0	4.3	1.1	0.4	0.0	0.1	1,121
137R	23.7	17.5	29.6	0.4	13.5	1.8	3.1	1.0	0.1	3.8	3.8	0.6	0.2	0.9	1,057
153G	15.4	21.8	30.6	0.1	23.3	1.1	1.2	0.7	0.0	2.7	3.7	0.3	0.6	0.1	1,039
153R	1.0	40.4	13.0	0.5	28.5	1.3	0.0	0.4	0.0	2.9	8.9	0.5	0.5	0.7	1,034
168A	3.9	30.5	29.1	0.1	23.9	2.0	5.7	1.3	0.0	4.2	0.2	0.1	0.2	1.1	1,069
170R	1.8	38.9	14.0	0.2	30.1	1.2	0.1	1.4	0.0	2.4	7.6	1.7	0.3	0.3	1,082
320G	35.5	25.5	3.1	0.2	12.0	1.8	9.0	3.2	6.3	1.5	0.6	0.5	0.8	0.0	1,084
320R	5.1	45.7	10.3	1.2	14.1	2.6	0.0	1.2	0.0	0.5	17.6	0.6	0.4	0.7	1,095
630G	17.3	21.2	24.3	1.0	8.8	1.9	12.0	2.0	8.8	0.6	1.3	0.5	0.2	0.1	1,424
630R	1.0	55.1	15.9	0.9	5.8	1.6	0.0	1.7	6.0	0.6	8.0	2.3	0.8	0.1	1,408

G = reference sample, R = red-stained sample, A = Alter sample without red-staining, Pl= fresh plagioclase (in R = albite), Alt. Pl = altered plagioclase (in G: plagioclase, albite, sericite, prehnite, epidote, [K-feldspar], in R: albite, K-feldspar, sericite, prehnite, epidote), Kfsp = fresh K-feldspar, Alt. Kfsp = altered K-feldspar, Qz = quartz, Op = Opaque minerals, Bt = biotite, Tit = titanite, Amf = amphibole, Epi = epidote, Chl = chlorite (incl. traces of titanite, muscovite, prehnite and biotite), Preh = prehnite, Cc = calcite, Imp = impregnated (voids, highly porous sections etc), No = number of counted points over each thin section.

According to the International Union of Geological Sciences /Le Maitre 2002/, the classification of rocks should be based on the modal composition. QAP-modal classification of the reference samples is found in Figure 7-1. In this classification all of the sericitized plagioclase is plotted as plagioclase. Since the plagioclase crystals of the red-stained samples generally are completely replaced by K-feldspar, albite and other secondary minerals, the red-stained samples could not be properly classified in the QAP-classification in Figure 7-1. The content of albite, K-feldspar and plagioclase, in the red samples differ somewhat. The red-stained samples have been plotted in Figure 7-1, with the assumption that albite and K-feldspar make up half of the plagioclase pseudomorphs each, which is an over simplification. The heterogeneity of the samples also makes the QAP-classification imprecise.

7.1.2 Mineralogy of the reference rock

Macroscopically, the unaltered reference rock is grey or sometimes reddish-grey, medium to coarse-grained and contains large K-feldspar phenocrysts. The reference rock samples show quite different modal compositions, with a cluster of samples in the granite field, one sample in the quartz monzonite field and one sample in the quartz diorite field. The thin section of the sample in the quartz diorite field (320G) is not representative since it lacks K-feldspar phenocrysts, which evidently are included in the drill core sample. The rocks with a high amount of biotite and amphibole are darker in colour. These minerals are often found in clusters and in some samples these minerals have been partly replaced by chlorite which gives the rock a somewhat greenish colour. The epidote content varies between the samples. The samples in the granite field (108G, 137G, and 153G) have a higher amount of K-feldspar and quartz and a lower amount of plagioclase and generally biotite as well, than samples 320G and 630G. Amphibole (hornblende) is generally only present in the samples 320G and 630G.

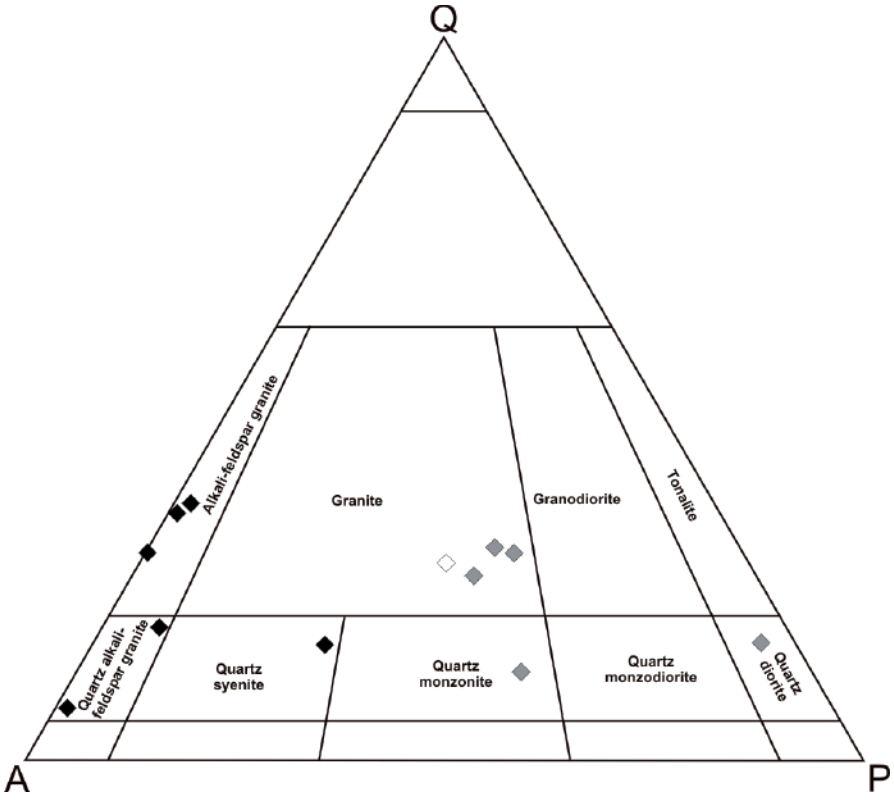

Figure 7-1. *QAP modal classification /Streckeisen, 1976, 1978/ of reference samples (grey), red-stained samples (black) and altered sample 168A (white). See text for details.*

The plagioclase crystals in the reference rock are often altered to sericite, albite, epidote and subordinately K-feldspar. About 40–60% of the plagioclase-counts in the reference rock have been counted as altered plagioclase. This alteration is however not as extensive as the alteration in the red-stained plagioclases, where the whole crystal commonly is replaced. In the reference rock the original plagioclase is often present between the alteration products.

The modal contents of opaque-minerals (commonly magnetite and hematite) and titanite in the reference samples are quite low (< 2%). The titanite content is occasionally very high (3%) and is generally highest in samples 320 and 630. The euhedral titanite crystals are quite large, up to 2 mm in length. The epidote content is generally quite high in the reference rock, but it varies to a large extent. Prehnite is common in the reference rock, as a secondary mineral in altered plagioclase, but also as bigger individual aggregates which might be secondary as well.

Biotite is often quite fresh in the reference samples but in some samples (especially in 153G) it has been slightly altered to chlorite, fine-grained titanite, muscovite, prehnite and possibly Ti-oxide. This indicates that the hydrothermal alteration reaches further from the fracture rim than the red-staining does, as suggested by /Landström et al. 2001/.

7.1.3 Mineralogy of the red-stained rock

The mineralogy of the rock is gradually changed with decreasing distance from the fractures. The texture of the rock is however well preserved and secondary minerals replace original minerals in a pseudomorphic manner. The only small textural changes occur in micro-fractured sections, especially in quartz crystals and K-feldspar phenocrysts.

The modal compositions of the samples are presented in Figures 7-2 and 7-3. The most striking features of the alteration adjacent to the fractures are plagioclase alteration, chloritization of biotite (and hornblende), and increased prehnite content. Further, hematite is replacing magnetite to a slightly higher degree in the red-stained samples than in the reference samples. The chloritization of biotite sometimes ranges further into the wall rock than the red-staining.

From point-counting it is evident that almost all fresh plagioclase have been completely altered and replaced by secondary minerals. The K-feldspar content varies widely and is increased in some red-stained samples and decreased in others. Quartz may be micro-fractured and thus counted as impregnation or as secondary minerals occurring in the micro-fractures.

The biotite (and amphibole) content is always lower in the red-stained samples compared to the reference rock. The chlorite content is higher in the red-stained samples than in the reference samples. However, in sample 630 the decrease of amphibole in the red-stained sample is much smaller than the decrease of biotite, which suggests that amphibole was more resistant to the hydrothermal alteration than biotite.

The prehnite content is higher and the epidote content is somewhat lower in most of the red-stained samples compared to the reference samples. The higher contents of epidote in the reference samples may however depend on sample heterogeneities. Prehnite is more common in altered plagioclase crystals in the red-stained rock and is counted is counted as “altered plagioclase” in the point-counting. Micro-fractures and porous parts recognised as ink-impregnations are more common in the red-stained samples. These parts occur in cross cutting fractures in quartz, in porous parts of chlorite, prehnite, altered plagioclase, and along grain boundaries.

Since titanite is heterogeneously distributed in the rock, the modal change is rather misleading. Secondary titanite in biotite pseudomorphs is often too small to be counted.

Magnetite is replaced by hematite to a slightly higher degree in the red-stained samples than in the reference samples, but the variation in magnetite/hematite-ratio varies a lot in both red-stained samples and red-stained samples. The magnetite in reference samples 108G, 320G and 630G is occasionally rather fresh. In reference samples 137G and 153G the magnetite is commonly replaced by hematite. The replacement of magnetite by hematite is commonly incomplete and remnants of magnetite are common in the pseudomorphs. In Table 7-2 the opaque-minerals from the point-counting is presented.

Fine-grained Fe-oxides in plagioclase crystals are too small to be point-counted. Pyrite is present in some samples. Secondary pyrite formed after the major oxidation/hydrothermal event is present in sample 153R.

A description of the mineralogical features of the altered but not red-stained sample (168A) is found in Section 7.6. Analyses from sample 168A are however occasionally included in tables and plots in this section.

The clay mineral content is generally low. Clay minerals may be found in secondary prehnite, in altered plagioclase and K-feldspar and in micro-fractures along with hematite and/or Fe-oxyhydroxide.

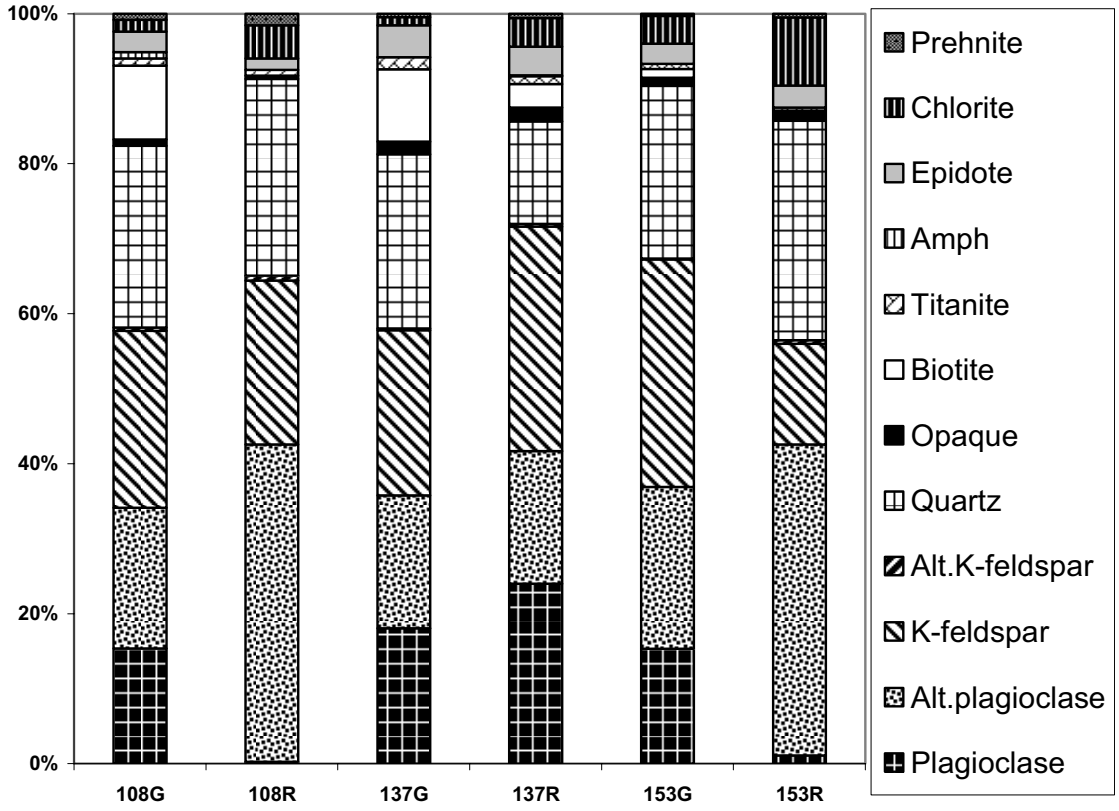

Figure 7-2. *Modal analyses of samples 108G, 108R, 137G, 137R, 153G and 153R. G = reference sample, R = red-stained sample.*

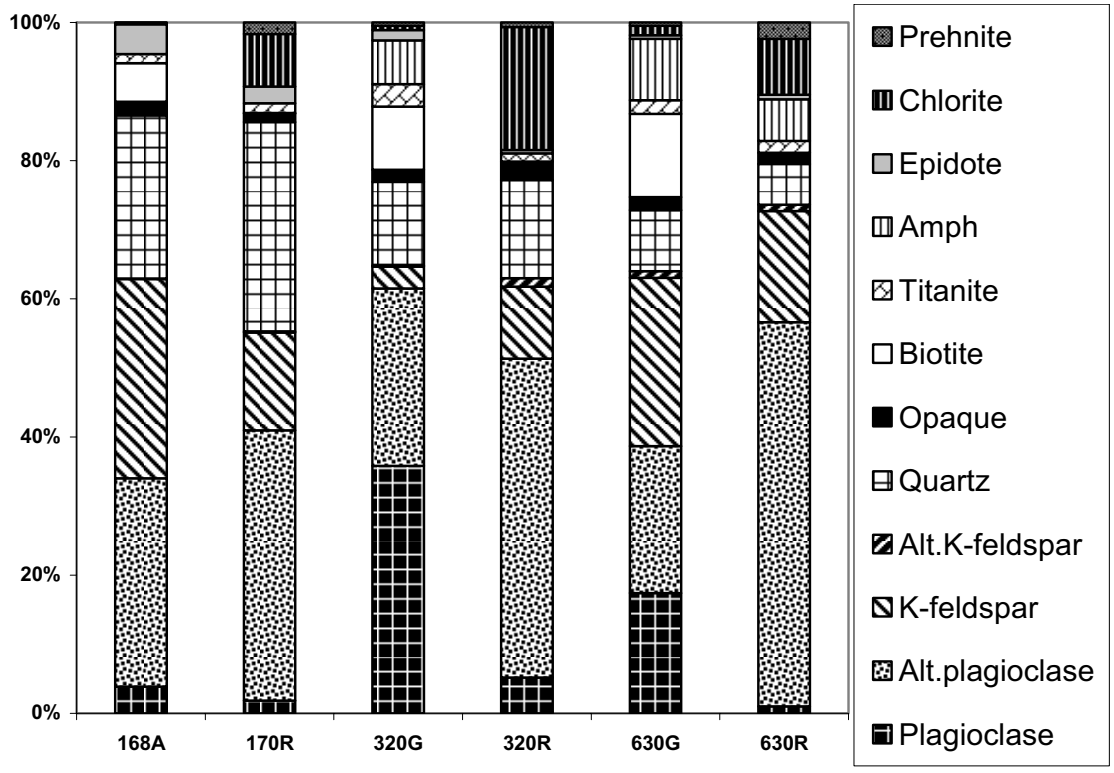

Figure 7-3. *Modal analyses of samples 168A, 170R, 320G, 320R, 630G and 630R. G = reference sample, R = red-stained sample, A = altered but not red-stained sample.*

Table 7-2. Detailed point-counting of the opaque minerals from Table 7-1.

Sample	Hematite	Magnetite	Hematite + Magnetite	Pyrite	Total counts
108G		10			10
108R		5			5
137G	3		16		19
137R	12		6		18
153G	1		10		11
153R	2		10	2	14
168A	16		5		21
170R	10		3		13
320G		8	10	1	19
320R	5		25		30
630G	1	17	8		26
630R	2	10	12		24

7.2 Mineralogical features

In this section the most important features of the minerals in the red-stained rock compared to the reference rock is discussed, along with micro-photographs, SEM-images and SEM-EDS analyses.

7.2.1 Quartz

Quartz was not heavily altered, dissolved or deformed during the hydrothermal alteration. Undulose extinction and micro-fracturing are however more common in the red-stained samples than in the reference samples (Figure 7-4). The micro-fractures are sometimes filled by fine-grained minerals, among others Fe-rich minerals. The quartz crystals remain transparent in the red-stained rock.

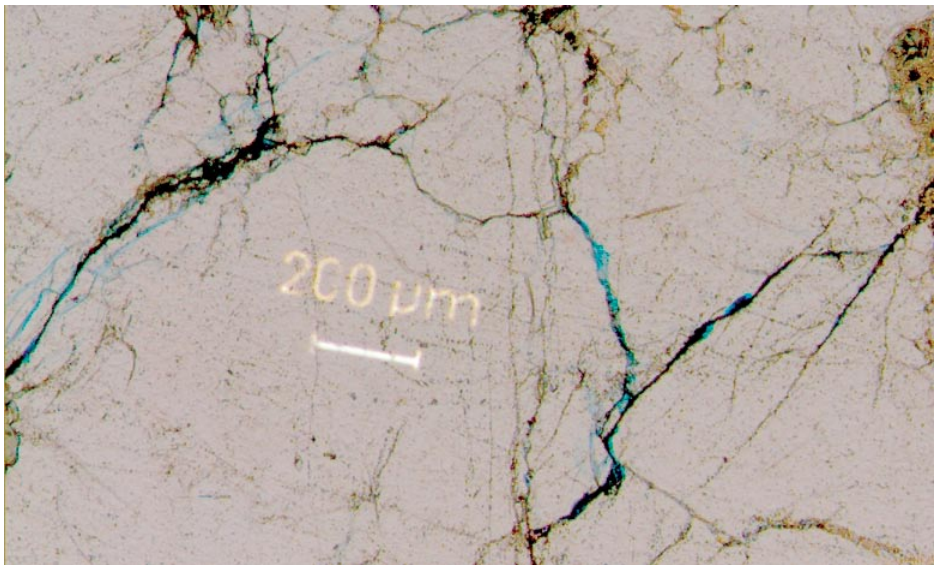

Figure 7-4. *Microphotograph, showing ink-impregnated (blue) micro fractures in quartz. Thin section 153R. Plain polarized light.*

7.2.2 K-feldspar

K-feldspar is present as primary and secondary crystals. The primary crystals are microcline crystals and perthite phenocrysts (K-feldspar with albite inclusions, Figure 7-5) that are mostly preserved during alteration. The secondary K-feldspar, possibly adularia, is found along with albite in pseudomorphs after plagioclase in the red-stained rock. The perthite is largely unaltered during the hydrothermal alteration, but micro-fractures and a small degree of secondary sericite may be present. Chemistry of representative K-feldspar crystals is found in Table 7-3.

The BaO-content varies widely between different crystals. However, K-feldspar in perthite generally has higher BaO-content (up to about 1.58%) than microcline and secondary K-feldspar. The K-feldspar found in altered plagioclase is discussed in the "Plagioclase section".

Table 7-3. Selected SEM-EDS analyses of K-feldspar, * = below detection limit.

Microcline	Na_2O	Al_2O_3	SiO_2	K_2O	FeO	BaO	Total
108G	0.54	18.00	63.98	16.19	*	0.53	99.24
320R	0.49	18.20	64.23	16.08	*	0.82	99.82
K-feldspar in perthite							
108G	0.66	18.25	63.81	16.03	*	0.56	99.31
320R	0.66	18.69	64.34	15.67	*	1.17	100.53
K-feldspar in plagioclase pseudomorphs							
108R	0.21	18.55	63.61	16.46	*	0.61	99.44
153R	0.59	19.62	62.62	15.13	0.21	1.07	99.24
320R	*	18.35	65.10	16.92	*	0.19	100.56
630R	*	19.37	63.44	16.01	*	0.75	99.57

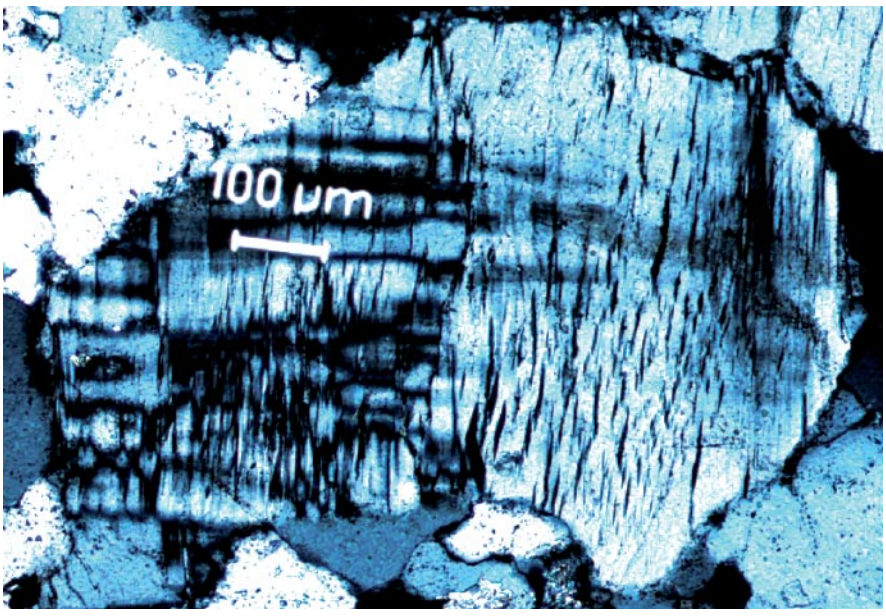

Figure 7-5. *Microphotograph of basically unaltered microcline with tweed-twinning (left) and perthite (right). Thin section 108R, +nic.*

7.2.3 Primary and altered plagioclase

Plagioclase is the most abundant mineral in the samples studied. In the unaltered samples, fresh, unaltered plagioclase crystals are common, but most commonly they have been partially altered to sericite, albite, prehnite, epidote and rarely K-feldspar. The plagioclase crystals in the red-stained samples are as a rule completely replaced by the low temperature paragenesis of albite, K-feldspar, sericite, prehnite, hematite and more rarely epidote and very seldom calcite. Porous and clouded plagioclase is by far the most characteristic feature in the red-stained samples. The red-staining becomes very prominent since plagioclase originally makes up about 35–50% of the modal composition of the rock.

Plagioclase in reference samples

The primary anorthite-content of plagioclase is about 24–30% (average 27%). Representative analyses are found in Table 7-4. The FeO-content in the primary plagioclase is quite small and the average content is < 0.1% (from 11 analyses).

The plagioclase crystals are normally twinned according to the albite-law but also Carlsbad-twinning is common. The primary plagioclase in the reference samples is in most cases partially replaced by alteration minerals such as sericite, albite and epidote, however, complete replacement is not observed (Figure 7-6). Plagioclase in the reference samples is usually colourless in plain polarised light. The sericitized and altered parts are somewhat more porous and clouded, which gives a slightly stronger colour (Figure 7-7). This faint colouration effect, increases gradually with increased alteration of the plagioclase in the reference samples. The primary plagioclase has low porosity in contrast to the plagioclase pseudomorphs in the red-stained samples.

Table 7-4 Selected SEM-EDS analyses of unaltered plagioclase, *=below detection limit.

	Na_2O	Al_2O_3	SiO_2	K_2O	CaO	FeO	Total	An%
108G	8.52	23.67	62.38	*	5.41	*	99.98	26.00
137G	8.33	23.45	62.19	0.78	5.00	*	99.75	25.00
153G	8.80	23.68	62.80	*	4.97	0.20	100.45	24.00
320G	8.33	24.56	61.52	0.18	6.08	*	100.67	29.00
630G	8.22	23.97	61.75	0.39	5.55	0.27	100.15	27.00
Av.(n=11)	8.36	24.02	61.70	0.19	5.65	<0.1	100.01	27.00

Av.(n=11) = average value from 11 analyses of unaltered plagioclase crystals.

Whole crystal-analyses (SEM-EDS) of plagioclase (Table 7-5) mostly show higher K_2O-, FeO- and MgO-contents compared to the SEM-EDS-spot analyses of unaltered parts of plagioclase (Table 7-4). This is caused by sericite and possibly also K-feldspar in the more altered part of the crystal. The Na_2O-content and CaO-content are somewhat lower in the whole crystal-analyses, for the same reasons. Some crystals are fairly unaltered and some heavily sericitized crystals have K_2O-values of up to 2.3%, but the average K_2O-content from 23 whole crystal-analyses is 1.1%.

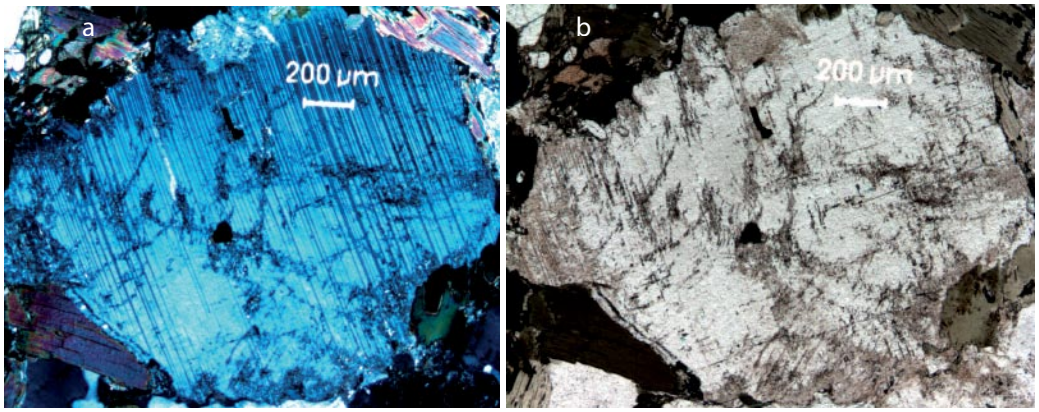

Figure 7-6. *Microphotographs of unaltered plagioclase from sample 630G, +nic (a), plain polarised light (b).*

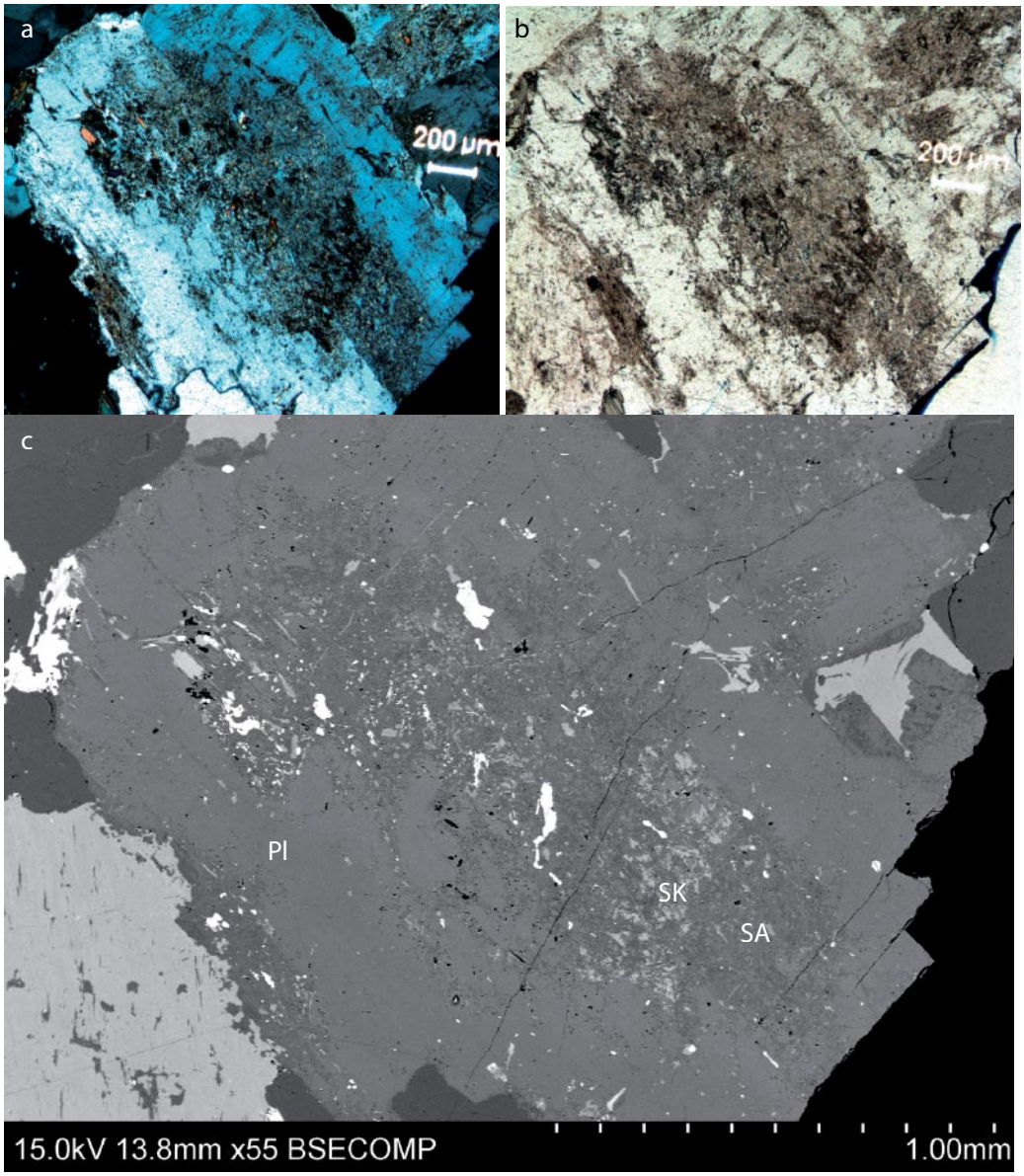

Figure 7-7(a-b-c). *Microphotographs (a,b) and SEM-image(c) of sericitized plagioclase from sample 108G, +nic (left), plain polarized light (right). In c Pl = fresh plagioclase, SK = sericite and K-feldspar and SA = sericite and albite.*

Table 7-5. Selected SEM-EDS analyses of whole plagioclase crystals from reference samples, *=below detection limit.

	Na_2O	MgO	Al_2O_3	SiO_2	K_2O	CaO	FeO	Total
108G	8.24	*	23.63	61.18	0.35	5.46	0.26	99.12
137G	7.93	0.17	24.02	61.41	0.93	5.00	0.37	99.83
153G	8.72	*	23.50	63.34	1.18	3.19	*	99.93
320G	8.11	*	23.65	61.60	1.32	4.72	0.42	99.82
630G	7.82	*	24.19	60.76	1.84	4.38	0.28	99.27
Av.(n=23)	8.05	<0.10	23.80	61.62	1.10	4.75	0.36	99.74

Av.(n=23) = average value from 45 analyses of whole plagioclase crystals.

Table 7-6 shows SEM-EDS analyses of sericite from the altered parts of plagioclase crystals in both reference samples and red-stained samples.

Table 7-6. Selected SEM-EDS analyses of sericite in plagioclase crystals, *=below detection limit.

	Na_2O	MgO	Al_2O_3	SiO_2	K_2O	FeO	BaO	Total
153R	0.19	0.26	35.90	48.11	10.74	1.02	*	96.22
168A	0.30	1.64	30.67	45.51	10.68	3.62	1.10	93.52
320R	*	1.57	28.15	49.50	10.93	3.57	*	93.72
630R	0.24	0.10	35.23	46.79	10.99	0.71	*	94.06

Plagioclase in red-stained samples

Plagioclase in the red-stained samples is commonly completely replaced by the secondary minerals; albite, K-feldspar, sericite, prehnite, Fe-oxides and epidote. Albite, K-feldspar and sericite are by far the most abundant secondary minerals in the pseudomorphs. The primary-anorthite content is altered to albite and prehnite, epidote and calcite, in the pseudomorphs, in voids, or in fracture fillings are formed. The replacement of plagioclase is pseudomorphic, i.e. the crystal shape is maintained after alteration. The primary albite-twinning of the plagioclase remains in many of the secondary pseudomorphs although the mineralogy is completely changed (Figure 7-8). The replacement generally features an intense red-staining of the secondary minerals in the plagioclase pseudomorphs. The intensity of the red-staining varies widely within crystals and between different crystals.

The replacement of primary plagioclase is associated with an increased porosity within the secondary grains. This is clearly visible in the petrographic microscope using reflective light (Figure 7-9).

Comparisons of microphotographs and back-scattered SEM-images clearly show that the intensity of the red-staining within crystals is associated to secondary minerals. Figure 7-10 shows that the most intense red-staining in the pseudomorphs occurs where K-feldspar is the dominant mineral. In albite-rich parts of the crystal, the red-staining is weaker, although still intense compared to surrounding crystals.

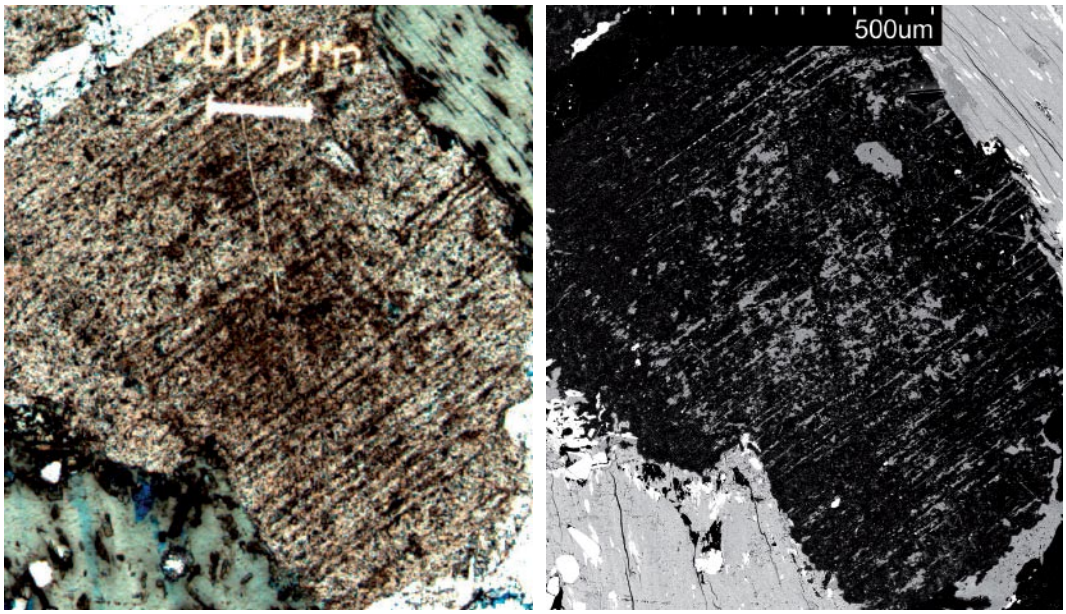

Figure 7-8. *Microphotograph (a, plain polarized light) and back-scattered SEM-image (b) of albite- and K-feldspar-rich pseudomorph after plagioclase, from sample 320R. Note the albite-twinning, inherited from the primary plagioclase.*

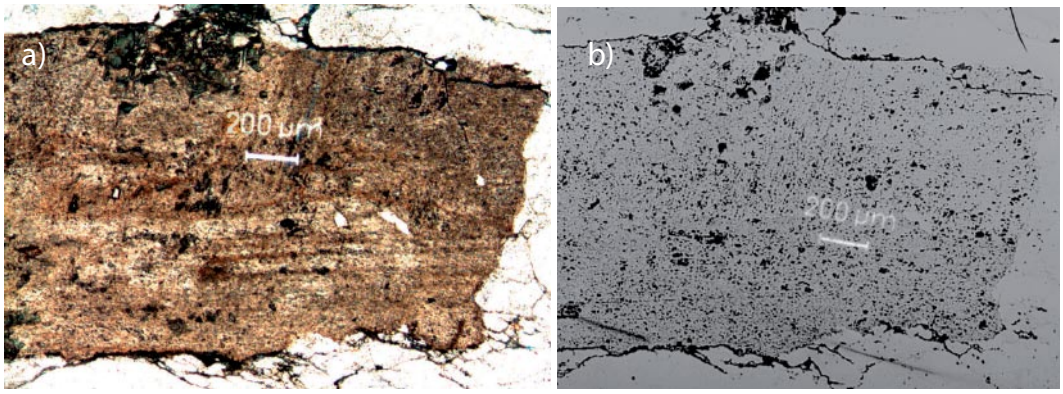

Figure 7-9. *Microphotographs of albite and K-feldspar rich pseudomorph after plagioclase, from sample 153R. Plain polarized light (a) and reflective light (b). Note the high porosity in the plagioclase pseudomorph (right) compared to surrounding quartz crystals*

SEM-investigations show that the inherited albite-twinning in the plagioclase pseudomorphs consists of an intergrowth of albite and K-feldspar (Figure 7-11). The red-staining is more intense in the inherited twins occupied by K-feldspar, while albite-rich parts are less red-stained. The inherited twins are occasionally somewhat distorted, which results in a patchy extinction of the twin-lamellae.

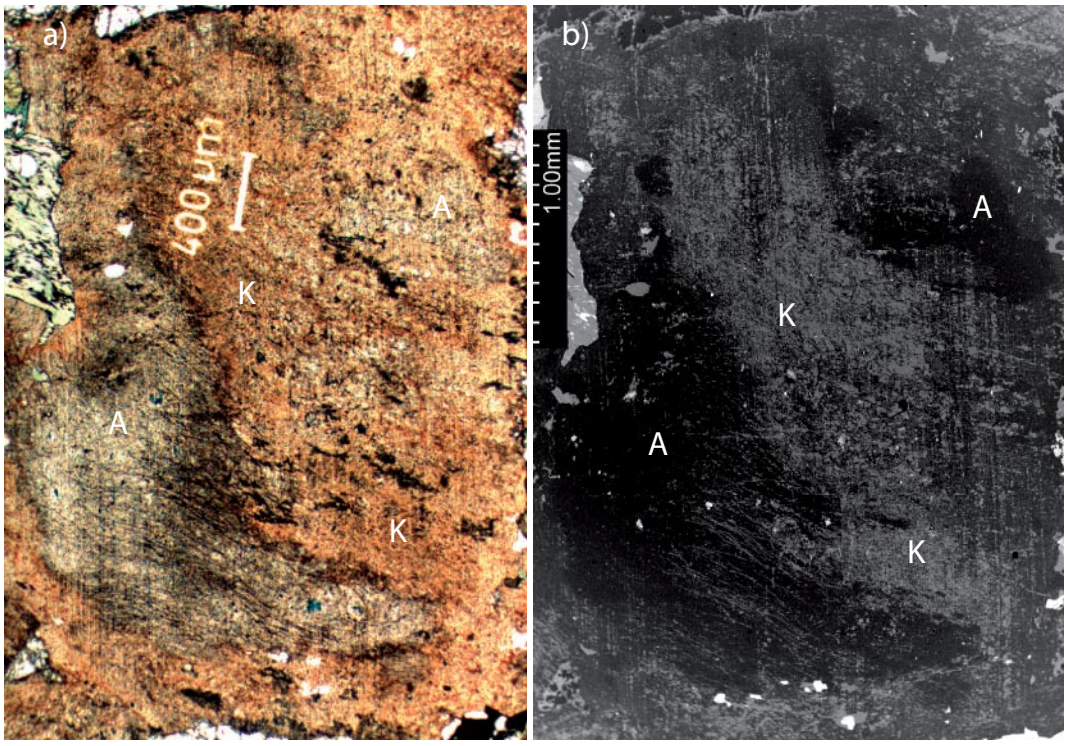

Figure 7-10. *Microphotograph (a) and back-scattered SEM-image (b) of red-stained pseudomorph after plagioclase, from sample 630R. "A"=albite, "K"=K-feldspar.*

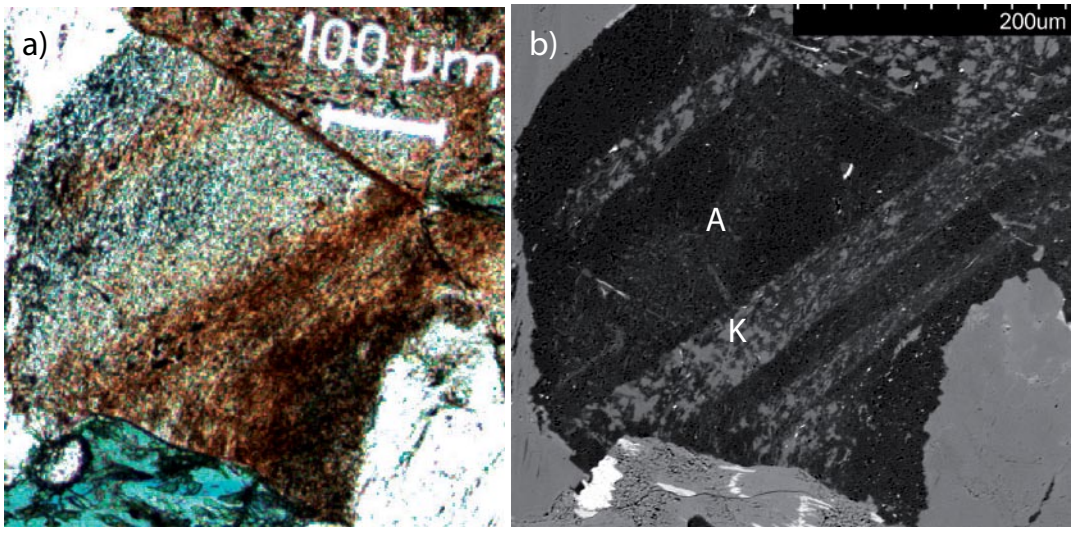

Figure 7-11. *Microphotograph (a) and back-scattered SEM-image (b) of red-stained pseudomorph after plagioclase with inherited twinning, from sample 630R. "A"=albite, "K"=K-feldspar (with minute Fe-oxide inclusions).*

The red-staining of albite and K-feldspar is caused by minute inclusions of Fe-oxides in the micro-pores, formed during the alteration and replacement of primary plagioclase. The secondary albite and K-feldspar are fairly equally porous but Fe-oxides are more commonly found in pores in K-feldspar than in albite (Figure 7-12). This may be one of the reasons why K-feldspar is more intensively red-stained than the albite. The high amount of micro pores makes the crystals look cloudy.

Some plagioclase pseudomorphs are cross-cut by micro-fractures filled with dark brown/ black/red Fe-oxides and possibly Fe-oxyhydroxides (Figure 7-13). These fractures were obviously induced and filled subsequently to the replacement of plagioclase, and thus subsequently to the major red-staining of the plagioclases. It is however difficult to determine how long time it was between the red-staining of the plagioclase pseudomorphs and the sealing of the Fe-oxide/Fe-oxyhydroxide filled fractures.

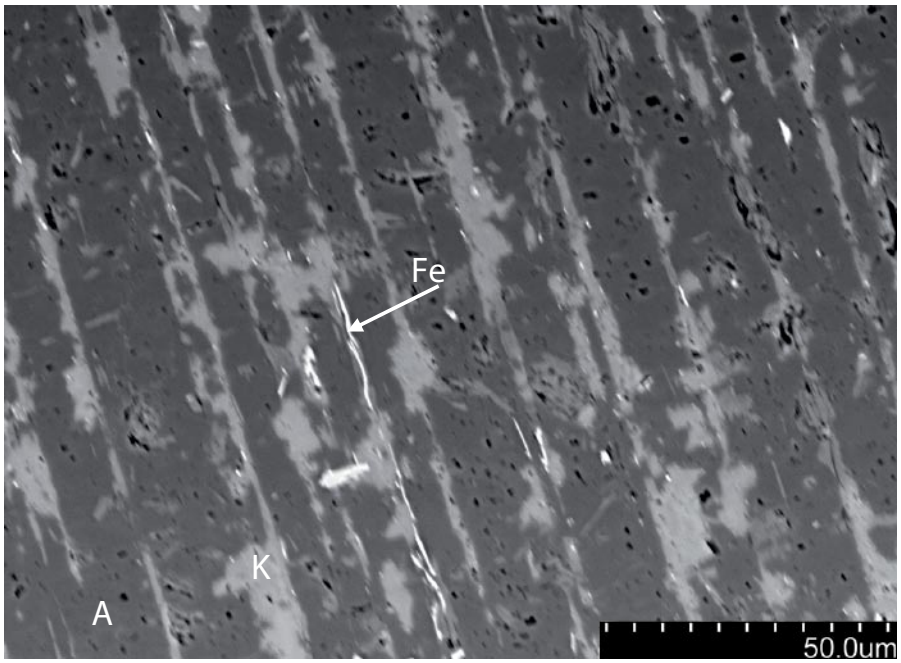

Figure 7-12. *Back-scattered SEM-image of twin-lamellae inherited from primary plagioclase, occupied by porous K-feldspar (K) with Fe-oxide inclusions (Fe), and albite (A) with less Fe-oxide inclusions. Sample 108R.*

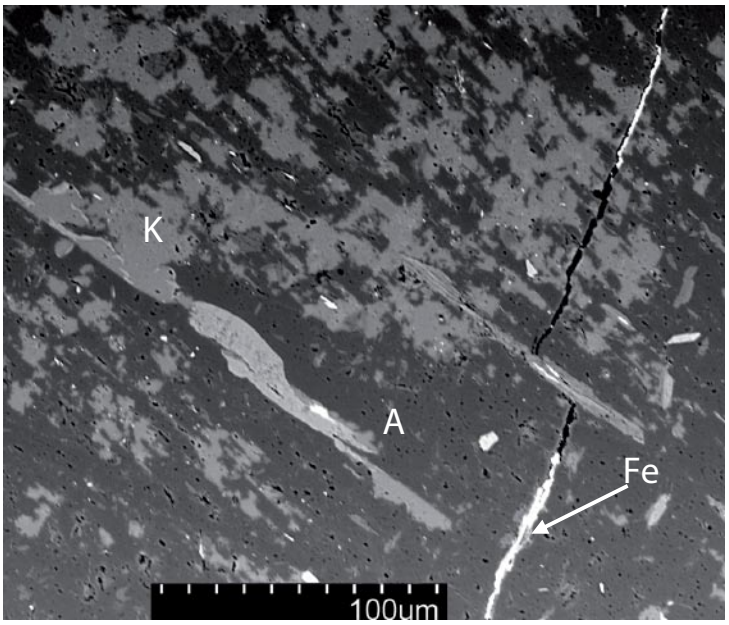

Figure 7-13. *Back-scattered SEM-image of highly porous albite (A), K-feldspar (K) with Fe-oxide inclusions, and fine-grained Fe-oxides/Fe-oxyhydroxides (Fe) in a micro-fracture in plagioclase pseudomorph (sample 630R).*

SEM-EDS analyses of pure secondary albite and K-feldspar in altered plagioclase from the red-stained samples show that the albite generally has FeO contents below < 0.1%, (Table 7-7).

Selected whole crystal analyses (SEM-EDS) of the whole plagioclase pseudomorphs are shown in Table 7-8. These analyses show that the K_2O-content is very high, with an average of about 3.5%, caused by increased K-feldspar and sericite contents. The average FeO- and MgO-contents are slightly higher than in the unaltered samples, which may be explained by slightly higher sericite and Fe-inclusion contents, and possibly Fe-rich minerals in micro-fractures.

Comparisons between the whole crystal-analyses of plagioclase crystals in the reference samples (Table 7-5) and pseudomorphs after plagioclase in the red-stained samples are shown in Figures 7-14, 7-15, and 7-16.

Figure 7-14 shows that the $K_2O/(K_2O+CaO)$-ratio is higher in the red-stained samples compared to reference samples and that FeO-content is generally higher on average in the red-stained samples. Diffuse positive correlations between FeO-contents and $K_2O/(K_2O+CaO)$-ratio, are related to increasing sericite-contents, and grade of alteration.

Figure 7-15 shows the CaO versus Na_2O-content in the red-stained samples compared to the reference samples. The CaO-content is consistently higher in the reference samples. The Na_2O-content in the red-stained samples is somewhat different from the reference samples. This mainly depends on the K-feldspar/albite-ratio in the altered plagioclase crystals.

Table 7-7. Selected SEM-EDS analyses of albite in plagioclase pseudomorphs from red-stained samples, *=below detection limit.

	Na_2O	Al_2O_3	SiO_2	K_2O	CaO	FeO	Total
137R	11.36	19.55	68.20	*	0.35	*	99.46
630R	11.24	19.78	68.21	0.13	0.36	*	99.72
Av.(n=9)	11.36	19.61	68.26	0.09	0.24	0.06	99.64

Av.(n=9) = average value from 9 analyses of albite.

Table 7-8. Selected SEM-EDS analyses of whole plagioclase pseudomorphs from red-stained samples, *=below detection limit.

	Na_2O	MgO	Al_2O_3	SiO_2	K_2O	CaO	FeO	Total
108R	8.25	*	21.22	65.89	4.31	0.46	0.55	100.68
137R	8.47	0.29	23.15	63.48	2.53	1.60	1.13	100.65
153R	8.10	0.34	22.95	63.21	3.60	0.97	0.76	99.93
170R	8.47	*	22.24	63.93	3.08	2.10	0.55	100.37
320R	8.15	*	20.65	64.80	4.58	0.45	0.84	99.47
630R	8.14	*	22.50	64.12	3.83	1.35	0.60	100.54
Av.(n=33)	8.26	0.15	21.81	64.36	3.46	1.09	0.66	99.79

Av.(n=33) = average value from 33 analyses of whole plagioclase pseudomorphs.

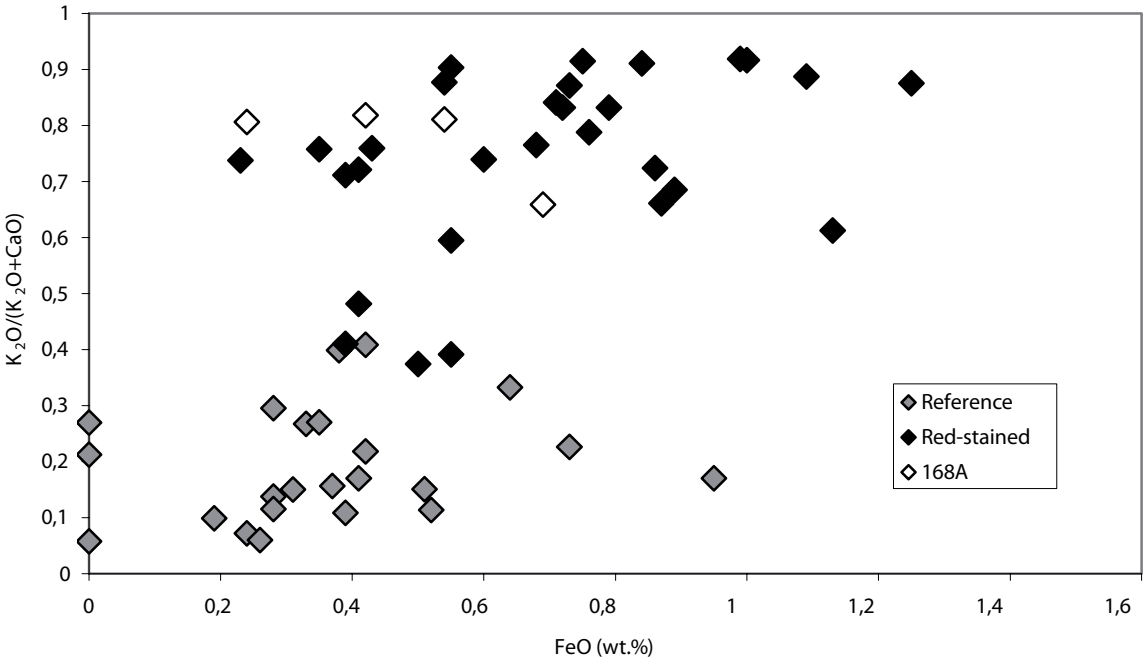

Figure 7-14. *Plot of $K_2O/(K_2O+CaO)$ vs FeO from SEM-EDS analyses of whole plagioclase crystals/pseudomorphs from reference samples, red-stained samples and sample 168A.*

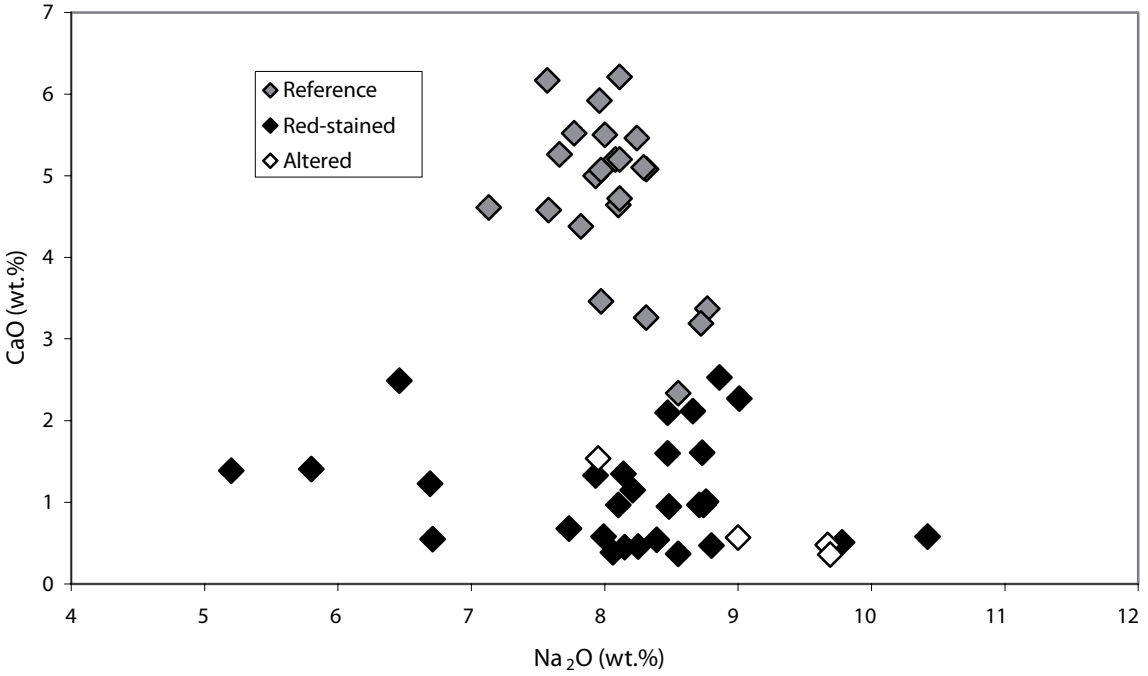

Figure 7-15. *Plot of CaO vs Na_2O from SEM-EDS analyses of whole plagioclase crystals/ pseudomorphs from reference samples, red-stained samples and sample 168A.*

Figure 7-16 shows Al_2O_3-contents versus SiO_2-contents in the red-stained samples compared to the reference samples. The Al_2O_3-content is generally lower and the SiO_2-content is generally higher in the red-stained rock. This is mainly dependent on the removal of the anorthite content in plagioclase ($CaAl_2Si_2O_8$) and the increase in albite ($NaAlSi_3O_8$) and K-feldspar ($KAlSi_3O_8$) in the red-stained samples. The low Al_2O_3-content and high SiO_2-content indicates that albite and K-feldspar dominates over sericite (high in Al_2O_3, low in SiO_2, see Table 7-6) in plagioclase. The stabilization of K-feldspar before muscovite in the red-stained granite was also noted by /Eliasson 1993/. This indicates a rather high activity of K+ in the hydrothermal solution /Beane and Titley 1981/, as shown by the whole rock chemistry analyses (Section 7.3).

Replacement processes

The replacement of primary plagioclase by albite (and K-feldspar) is rather complex and have been described or briefly reported in many earlier studies e.g. /O'Neil 1977, Kastner and Siever 1979, Saigal et al. 1988, Morad et al. 1990, Slaby et al. 1990, Slaby 1992, Lee and Parsons 1997, Petersson and Eliasson 1997, Lee and Parsons 1998, Ennis et al. 2000, Larsson et al. 2002, Putnis 2002, Holness 2003/. Inherited twins and inherited optical orientation in plagioclase pseudomorphs have been reported by /Morad et al. 1990, Slaby et al. 1990, Petersson and Eliasson 1997, Taboada and Garcia 1999, Holness 2003/. /Putnis 2002/ argues that the parent crystal will have crystallographic control over the product, even when all bonds may have been broken in the dissolution process.

Plagioclase alteration and replacement are dependent on a large number of parameters like temperature, pressure, pH, dissolution rates, time, solution composition, mineral (solid) composition, closeness to equilibrium, mineral surface area etc. One of these processes, where the primary plagioclase is replaced by secondary minerals, is the dissolution-reprecipitaion process, described by e.g. /Slaby 1992, Ennis et al. 2000, Larsson et al. 2002, Putnis 2002, Holness 2003/. This process (albitization and/or "microclinization") results

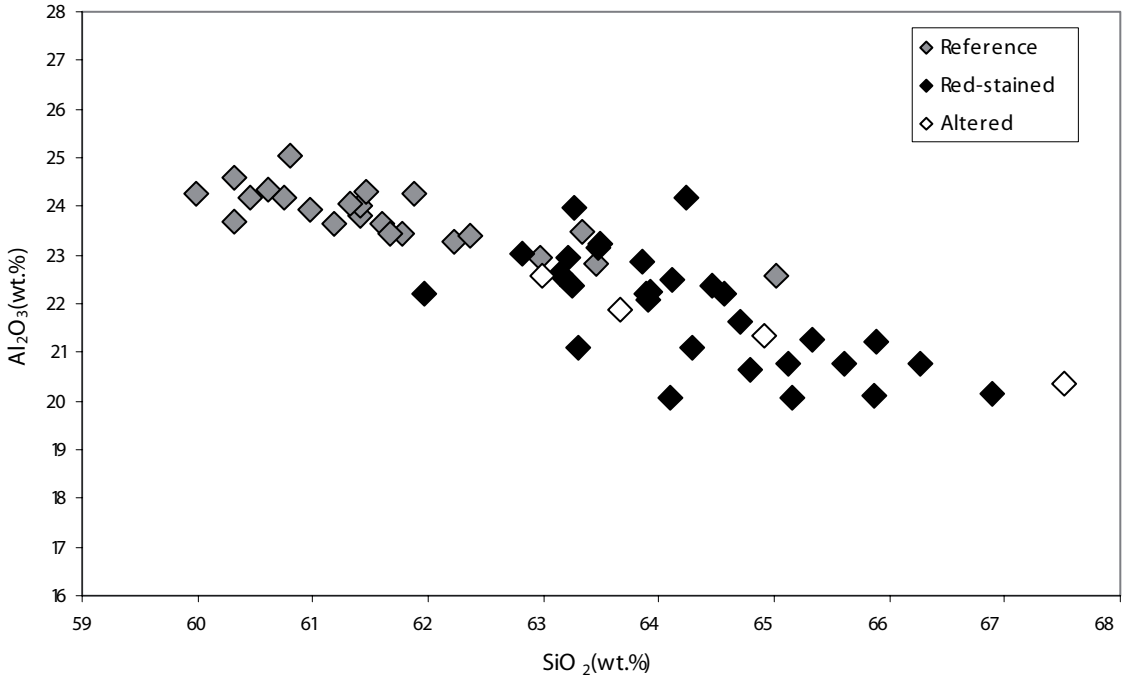

Figure 7-16. *Plot of Al_2O_3 vs SiO_2 from SEM-EDS analyses of whole plagioclase crystals/ pseudomorphs from reference samples, red-stained samples and sample 168A.*

in a sharp compositional gradient between the host and the secondary mineral /Putnis 2002/ and often feature micro-porosity in the secondary mineral /Morad et al. 1990, Lee and Parsons 1997, Putnis 2002/. This occurs whenever the amount precipitated is less than the amount dissolved and depends on solubility and composition of the solid and the fluid phases. In the presence of a fluid phase, comparatively small differences in free energy are sufficient to drive the re-crystallization by the dissolution re-precipitation process /Putnis 2002/. Exchanging cations through a "passive" aluminosilicate structural framework often, if not always, involves re-crystallization of the entire structure /O'Neil 1977/. However, /Krauskopf and Bird 1995/ using data from /Busenberg and Clemency 1976, Helgeson et al. 1984, Wollast and Chou 1985/ describe alteration of plagioclase that is mainly caused by formation of a surface layer of the feldspar that has been altered by partial loss of the alkali metals. The dissolution rate is controlled by reactions at the solution-mineral interface and not by the rate of ion diffusion away from the mineral into solution. This would involve a passive Al-Si network while the cations are exchanged. /Orville 1963, Lagache and Weisbrod 1977/ showed that fluid flow in combination with a temperature gradient in a rock containing two alkali feldspar phases (or in a system in which two feldspars are in chemical communication), will result in redistribution of alkalis, which is also suggested in this study.

In conclusion, the presence of elevated micro-porosity in the secondary minerals of the plagioclase pseudomorphs as well as the local sharp compositional contrasts between K-feldspar and albite, may suggest a dissolution-reprecipitation process. It is however difficult to discern whether the plagioclase crystals have been completely dissolved or if an Al-Si structural network remained in the host crystal and exchange mainly progressed as cation exchange. The plagioclase crystals are sometimes replaced in a well structured manner with inherited twinning and sometimes in an unstructured manner. This suggests that the replacement of plagioclase have involved different processes. The order-disorder in the secondary albite, and presence or absence of twins may be controlled by the composition of the solution affecting the speed of albite growth /Slaby 1992/.

7.2.4 Magnetite, hematite and pyrite

Magnetite is the most common opaque mineral in the reference samples (Figure 7-17) and is replaced by hematite in the red-stained samples, but also often in the reference samples. The magnetite crystals commonly occur in close relationship to chloritized or unaltered biotite and to some extent, to titanite and amphibole. The replacement of magnetite by hematite is commonly incomplete and remnants of magnetite are commonly visible in the pseudomorphs (Figure 7-18).

Fine-grained Fe-oxides are present in plagioclase pseudomorphs. These Fe-oxides are often too small to be analysed by SEM-EDS, but the few analyses that have been performed indicate that it consist of hematite. Fine-grained Fe-oxide/Fe-oxyhydroxide is present in micro-fractures cutting through crystals of mainly quartz, plagioclase and K-feldspar. These crystals are also too small to be analysed properly with SEM-EDS. The identification of goethite in one Mössbauer analysis (see Section 7.5) infers that some of the fine-grained Fe-rich minerals in the red-stained samples are Fe-oxyhydroxide. The Fe-oxides and possibly also Fe-oxyhydroxides in plagioclase may originate from break-down of magnetite to hematite, from Fe that is originally present in primary plagioclase, or from other reactions like chloritization of biotite.

Pyrite is present in some samples. Pyrite is common in some of the red-stained samples, where pyrite crystals have precipitated in voids and micro-fractures of the porous rock (Figure 7-19), probably during reducing conditions subsequently to the major red-staining event.

Figure 7-17. *Microphotograph of magnetite (Mt) from sample 320G, reflective light.*

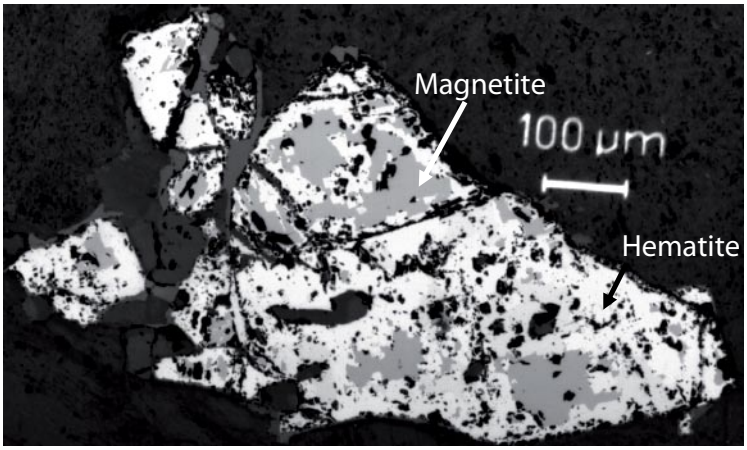

Figure 7-18. *Microphotograph of hematite partially replacing magnetite in a pseudomorphic manner, from sample 320R, reflective light.*

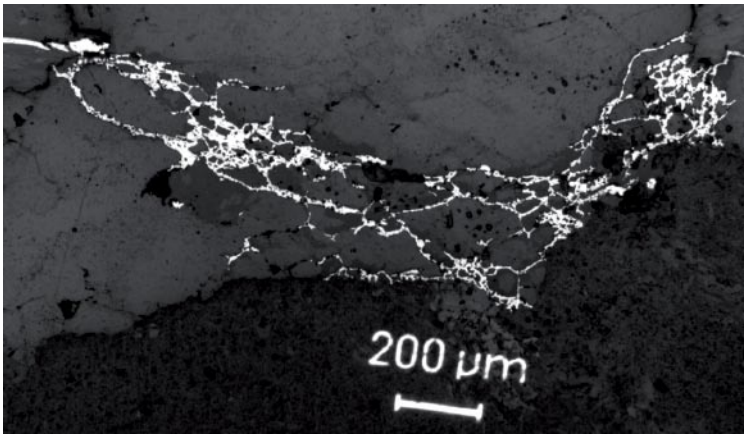

Figure 7-19. *Microphotograph of pyrite (bright mineral) in micro-fractures. Sample 153R, reflective light.*

7.2.5 Biotite

Biotite is commonly rather unaltered in the reference samples (Figure 7-20). Partial replacement of biotite by chlorite is observed in some reference samples, especially in sample 153G where a major part of the biotite content is replaced by chlorite (Figure 7-21). Biotite is commonly completely replaced by chlorite in the red-stained samples, except in sample 137R, where biotite is only partially replaced. The replacement is pseudomorphic and titanite, and subordinate prehnite, muscovite (especially in sample 137R), K-feldspar, quartz, fluorite and possibly Ti-oxides are present together with chlorite in the pseudomorphs.

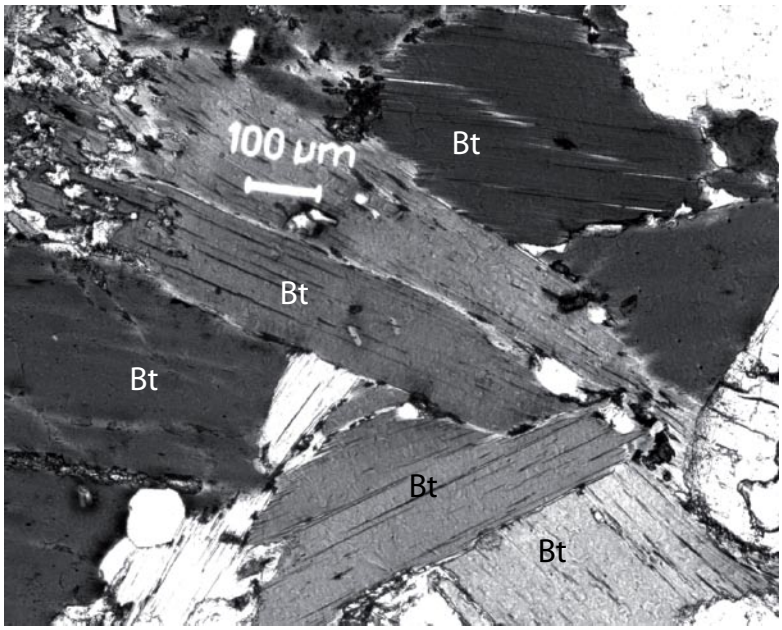

Figure 7-20. *Microphotograph of fresh biotite, from sample 108G. Plain polarized light.*

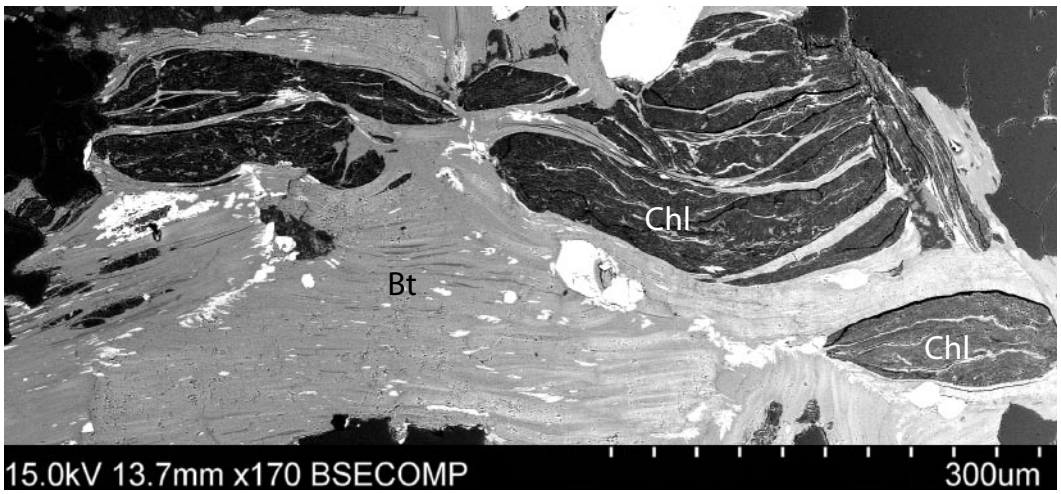

Figure 7-21. *Back-scattered SEM-image of partly chloritized (Chl) biotite (Bt) from sample 153G.*

The suggested simplified reaction is:

Biotite + H_2O (+Ca^{2+}) Chlorite ± Titanite ± Ti-oxide + K^+

These new crystals are formed along the (001)-cleavages of biotite. The Ti-content in biotite (Table 7-9) ranges from 1.5 to 2%. Even a small degree of chloritization gives intense potassium removal, as suggested by /Wilamowski 2002/. The released K^+ forms K-feldspar and sericite in the surrounding rock and sometimes K-feldspar and muscovite in the pseudomorph after biotite. In some samples prehnite is formed along with chlorite in biotite-pseudomorphs. This prehnite and the titanite can be formed by the Ca^{2+}, mainly released during plagioclase breakdown. Some Ca^{2+} may originate from hornblende alteration. /Ferry 1979/ suggested that Al-contents remained unchanged during chloritization of biotite while /Parneix et al. 1985/ suggested that the Al-content was variable at chloritization, although Al will not be transported for long distances since Al activity in hydrothermal fluids is very weak /Ellis and Mahon 1977/.

/Spear 1993/ proposes that the reaction biotite + H_2O = chlorite + K-feldspar, takes place below approximately 400°C, at conditions close to equilibrium, normally at a maximum depth of 16 km. /Wilamowski 2002/ argues that chloritization of biotite takes place at temperatures of approximately 300°C.

Table 7-9. Selected SEM-EDS analyses of biotite.

	MgO	Al_2O_3	SiO_2	K_2O	TiO_2	MnO	FeO	Total
108G	12.87	14.48	38.08	10.05	1.77	0.45	19.45	97.15
630G	13.59	14.02	37.44	9.63	1.75	0.49	18.59	95.51
Av.(n=10)	13.19	14.58	37.62	9.62	1.74	0.47	18.69	95.92

Av.(n=10) = average value from 10 analyses of biotite.

7.2.6 Amphibole

Amphibole is only present in samples 320 and 630. The only identified amphibole is hornblende (Table 7-10) and it is commonly found in clusters together with completely or partially chloritized biotite, magnetite and sometimes titanite. The highest amount of amphibole is found in sample 630G, where it constitutes 8.8 vol.% of the modal composition. Hornblende is partially replaced by chlorite in sample 630R and completely replaced by chlorite in sample 320R. Chloritization of hornblende results in mobilisation of Ca^{2+} and small amounts of Na^+ and K^+. The other major and minor elements are fixed in chlorite and titanite, which is sometimes formed together with chlorite. Some Ca^{2+} may also be fixed in the secondary titanite.

Table 7-10. Selected SEM-EDS analyses of hornblende.

	Na_2O	MgO	Al_2O_3	SiO_2	K_2O	CaO	TiO_2	MnO	FeO	Total
320G	1.15	12.33	7.18	46.54	0.95	12.17	0.94	0.55	16.70	98.51
630R	1.33	11.60	7.80	45.16	0.98	11.80	1.09	0.54	17.26	97.56

7.2.7 Chlorite

Chlorite is a common secondary mineral in the studied samples. It replaces biotite and some of the amphibole. Crystallisation of fine-grained titanite accompanies the chloritization (Figure 7-22). Other minerals that occasionally are found along with chlorite in the

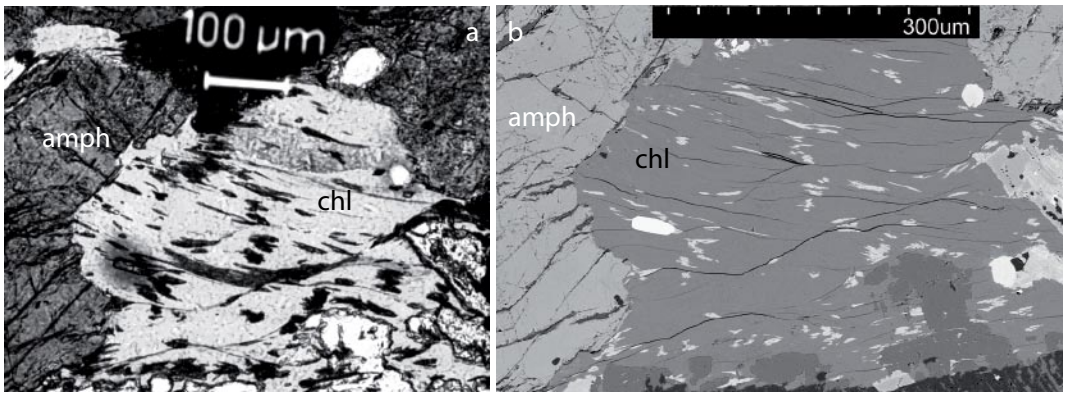

Figure 7-22. *Microphotograph (a, plain polarized light)) and back-scattered SEM-image of chlorite (chl, with minor inclusions of titanite=bright crystals) and amphibole (amph), from sample 630R.*

pseudomorphs after biotite are prehnite, muscovite (especially in sample 137R), K-feldspar, quartz, fluorite and possibly Ti-oxides. Impregnation by ink shows that chlorite is highly porous. SEM-EDS analyses show that the chlorite has a homogenous composition in all of the analysed red-stained and reference samples (Table 7-11). This is in contrast to what is found in chlorite formed in fractures.

SEM-EDS-analyses of fracture filling chlorites, from KSH01, KSH03, KLX02, KAS04 and KA1755A (Figures 7-23 and 7-24) /Drake and Tullborg 2004, 2005, 2006b/ shows that the chlorite in the wall rock has a similar composition as the fracture filling chlorite of generation 1 to 4 (Table 3-1), in accordance to the study of wall rock alteration at Simpevarp /Drake and Tullborg 2006c/. This suggests that the chloritization in the wall rock is coeval with these fracture fillings and is formed at similar hydrothermal conditions.

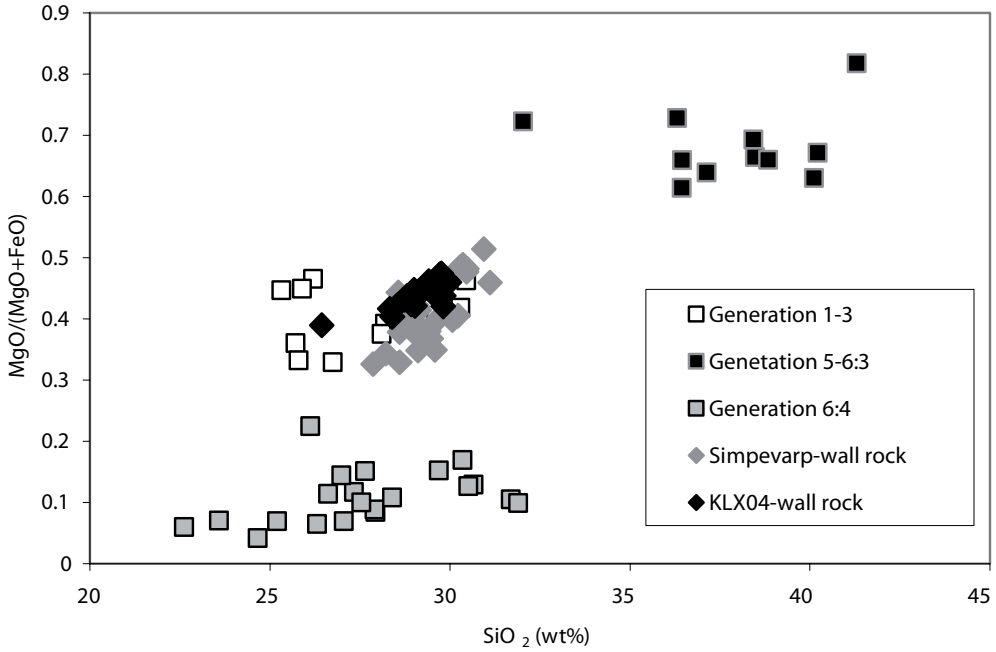

Figure 7-23. *Plot of MgO/(MgO+FeO) vs SiO_2 from SEM-EDS-analyses of the wall-rock chlorites from this study and from KSH01 and KSH03 at Simpevarp /Drake and Tullborg 2006c/, along with chlorites from fracture fillings from drill cores KSH01, KSH03, KLX02, KAS04 and KA1755A /Drake and Tullborg 2004, 2005, 2006b/.*

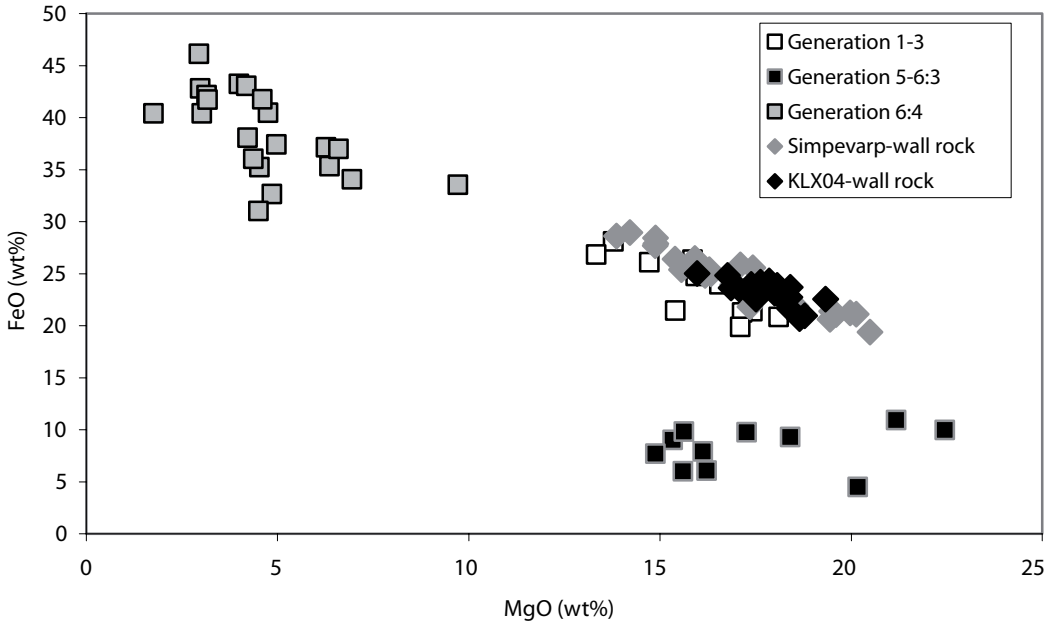

Figure 7-24. *Plot of FeO vs MgO from SEM-EDS-analyses of the wall-rock chlorites from this study and from KSH01 and KSH03(Simpevarp) /Drake and Tullborg 2006c/, along with chlorites from fracture fillings from drill cores KSH01, KSH03, KLX02, KAS04 and KA1755A /Drake and Tullborg 2004, 2005, 2006b/.*

Chlorite is generally formed at temperatures below about 400°C and pressures of a few kilobars /Deer et al. 1992/.

Table 7-11. Selected SEM-EDS analyses of chlorite, *=below detection limit.

	MgO	Al_2O_3	SiO_2	MnO	FeO	Total
108R	16.86	16.87	28.33	0.69	23.62	86.37
170R	18.40	15.83	29.00	0.69	22.74	86.66
320R	18.41	16.35	29.83	0.59	23.68	88.86
630R	17.63	16.40	28.53	0.57	24.19	87.32
Av.(n=19)	17.87	16.85	29.08	0.69	23.18	87.68

Av.(n=19) = average value from 19 analyses of chlorite.

7.2.8 Titanite

Euhedral titanite is found in all of the samples. The titanite contents may vary between the reference samples and related red-stained samples due heterogeneous distribution of titanite in the rock. Samples 320 and 630 have the highest amount of titanite. The crystals often show a primary core and a secondary rim (Figure 7-25). Titanite crystals with rims are found in red-stained samples as well as in reference samples. SEM-EDS analyses (Table 7-12) show that there is no distinct compositional difference, apart from small differences in REE:s, V and Sc, between the primary euhedral crystal (core), and the secondary rim. /Eliasson 1993/ documented changes in the REE-content between rims and core of titanite crystals from Äspö, which along with a presumed low mobility of Ti in the altered

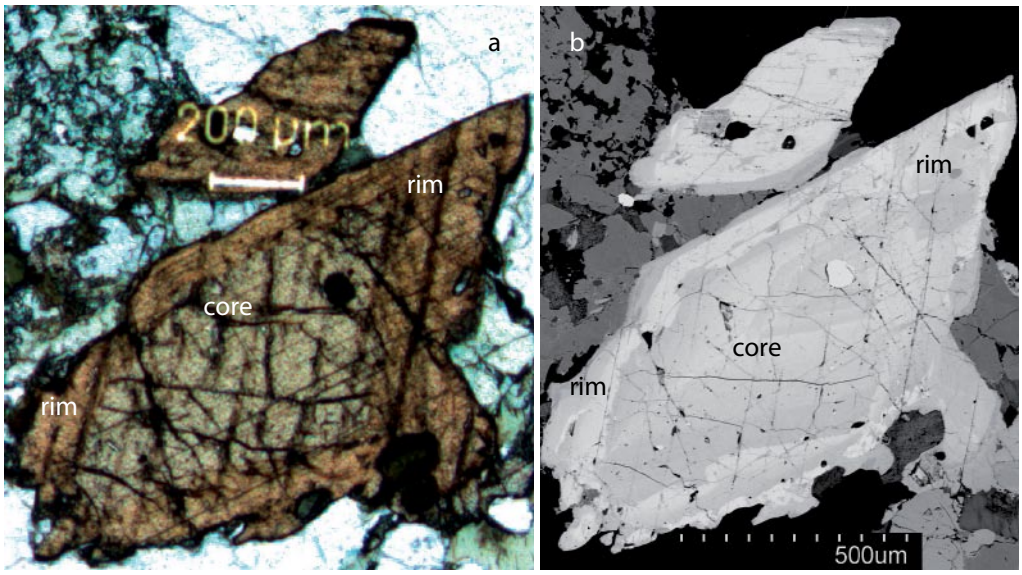

Figure 7-25. *Microphotograph (a) and back-scattered SEM-image (b) of euhedral titanite crystals with secondary rims, from sample 108G, plain polarized light.*

zone made him suggest that the Ti (in the rim) originates from biotite decomposition. Since titanite crystals with rims occur in co-existence with fresh biotite it is suggested that the initial rims are formed prior to biotite decomposition but the fact that the rims seem to be more distinct close to the fractures and that some samples lack rims might infer that the distinct rims are associated to biotite decomposition and hydrothermal alteration.

Titanite also occurs as fine-grained crystals, along with chlorite in biotite-pseudomorphs. These fine-grained crystals have high contents of Al, F, Fe, Mg and subordinately V and low contents of Ti and REE:s (Table 7-12,). The high F content is probably due to the presence of small fluorite crystals in relation to titanite in the pseudomorphs after biotite. Some contamination of associated chlorite might be included in these analyses due to the fine-grained nature of secondary titanite, resulting in higher contents of mainly Mg and Fe. These crystals are presumed to be grothite, a titanite high in Al and Fe^{3+}.

Table 7-12. Average values of SEM-EDS analyses of titanite (core, rim, grothite), based on 3-5 analyses each, *=below detection limit.

Titanite	MgO	Al_2O_3	SiO_2	CaO	TiO_2	FeO	V_2O_5	Ce_2O_3	Nd_2O_3	Sc_2O_3	F	Total
Core	*	1.31	28.96	25.91	36.09	1.84	*	1.48	0.46	*	*	97.36
Rim	*	1.40	29.29	26.49	35.86	1.66	0.10	0.70	0.31	0.28	*	98.46
Grothite	1.37	7.44	29.88	25.20	24.81	3.64	0.42	*	*	*	3.79	97.47

7.2.9 Epidote

The epidote content is commonly slightly higher in the reference samples than in the red-stained samples. This might depend on heterogeneous distribution of epidote in the samples or that epidote is more enriched in the reference samples than in the red-stained samples at the alteration. Late magmatic epidote may also be more altered in the red-stained rock.

Further, fine-grained epidote crystals in altered parts of plagioclase crystals are not included in the modal epidote content of the rock. The high amount of epidote in the reference rock might indicate that at least some of the epidote is late-magmatic, as suggested by /Eliasson 1993/ or that the formation of hydrothermal epidote reaches further into the wall rock to the fracture than the red-staining does. These epidote crystals are different in grain-size and morphology than the fine-grained crystals, found locally in saussuritic plagioclase. A major part of the epidote found in plagioclase pseudomorphs of the red-stained samples are thought to be formed by removal of Ca^{2+} (and Al^{3+}) from the altered plagioclase.

Epidote is a common a fracture filling in fractures with red-staining alteration of the host rock.

Table 7-13. Selected SEM-EDS analyses of epidote.

	Al_2O_3	SiO_2	CaO	MnO	FeO	Total
108G	22.68	38.24	23.48	0.31	13.20	97.91
137R	22.24	37.41	22.70	0.76	13.38	96.49
153R	22.21	37.38	23.16	0.54	13.40	96.69
Av.(n=14)	22.19	37.38	23.06	0.38	13.24	96.25

Av.(n=14) = average value from 14 analyses of epidote.

7.2.10 Prehnite

Prehnite is the most common mineral filling in voids and minor fractures in the red-stained samples. Along with some calcite and K-feldspar, it is also the most common mineral filling in the major fractures that probably worked as conduits for the hydrothermal fluids causing the red-staining. Prehnite is commonly present in both the reference samples and the red-stained samples but the modal content is normally higher in the red-stained samples, where it commonly fills voids and is rarely replacing biotite (along the [001]-cleavage) and very rarely amphibole. Prehnite is found as irregular rounded inclusions within amphibole crystals, commonly in the middle of the crystals. These observations are similar to those made by /Tulloch 1979/, who studied the alteration of biotite in granitoids and suggested the reaction: biotite + anorthite (component in plagioclase) + H_2O = prehnite + chlorite + K-feldspar + titanite + muscovite to take place.

The prehnite is thought to be secondary and related to hydrothermal alteration. Prehnite is rather common in the completely replaced plagioclase pseudomorphs in the red-stained rock, but it is also found to a smaller degree in partially altered plagioclase in the reference sample. The prehnite content in these pseudomorphs is very much lower than the albite-content and the K-feldspar-content in the pseudomorphs. The contents of prehnite and epidote are fairly equal in the altered plagioclase, although the prehnite/epidote-ratio in altered plagioclase has not been studied in detail.

Some of the euhedral prehnite crystals are slightly altered to fine-grained crystals, possibly clay-minerals. Ink impregnation reveals that the prehnite crystals are rather porous.

The SEM-EDS analyses (Table 7-14) are similar to analyses of fracture-filing prehnite from KSH01 and KLX02 /Drake and Tullborg 2004, 2005/.

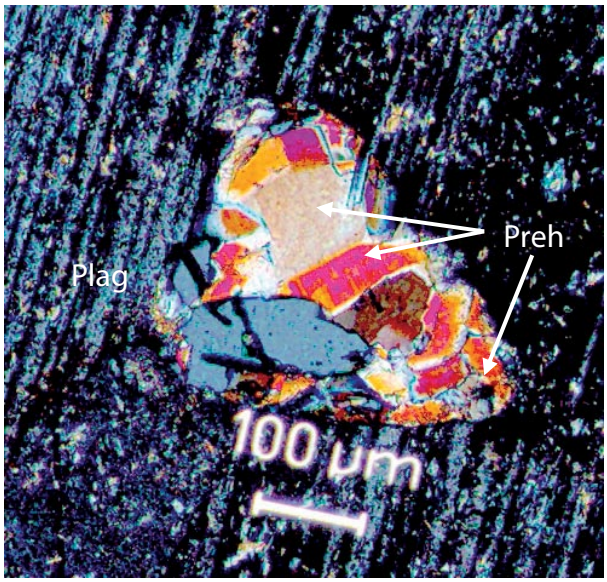

Figure 7-26. *Microphotograph of unaltered, secondary prehnite (Preh) in an altered red-stained plagioclase pseudomorph (Plag). From sample 108R, +nic.*

Table 7-14. Selected SEM-EDS analyses of prehnite.

	Al_2O_3	SiO_2	CaO	FeO	Total
630R-1	21.82	43.43	27.59	2.76	95.60
630R-2	19.86	42.82	26.91	5.45	95.04

/Liou et al. 1983/ carried out experiments of the stability of prehnite and epidote under certain temperatures and pressures, in which the upper prehnite stability is set to 405°C at 2 kbar. /Deer et al. 1992/ report the upper stability of prehnite to occur at 400° at 2–4 kbar, and that prehnite-pumpellyite facies in natural environments at 3 kbar has been estimated to form at ~ 250–380°C. /Bucher and Frey 2002/ show that the upper pressure limit of prehnite is about 5 kbar, but that a more realistic value is around 3 kbar. This temperature and pressure range is thought to be valid for the hydrothermal alteration in this study.

The lack of laumontite, which replaces prehnite at lower temperatures /Tullborg 1997, Drake and Tullborg 2004, 2005/ and has an upper stability of about 260–280°C /Frey et al. 1991/ or 230–260°C /Bucher and Frey 2002/, suggests that the temperature of alteration is higher than so.

7.2.11 Muscovite

Muscovite is sometimes replacing biotite (Figure 7-27). This replacement is most common in the red-stained samples, especially in sample 137R, but it has also been noticed in the reference samples. Muscovite is however more common as fine-grained sericite crystals in altered plagioclase (cf Table 7-6 and Section 7.2.3.), a feature that is most common in the red-stained samples. Muscovite was not counted in the "point-counting" since it was problematic to distinguish these often fine-grained secondary minerals from other minerals such as prehnite, chlorite, epidote etc.

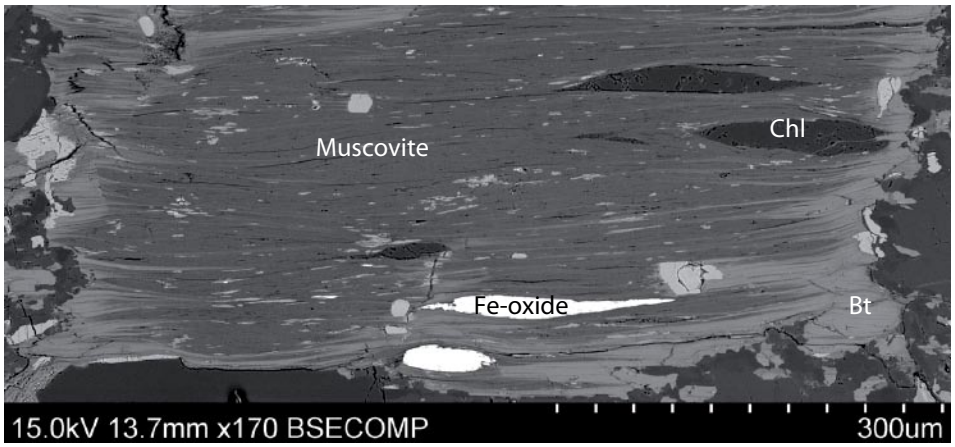

Figure 7-27. *Back-scattered SEM-image of a biotite crystal that is almost entirely replaced by muscovite and chlorite (Chl). The Fe-oxide might be secondary. Sample 137R.*

7.3 Porosity and density

Results and interpretations from measurements of density and porosity are presented in this section.

A description of the porosity and density properties of the altered but not red-stained sample (168A) is found in Section 7.6. Values of porosity and density from sample 168A are however included in the diagrams in this section.

7.3.1 Density

The density is lower in all of the red-stained samples compared to the reference samples (Figure 7-28). This is due to break down of primary minerals and formation of lighter, often OH-bearing, secondary minerals, increased micro-porosity in secondary minerals and an increased amount of micro-fractures in the altered rock. The largest difference is found in sample 320, because of high amounts of micro-fractures and voids in the red-stained sample.

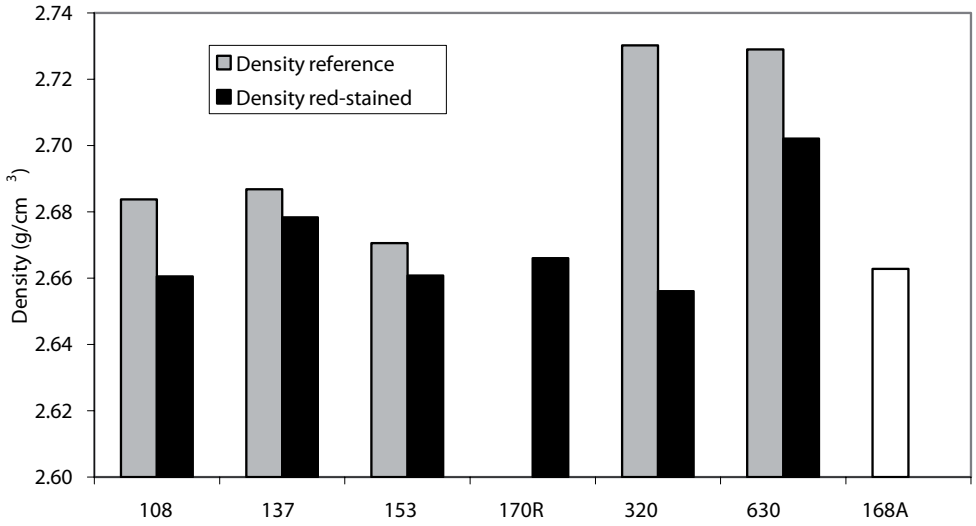

Figure 7-28. *Density values for reference samples, red-stained samples and sample 168A.*

7.3.2 Porosity

The porosity in the samples is made up of micro-fractures, intragranular pores and pore space along grain boundaries. Results from measurements of total porosity are shown in Figure 7-29.

Most of the red-stained samples have higher porosity compared to the reference samples, especially sample 320R which has a high amount of micro-fractures and voids. Since the reference sample 137G also has a high amount of micro-fractures it has a higher porosity than that in the red-stained sample 137R.

The porosity in the examined samples is mainly due to micro-fractures and microscopic pores of different geometry and occurrence. In accordance with studies of altered rock at Äspö HRL /Mazurek et al. 1995/ the following porosities are distinguished; grain-boundary porosity, trans-granular porosity, micro-fractures, sheet silicate porosity and solution porosity.

Grain-boundary porosity is made up of planar micro-pores aligned along the grain boundaries of quartz or feldspars. This type of pore-space occasionally constitutes an interconnected network in the rock matrix. Trans-granular porosity is made up of planar micro-pores cross-cutting minerals, mostly feldspars, very often along crystallographic cleavage planes of the minerals. Micro-fractures cutting through the primary and secondary minerals are numerous in this study and have controlled migration of hydrothermal fluids to a large extent. Sheet silicate porosity is due to planar micro-pores along the basal planes, at the rims or within sheet silicates, such as biotite or chlorite. This porosity is observed parallel to the basal sheets of chlorite pseudomorphs after biotite. Solution porosity is formed during metamorphic events when hydrothermal fluids penetrate through the rock matrix. Unstable minerals are partly dissolved and an irregular-shaped microscopic pore space is created. These pores are identified as cloudy regions in the crystals that are mostly aligned along grain boundary or trans-granular pores. These pore spaces are quite prominent within plagioclase in this study (cf Figure 7-9), and to a smaller degree in microcline. The pores contain variable amounts of inclusions of secondary nature, e.g. hematite.

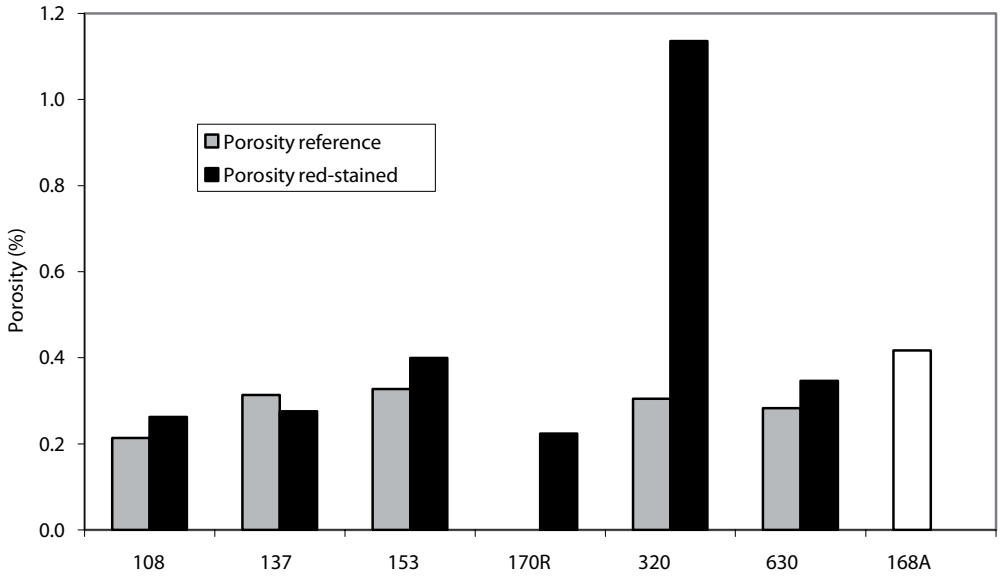

Figure 7-29. *Porosity values for reference samples, red-stained samples and sample 168A.*

The above mentioned features are more prominent in the red-stained samples than in the reference samples. Similar pore-space features have been documented in altered granite from Äspö, using the more advanced ^{14}C- and ^{3}H -PMMA-techniques /Kelokaski et al. 2001/.

The trend of higher porosities in the altered rock is in accordance with earlier studies from the area /Eliasson 1993, Mattsson and Thunehed 2004, Savukoski 2004, Savukoski and Carlsson 2004, Börjesson and Gustavsson 2005, Savukoski 2005ab/ (see also Section 9.2).

7.4 Whole rock chemistry

Twelve samples were analysed for major elements, minor elements, trace elements and LOI at Analytica AB Sweden. The result is shown in Table 7-15. Results of REE-analyses are shown in Table 7-16. The normative changes are obtained from the following equation:

$$\Delta C_i = (C_i^A / C_i^0) - 1$$

where ΔC_i is the normative change in concentration of element *i*, C_i^A is the measured concentration of element *i* in the red-stained rock and C_i^0 is the measured concentration of element *i* in the reference sample. The ΔC_i-value is then multiplied by 100 to give the changes in per cent.

There exist many methods for evaluating the most representative change in chemical composition of an altered rock compared to a reference rock. One method is to assume that some elements, e.g. Zr, Hf, Ti, Ta, Nb, Al, Y, P and REE are immobile during low-grade metamorphic and hydrothermal alteration. The changes of the other analysed elements are then correlated to the change of the immobile elements. Some elements that have been considered as immobile have however been shown to be mobile under certain, often extreme conditions /Kerrich and Fryer 1979, Ludden et al. 1982, Van Baalen 1993, van Gaans et al. 1995/.

The choice of elements to be used as references (immobile) needs to fulfil certain criteria:

1. to be analysed with high accuracy,
2. to be distributed relatively homogenously in the samples,
3. to be immobile in the samples scale, such that redistribution between mineral phases can be accepted.

In the study at Simpevarp, Ti, P and Y were used as “immobile” reference elements /Drake and Tullborg 2006c/. No method of evaluating the chemical differences in the altered rock compared to the reference rock has however been used in the present study since the criteria above were fulfilled. This is because the rock samples were highly heterogeneous, especially concerning the titanite content. The P content is somewhat enriched in the red-stained samples, which might be due to formation of secondary apatite. Changes in Zr and Hf are sometimes highly variable depending on the heterogeneous appearance of zircon. Further, the reproducibility of the changes in Ta, Nb, Zr and Hf were shown to be quite bad in the Simpevarp study and they vary quite much in the present study. Al, which was used as an immobile reference element in the study of red-stained rock at Äspö /Eliasson 1993/, is evidently depleted in all of the red-stained samples in the present study, in agreement with the study at Simpevarp, and disqualify this element as an immobile reference element.

Table 7-15. Chemical whole rock analyses.

	108G	108R	137G	137R	153G	153R	168A	170R	320G	320R	630G	630R
SiO2 (%)	69.4	68.9	67.4	67.6	68.4	68.2	68.6	67.4	60	60.2	59.2	57.7
Al2O3 (%)	14.7	14.6	15.6	15.4	15.2	14.7	14.8	14.9	17.7	17	18.3	17.6
CaO (%)	2.51	1.81	2.82	2.6	2.48	1.65	1.31	2.59	4.32	2.37	4.26	3.89
Fe2O3 (%)	2.94	3.02	3.28	3.15	3.19	3.51	3.47	3.2	5.23	5.28	5.57	5.77
K2O (%)	4.04	4.56	3.89	4	4.02	4.19	4.37	4.14	2.99	3.16	3.28	3.91
MgO (%)	1.09	1.28	1.17	1.22	1.28	1.4	1.3	1.35	2.15	2.47	2.36	2.73
MnO (%)	0.0532	0.0627	0.0576	0.0617	0.0629	0.0621	0.0612	0.0601	0.095	0.104	0.101	0.11
Na2O (%)	3.66	3.82	3.99	3.92	3.81	3.93	4.18	3.91	4.7	5.45	4.76	4.61
P2O5 (%)	0.157	0.16	0.183	0.188	0.184	0.194	0.19	0.173	0.359	0.374	0.359	0.403
TiO2 (%)	0.448	0.416	0.46	0.468	0.486	0.521	0.476	0.437	0.804	0.797	0.806	0.971
LOI (%)	0.7	1.3	0.6	1.1	0.9	1.3	1.2	1.3	0.8	2.1	0.9	1.8
Total (%)	99	98.6	98.9	98.6	99.1	98.4	98.8	98.2	98.3	97.2	99	97.7
Ba (ppm)	1,030	1,050	1,110	1,220	1,100	1,100	1,170	1,100	1,350	1,170	1,700	1,570
Be (ppm)	2.56	3.38	2.49	2.77	2.62	3.06	2.16	2.55	3.42	2.44	2.91	2.67
Co (ppm)	<6	<6	<6	<6	<6	6.24	<6	<6	8.97	11.4	9.75	9.37
Cr (ppm)	70.7	70	67.8	59.4	77.8	69.8	80.7	58.4	57.4	51.6	50.2	52.1
Cs (ppm)	2.11	1.7	2.41	2.98	2.92	2.05	1.92	1.99	2.61	1.75	2.52	1.9
Cu (ppm)	13.1	8.8	<6	8.62	21.9	21.1	31.6	14.2	38.1	29.4	31.4	28.2
F (%)	0.11	0.1	0.12	0.1	0.12	0.085	0.045	0.22	0.22	0.17	0.22	0.23
Ga (ppm)	26.6	24.4	26.6	25.1	27	25.3	26.2	27	34.1	29.3	34.5	32.9
Hf (ppm)	4.83	6.3	6.38	6.19	5.54	5.87	6.06	6.7	7.77	7.13	6.48	7.57
Mo (ppm)	<2	<2	<2	<2	<2	<2	<2	<2	<2	4.06	<2	<2
Nb (ppm)	9.26	8.53	8.41	9.18	10.7	12.5	14.8	8.47	17.4	15.5	10.2	14.6
Ni (ppm)	16.6	17.2	17	14.2	19.5	19.6	26	15.3	22.9	22.9	24.7	24.8
Rb (ppm)	110	132	112	104	105	122	130	116	89.5	101	85.1	149
S (ppm)	39.8	58.7	16.7	17.6	14.8	96.3	13	17.9	302	46.4	198	198

	108G	108R	137G	137R	153G	153R	168A	170R	320G	320R	630G	630R
Sc (ppm)	4.68	4.85	5.55	5.46	5.99	5.01	10	4.78	8.21	9.24	9.18	10.5
Sn (ppm)	1.89	2.1	2.06	2.27	2.1	1.86	2.48	2.28	2.78	3.21	2.19	3.08
Sr (ppm)	697	599	782	836	710	652	441	593	1,350	757	1,390	1,180
Ta (ppm)	1.04	0.99	1.01	0.856	0.852	1.13	1.44	0.797	1.64	1.56	0.852	1.3
Th (ppm)	11.8	13.5	16	15.9	16.5	20.1	13.4	13.1	23.1	18	15.6	16.8
U (ppm)	4.33	5.87	4.79	5.45	6.3	5.71	3.46	4.57	7.93	8.95	3.08	3.72
V (ppm)	42	40.7	44.9	43.6	45.7	45.4	42.3	46.1	84.9	88.7	92.6	96.8
W (ppm)	2.04	2.1	1.72	2.52	2.11	4.65	3.39	2.03	3.07	3.33	1.83	2.82
Y (ppm)	19	17.6	16.5	16.7	17.6	17.5	20.4	15.2	24.3	27.7	20.8	25.9
Zn (ppm)	53.9	52.7	47.4	55.2	42.6	87.6	62	48.8	101	94.5	99.5	104
Zr (ppm)	163	215	222	209	182	181	207	227	301	266	253	277

Table 7-16. Chemical whole rock analyses – Rare earth elements (ppm).

	108G	108R	137G	137R	153G	153R	168A	170R	320G	320R	630G	630R
La	38.1	39.7	41.9	40.4	42.7	41.6	38.9	35.2	61.1	61.4	51.8	58.6
Ce	84.5	83.4	93.1	87.1	95.6	93.4	94.9	80.2	142	146	121	142
Pr	9.66	9.1	10.3	9.7	11.5	10.3	10.5	9.01	16.5	17.5	14	16.7
Nd	33.6	30	32.3	34.6	38.1	35.1	35.7	29.7	56.1	62.7	51.2	61.6
Sm	5.99	4.39	4.55	4.89	5.94	5.55	5.87	4.48	7.99	8.76	7.45	10
Eu	0.953	0.816	1.08	1.03	0.984	0.966	0.98	0.741	1.7	1.76	1.67	1.81
Gd	3.82	3.57	3.46	4.01	4.18	3.14	3.58	2.21	4.06	4.48	4.04	5.1
Tb	0.766	0.664	0.672	0.666	0.757	0.817	0.744	0.636	1.1	1.17	1.06	1.25
Dy	3.31	3.51	3.07	2.68	3.65	3.35	4.02	2.97	4.06	4.87	3.87	4.83
Ho	0.648	0.638	0.66	0.588	0.677	0.688	0.774	0.603	0.827	0.893	0.748	0.976
Er	1.72	1.73	1.56	1.7	2.09	1.81	2.24	1.83	2.43	2.86	2.49	2.74
Tm	0.322	0.366	0.356	0.26	0.346	0.357	0.362	0.343	0.477	0.475	0.313	0.382
Yb	1.81	2.03	1.96	1.8	1.76	1.81	1.79	1.68	2.86	2.73	2.2	2.7
Lu	0.294	0.3	0.241	0.273	0.353	0.302	0.295	0.248	0.468	0.448	0.305	0.403

7.4.1 Classification of samples

Classification of the reference samples from various classification diagrams is shown in Table 7-17. This is based on chemical (and modal) analyses from this study along with classification of the samples from "Boremap". Classification based on modal analyses is left out since the rock is highly heterogeneous and the thin sections show variable amounts of K-feldspar phenocrysts. The samples 108G, 137G and 153G are classified as granite/granodiorite/quartz monzonite (adamellite), while the samples 320G and 630G are classified as quartz monzodiorite/monzonite.

A comparison between the principal modal alkali feldspar, plagioclase and quartz contents in a QAP-plot (Figure 7-1) and the normative chemical QAP-classification (Figure 7-31), shows that the alteration of feldspar phases, from plagioclase with an An-content 24–30% to albite and K-feldspar, will not influence the classification in Figure 7-31, but will give a serious influence on the classification in Figure 7-1. This is because CaO is partly fixed in secondary epidote and prehnite in the altered rock. The assumption (used in the modal QAP-plot) that all plagioclase is altered to K-feldspar and albite is exaggerated.

Table 7-17.

Sample	Depth	Rock type (mapping)	Rock type (TAS)*	Rock type (QP)**
108G	108.65–109.30	Ävrö Granite^	Granite"	Adamellite#"
137G	137.15–137.39	Ävrö Granite^	Quartz monzonite"	Granodiorite
153G	153.73–153.96	Ävrö Granite^	Granodiorite^^	Adamellite#"
320G	320.63–320.96	Ävrö Granite^	Monzonite	Quartz monzodiorite
630G	630.33–630.76	Ävrö Granite^	Monzonite	Quartz monzodiorite

* = /Le Maitre 1989/ – normative.
** = /Debon and Le Fort 1982/.
^ = Granite to quartz monzodiorite.
# = Quartz monzonite.
" = Borders to granodiorite.
^^ = Borders to quartz monzonite.

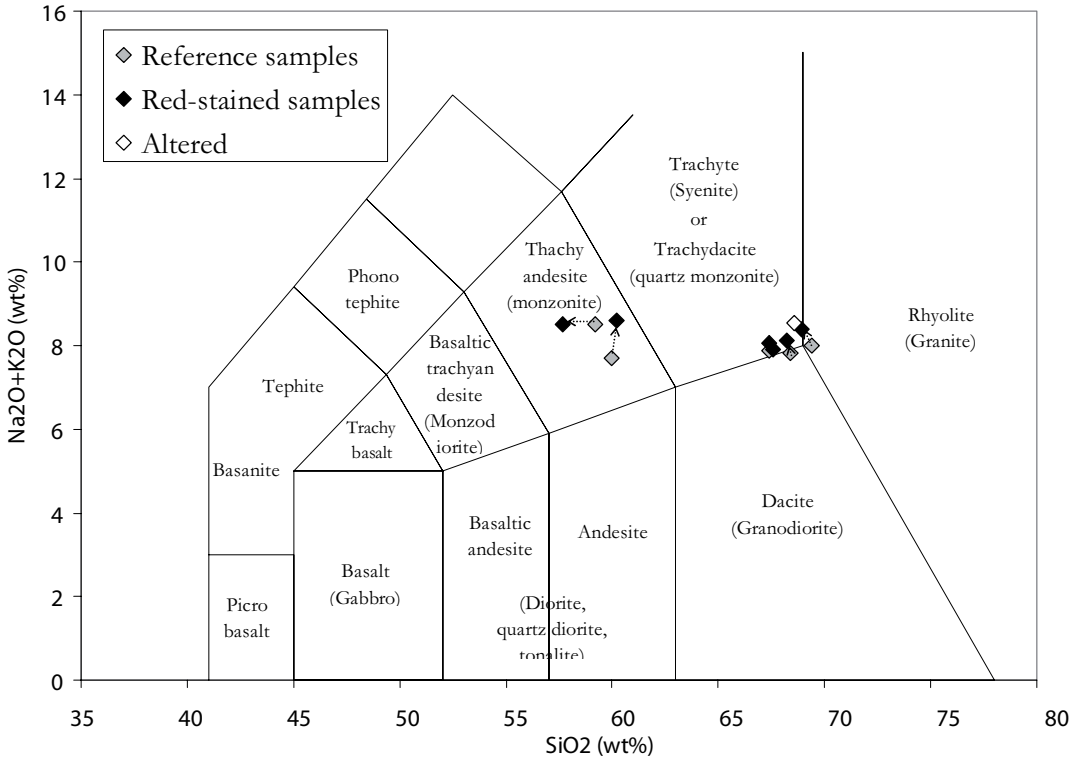

Figure 7-30. *TAS-diagram from /Le Maitre 1989/. Arrows show related samples. Reference samples (grey), red-stained samples (black) and sample 168A (white). Note that most of the red-stained samples have slightly higher Na_2O+K_2O-contents than the reference samples.*

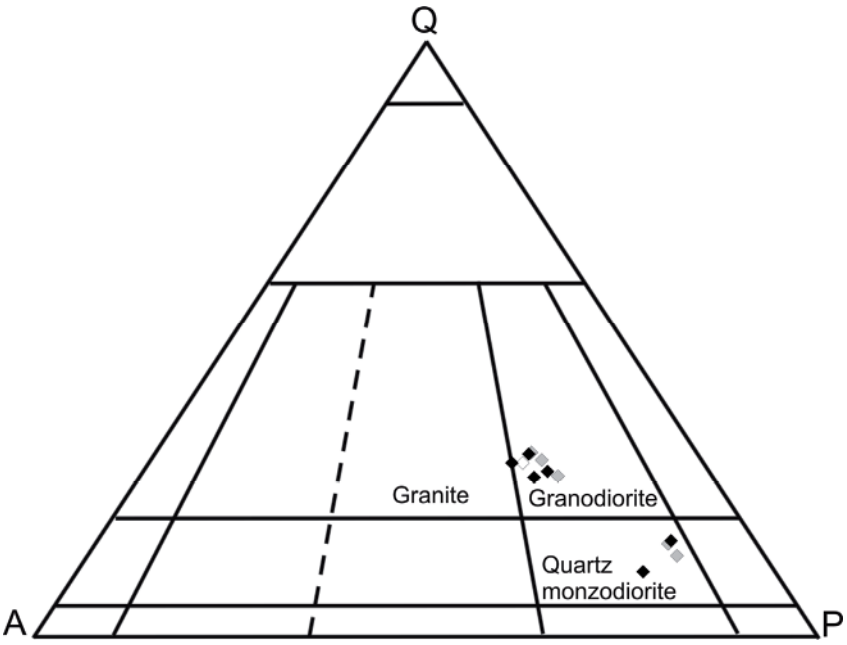

Figure 7-31. *Normative QAP-diagram of whole rock analyses /Le Maitre 1989/, constructed from whole rock chemical analyses using Newpet software. Q = Quartz, P = Plagioclase, A = Alkali. Reference samples are shown in grey and red-stained samples in black (sample 168A in white). All of the red-stained samples have higher alkali-contents than the corresponding reference samples have.*

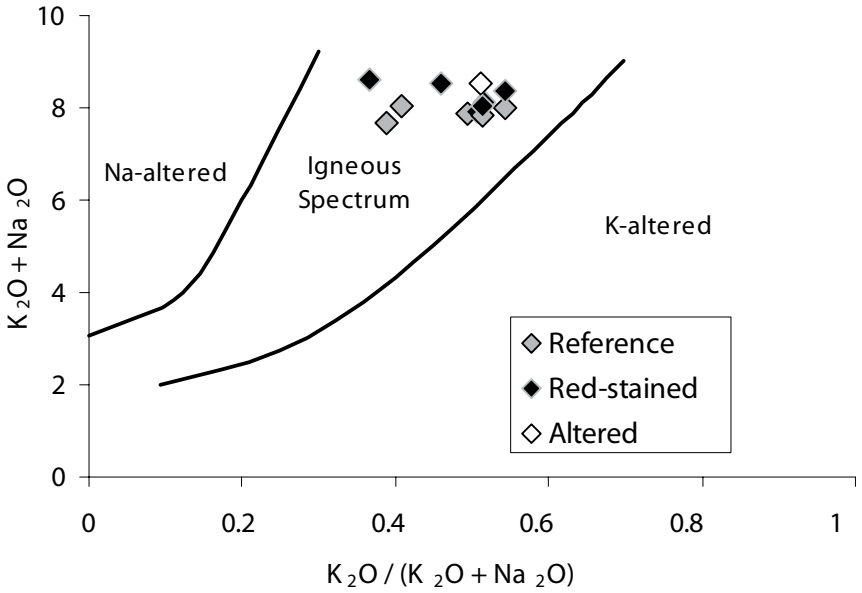

Figure 7-32. *Igneous spectrum diagram /Hughes 1973/ with plots of reference samples (grey), red-stained samples(black) and altered sample 168A (white).*

The reference samples and the red-stained samples plot in the "igneous spectrum" field of /Hughes 1973/ (Figure 7-32), indicating no major Na or K mobilisation. However, the "Na_2O+K_2O"-contents are higher in all of the red-stained samples compared to the corresponding reference sample and the increase in K is generally higher than the increase in Na.

7.4.2 Changes in element concentrations

In this section changes of each element in the red-stained samples compared to the reference samples are discussed, as well as the general abundance of most elements. Elements that are related, e.g. K, Rb, Ba and Cs may replace one another and are described collectively. Elements Co, Hf, Mo, Nb, Ni, Sn, Ta, W, Zn and Zr are not discussed in detail since the analyses of these show too low values and/or inconclusive results. However, the increase in W in the red-stained rock may be related to hydrothermal fluids related to the intrusion/ post-magmatic circulation of the Götemar granite, since W-rich minerals have been noticed in fracture fillings suggested to be related to the Götemar granite /Drake and Tullborg 2006a/.

Since it was not possible to collect a nearby reference samples to the red-stained sample 170R, sample 153G was chosen as a comparison. This was done since the chemistry (based on TAS- and QAP-classification) and density of these samples are similar and that these samples are from similar depths. Description of the elemental changes of the altered but not red-stained sample (168A) compared to reference sample 153G is found in Section 7.6. Normative changes in concentrations of different elements between sample 168A and 153G are however included in diagrams of this section.

SiO_2

SiO_2 can be considered as more or less constant during alteration, although re-distribution in situ is proposed. The normative absolute changes are about –2.5 to +0.3% and no conclusive trend of enrichment or depletion is found. However, some silicon is leached from the rock and is incorporated in prehnite, chlorite, quartz and epidote in fractures.

Al_2O_3, Be and Ga

Al_2O_3 is depleted in all of the red-stained samples compared to the reference samples (Figure 7-33). The depletion is generally 0.7–4%. The depletion of Al_2O_3 is thought to reflect break-down of the anorthite-content in plagioclase, which is replaced by albite and K-feldspar mainly. The crystallization of secondary prehnite and epidote is insufficient to fix all of the excess Al. Excess Al may also be included in formation of prehnite, chlorite and epidote in fractures. /Eliasson 1993, Stosnach and Mengel 1998/ were not able to detect changes in Al_2O_3 in their studies.

In the study of red-stained wall rock from Simpevarp /Drake and Tullborg 2006c/ it was shown that depletion of Be and Ga apparently is related to the depletion of Al_2O_3. Results from the present study show Be increase in three of the red-stained samples while the Ga content is depleted in all of the red-stained samples. Depletion of Ga may be related to albitization of plagioclase as proposed by e.g. /Bailey 1971/. Be may possibly be correlated with Al since they both are ions of similar size /Bailey 1971/.

CaO and Sr

CaO is mainly depleted in the red-stained rock compared to the reference rock, except for sample 170R and sample 153G (Figure 7-34). The depletion in CaO is about 8 to 47%. The general depletion in CaO is evidently caused by alteration of plagioclase and removal of the anorthite-content, which is replaced by albite and K-feldspar mainly. The excess CaO is involved in growth of secondary prehnite and smaller amounts of epidote in altered plagioclase pseudomorphs. Occasionally, prehnite is also found in pseudomorphs after biotite in association with chlorite. Secondary prehnite and additional calcite is also found in voids and in micro-fractures in the red-stained rock. This growth of Ca-rich secondary minerals is commonly not enough to compensate for the break-down of primary Ca-rich

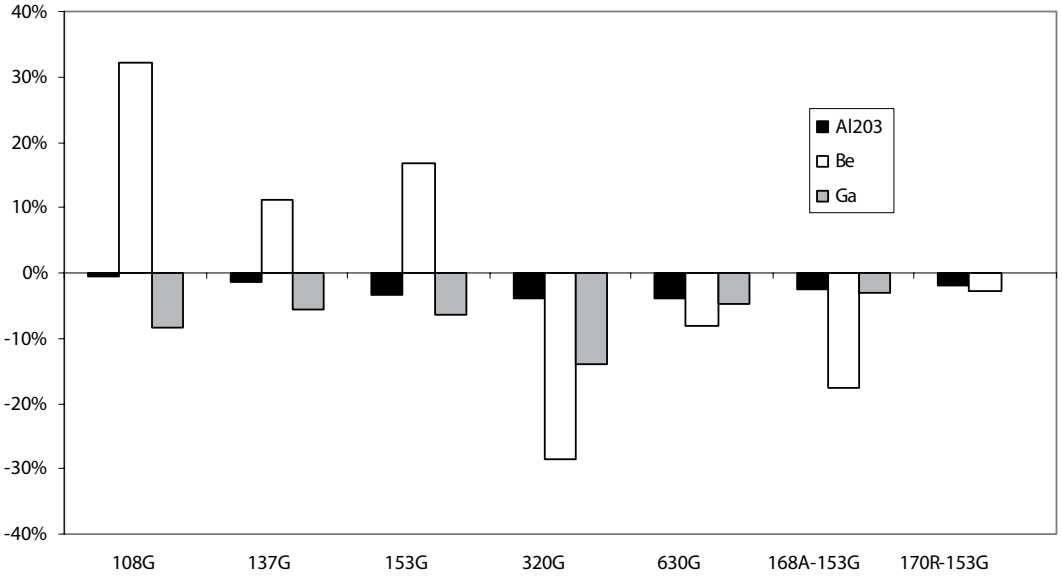

Figure 7-33. *Plot of normative changes for Al_2O_3, Be and Ga between red-stained samples and reference samples.*

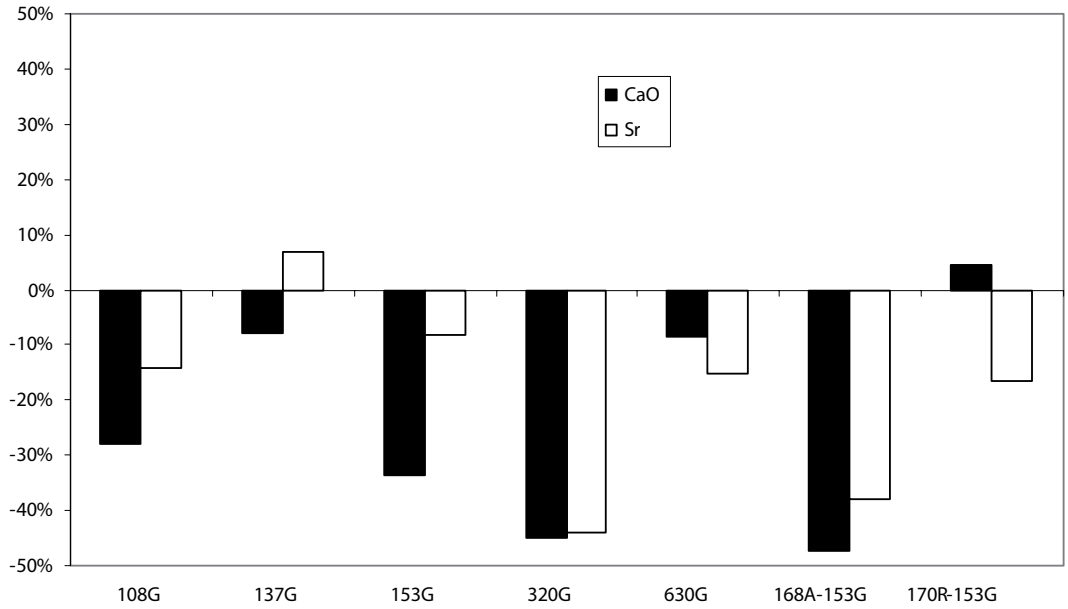

Figure 7-34. *Plot of normative changes for CaO and Sr between red-stained samples and reference samples.*

minerals. A large part of the CaO content is removed from the rock and is involved in formation of fracture minerals like prehnite, epidote and calcite. Higher value of CaO in fracture coatings compared to the wall rock is a common feature in the area /Landström and Tullborg 1995, Tullborg 1995, Landström et al. 2001/. The generally higher epidote contents in the reference rock may also influence the apparent depletion of CaO in the red-stained rock compared to the reference rock.

Changes in Sr are closely related to the changes in CaO (Figure 7-34), except in sample 137R, where some of the primary plagioclase is preserved in the red-stained rock and where the red-stained rock is enriched in epidote. This sample is also the least red-stained of the red-stained samples in this study. Sr is mainly hosted in Ca-bearing minerals since the ions Sr^{2+} and Ca^{2+} have similar properties and exchange easily. However, the Sr/Ca-ratios in Ca-minerals are quite different for different minerals, e.g. calcite has a much lower Sr/Ca ratio than for example plagioclase. Epidote, in contrast, have shown preferential uptake of Sr (cf earlier studies from Äspö /Landström and Tullborg 1991, Stosnach and Mengel 1998/). The depletion in Sr (except in sample 137R) is related to the alteration of primary plagioclase. Some Sr may be incorporated in secondary epidote, prehnite and possibly also calcite in plagioclase pseudomorphs, in voids, in micro-fractures in the altered rock and as fracture minerals in major fractures. However, the uptake of Sr in secondary minerals within the studied rock volume is insufficient to compensate for all the excess Sr. However, Sr content in prehnite has not been studied in detail.

Fe_2O_3, MgO, MnO, TiO_2, Cr, Sc, V and Y

The iron content measured by whole rock analyses is expressed as Fe_2O_3. The content of Fe and related elements are higher in samples 320 and 630 than in the other samples since these two samples have higher amounts of biotite, amphibole, chlorite and opaques. The variation in iron-contents is very small, although a trend of small enrichments of iron is found in the red-stained samples compared to the reference samples (except sample 137R).

This may be due to the chloritization of biotite, since chlorite has a higher amount of iron than biotite. In the sample 137R biotite is replaced by muscovite to a higher degree than in the other samples. Since the Fe-content of muscovite is lower than that of biotite, the red-stained sample 137R is depleted in iron.

The chloritization of biotite may also be responsible for the enrichment of MgO and MnO in the most of the red-stained samples, since chlorite contains more of these elements than biotite does (Figure 7-36, Tables 7-9 and 7-11). Mn has been reported to be more redistributed during weathering than other redox sensitive elements like Fe and V, possibly

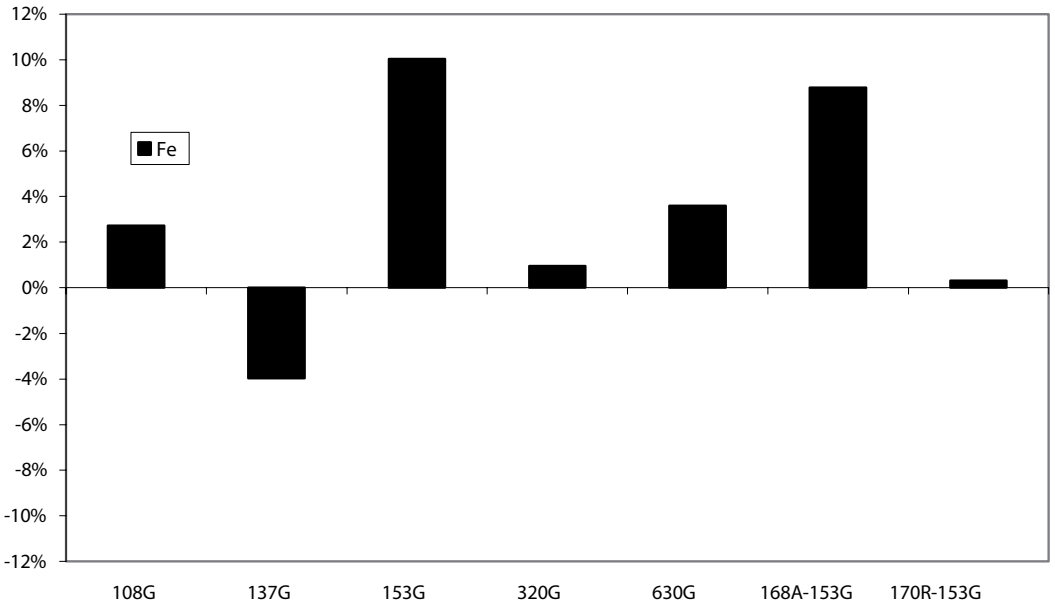

Figure 7-35. *Plot of normative changes for Fe_2O_3 between red-stained samples and reference samples.*

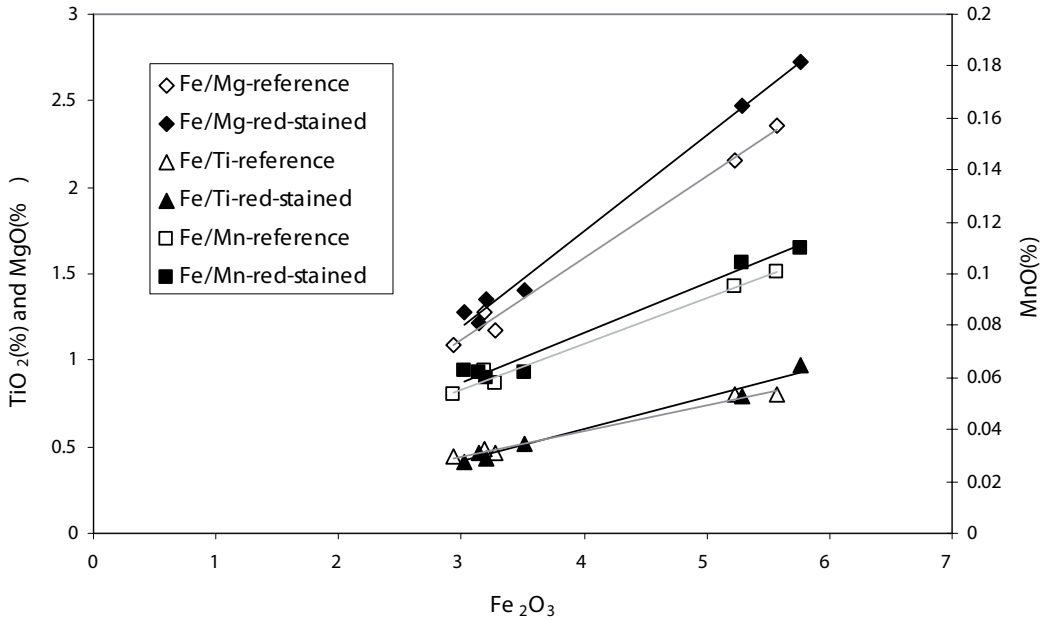

Figure 7-36. *Plot of Fe_2O_3 content vs TiO_2 (left y-axis), MgO (left y-axis) and MnO (right y-axis). Black and grey lines are trend-lines for the red-stained samples and reference samples, respectively.*

as Mn^{2+} which may become absorbed on Fe(III)-oxide phases or precipitated as an insoluble Mn(III,IV)-oxide during oxidation /van der Weijden and van der Weijden 1995/. This is in agreement with the Mn-enrichment in the red-stained samples. The Fe-related elements TiO_2, Sc, V and Y show variable changes between the red-stained samples and the reference samples. The changes in Ti-content may be related to the heterogeneous distribution of titanite in the rock. TiO_2 is also contained in biotite (which is more frequent than titanite) and subordinately in hornblende. Secondary titanite (grothite) is formed during chloritization of biotite which indicates that Ti is redistributed during alteration. Earlier studies in the area have shown significantly lower Ti values in fracture coatings than in the host rock which indicate very low mobility of Ti /Tullborg 2002/. Cr is depleted in all but one of the red-stained samples and is probably the result of hematitization of magnetite. V is commonly found as a trace element in Fe-bearing minerals and V and Fe are often correlated during weathering/alteration e.g. /van der Weijden and van der Weijden 1995/. Y is mainly fixed in titanite /Stosnach and Mengel 1998/ and is thus in close relation to the TiO_2–content. Some Y may however be incorporated in epidote.

K_2O, Ba, Cs and Rb

K and Rb are commonly highly enriched in the red-stained samples (except in sample 137R), while Cs is depleted (except in sample 137R). The differences in Ba are inconclusive. The normative enrichment in K_2O is about 3–20% and in Rb about 10–75%, while the depletion in Cs is 20–35%, although exceptions are found (Figure 7-37). The ions Ba^{2+}, Rb^+ and Cs^+ have similar properties as K^+ (size and/or charge) and may replace K^+ in the structure of K-bearing minerals such as K-feldspar (preferably Ba) , biotite and sericite (preferably Rb and even more so Cs) and subordinately hornblende and are thus enriched in these minerals. The enrichment of K_2O in the red-stained rock is related to extensive growth of secondary K-feldspar (adularia) and to some extent sericite in altered plagioclase crystals. Biotite is generally fresh in the reference samples but partial replacement of biotite by chlorite in some of these samples may have lead to K_2O depletion. This is since

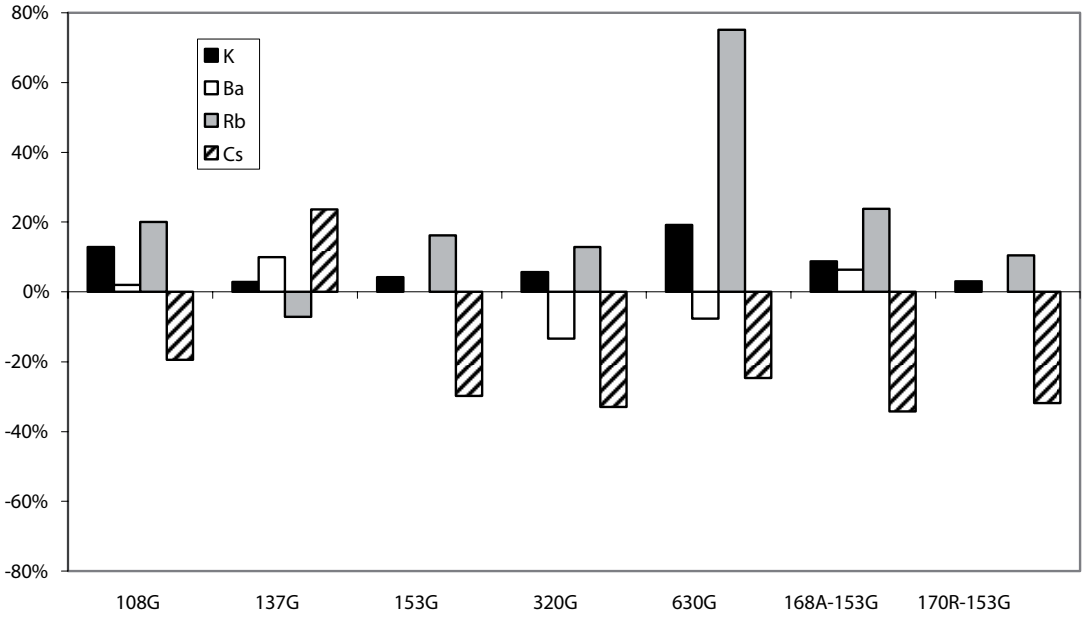

Figure 7-37. *Plot of normative changes for K_2O, Ba, Rb and Cs between red-stained samples and reference samples.*

the K-content of biotite is intensively depleted in the initial stage of the chloritization /Wilamowski, 2002/. In samples 137R the biotite is replaced by muscovite to a higher degree than in the other samples. This sample is also less red-stained and has the lowest increase in secondary K-feldspar in altered plagioclase. This might be the case why this sample is depleted in K_2O compared to the reference rock. In the samples with low increase in K_2O or K_2O-depletion, the Na_2O-content is increased. This reflects the alteration of plagioclase to albite and K-feldspar in the pseudomorphs after plagioclase (Figure 7-39).

The Ba-content is dependent on the K-feldspar content in the rock. The BaO content is up to 1.58% in the microperthitic K-feldspar phenocrysts but groundmass K-feldspars and secondary K-feldspar in altered plagioclase have somewhat lower content of BaO. The BaO content in the rock depends also on the BaO content in different K-feldspar crystals

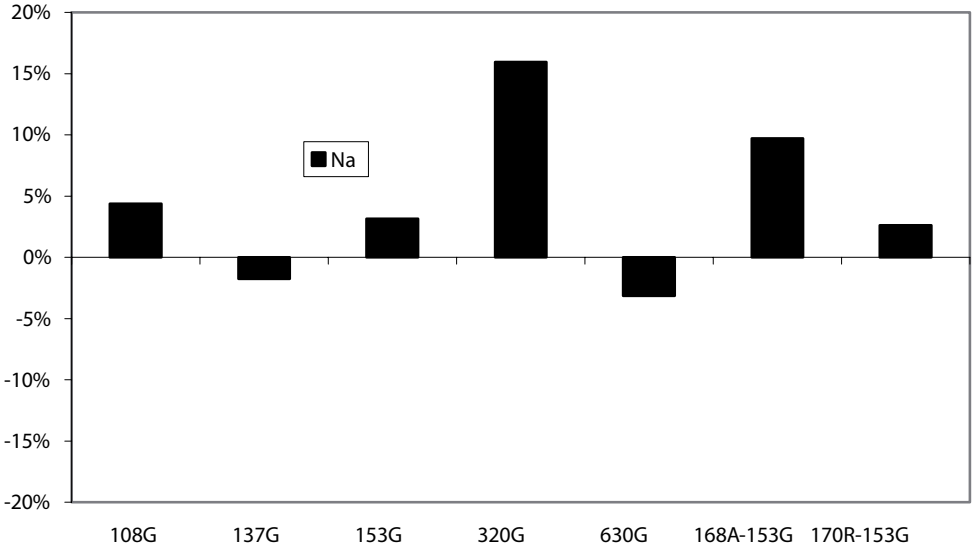

Figure 7-38. *Plot of normative changes for Na_2O between red-stained samples and reference samples.*

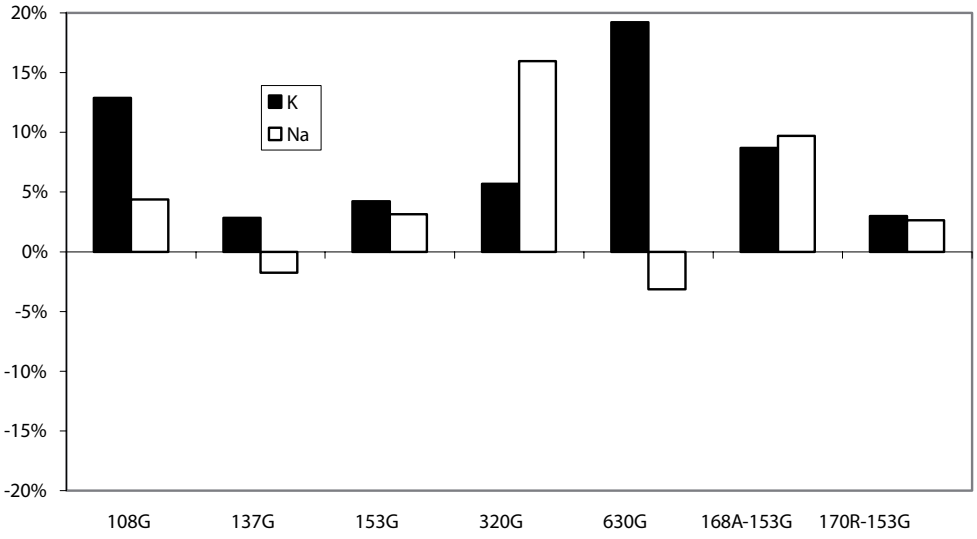

Figure 7-39. *Plot of normative changes for K_2O and Na_2O between red-stained samples and reference samples.*

as shown by SEM-EDS analyses (cf analyses in appendix). Sericite and biotite contain some BaO as well, but the content is usually lower than that in the K-feldspars. The Ba-content is slightly enriched in most of the samples, because of secondary K-feldspar in the red-stained samples.

The depletion of Cs is related to the chloritization of biotite. Since Cs is more compatible in biotite (and muscovite) than in K-feldspar /De Albuquerque 1975/ break down of biotite will result in excess Cs that is not entirely incorporated in secondary K-feldspar. The enrichment of Cs in sample 137R may be due to the formation of muscovite in biotite pseudomorph, since Cs is more compatible in muscovite than in K-feldspar, and that the amount of secondary K-feldspar in this sample is rather small. Rb is mainly hosted in biotite /Stosnach and Mengel 1998/ but Rb is not as compatible in biotite as Cs is. Rb is only slightly enriched in biotite compared to K-feldspar /De Albuquerque 1975/. The large enrichment in the Rb-content in the red-stained samples in the present study shows however that Rb must be highly compatible with secondary K-feldspar, with a few exceptions. /Gebel et al. 1999/ reports significantly lower concentrations of Cs and Rb in secondary chlorite than in primary biotite, which is in accordance with the results from the present study. Enrichment of Rb and depletion of Cs may also support the observations from e.g. microscopy and SEM-EDS where secondary K-feldspar dominates over secondary sericite. This may also explains the depletion of Rb in sample 137R, where secondary muscovite is common and secondary K-feldspar is less common than in the other red-stained samples.

Na_2O

Na_2O is enriched in the red-stained rock (except in samples 137 and 630) as a result of albitization of plagioclase. The enrichment is normally about 3–16% (Figure 7-38).

In the red-stained samples where the Na_2O-content is less than in the reference samples, the enrichment in K_2O-content is generally larger than the depletion in Na_2O (Figure 7-39). This is a strong indication on how extensive replacement of primary plagioclase was by secondary albite and K-feldspar during the hydrothermal alteration. The increase in K_2O+Na_2O is smallest in sample 137R where parts of the primary plagioclase are preserved, the enrichment of secondary albite and K-feldspar is smaller, and the intensity of the red-staining is lower than in the other red-stained samples.

P_2O_5

P_2O_5 is considered to be fixed in apatite during alteration, which is in agreement with studies of e.g. /Stosnach and Mengel 1998, Tullborg 2002/. The P_2O_5-content is however increased in most of the red-stained samples, possibly due to formation of secondary apatite, which has been identified in fracture fillings in drill core KSH01 /Drake and Tullborg 2004/. However, no secondary apatite has been identified in the present study. Changes in P_2O_5 generally correlate quite well to changes in TiO_2.

The total chemical content and the Loss on Ignition (LOI)

The sum of the analysed elements is lower and LOI is higher in the whole rock analyses of the red-stained rock compared to the reference rock. The increase in LOI (Figure 7-40) and decrease in total values in the red-stained samples reflect a higher amount of “crystal-bound” water and indicate presence of secondary mineral phases (e.g. chlorite, sericite and prehnite).

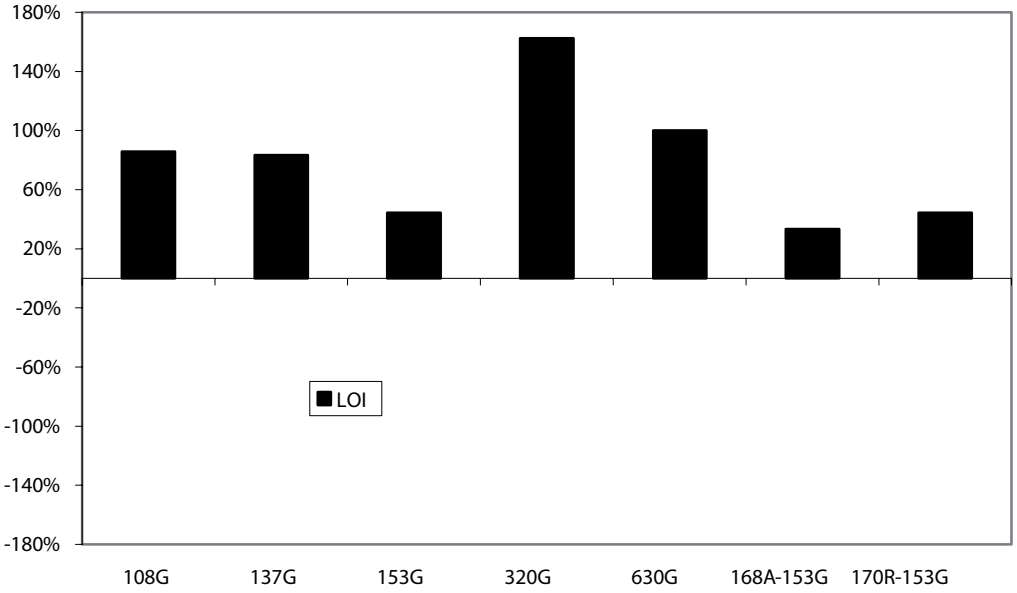

Figure 7-40. *Plot of normative changes for LOI between red-stained samples and reference samples.*

Cu and S

Sulphur and Copper is dominantly found in accessory sulphides, mainly pyrite (S) and some chalcopyrite (S and Cu). The depletion of Cu and S in some of the red-stained samples reflects corrosion and break-down of the sulphide due to oxidation. The enrichment of S mainly, and to a lesser degree Cu, is due to the presence of secondary pyrite and subordinate chalcopyrite in the red-stained samples. These sulphides were formed after the major hydrothermal alteration of the rock. The normative change in S is commonly larger than that of Cu (Figure 7-41).

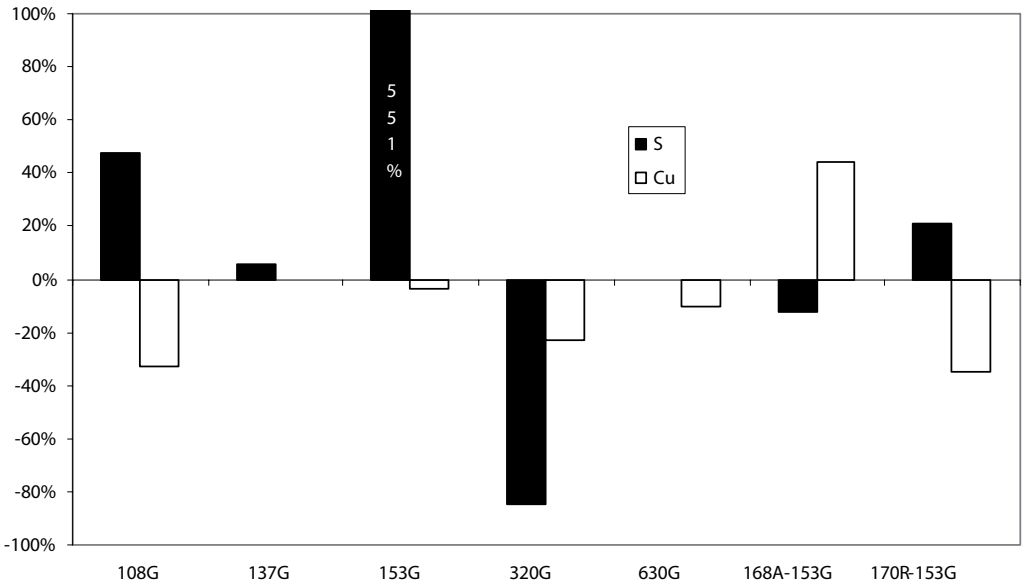

Figure 7-41. *Plot of normative changes for S and Cu between red-stained samples and reference samples. In sample 137G the Cu-content is below detection limit. Note that the S-enrichment in sample 153 is 551% and is out of space in this diagram.*

Th and U

Four of six red-stained samples are enriched in U (Figure 7-42). Th is enriched in some samples and depleted in some samples. In another study, /Stosnach and Mengel 1998/ reported that Th and U are predominantly fixed in titanite. U may however also be present in sub-microscopic U-rich phases along grain boundaries and in U-rich silicates in micro-fractures, as seen in studies of the fracture fillings in the area /Drake and Tullborg 2006ab/. The U in these phases may be mobilised as U(VI) during oxidizing conditions, by diffusion in pores and micro-fractures, as proposed by /Landström et al. 2001/ such that the U-concentration is enhanced in the red-stained rock where U(VI) is absorbed onto Fe(III)-minerals. This scenario may explain the higher U/Th-ratio in the red-stained rock, since Th is less redox sensitive than U and thus less mobilised during oxidizing conditions. It must however be noticed that the U and Th concentrations are very small and the reproducibility too poor to allow unequivocal conclusions to be drawn.

F

The F-content is generally lower in the red-stained rock than in the reference rock (Figure 7-43). The major F-bearing minerals in the samples, apart from fluorite that may be present in very small amounts in fractures and voids, are biotite and hornblende. Since these minerals are altered it is probably that F is mobilized. Studies of fracture mineralogy infer that fracture fillings that are coeval with the red-staining event include fluorite /Drake and Tullborg 2004, 2005/. Observations of fine-grained fluorite crystals present along with chlorite and titanite in pseudomorphs after biotite in some red-stained samples confirm redistribution and possibly mobilisation of fluorite during biotite alteration.

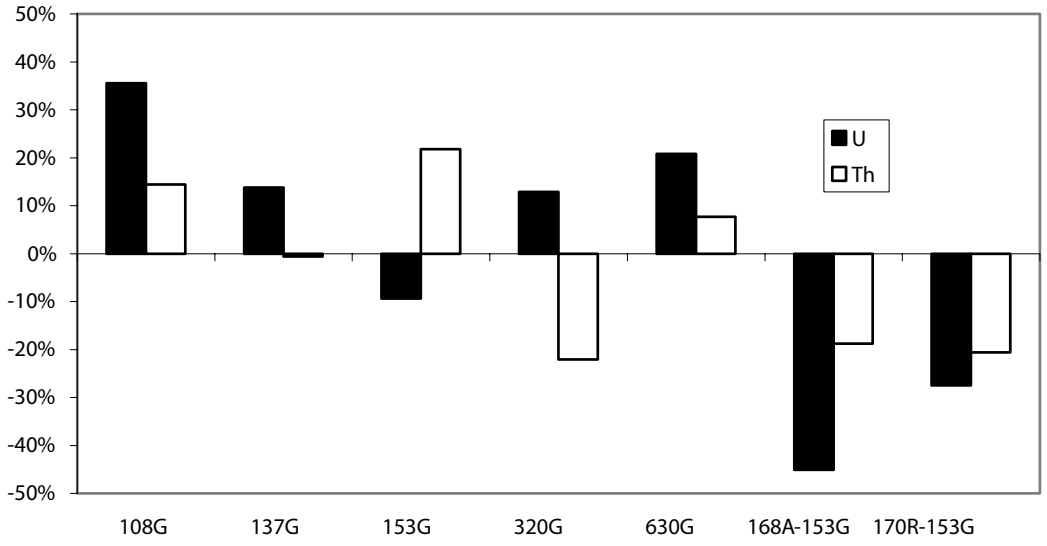

Figure 7-42. *Plot of normative changes for U and Th between red-stained samples and reference sample.*

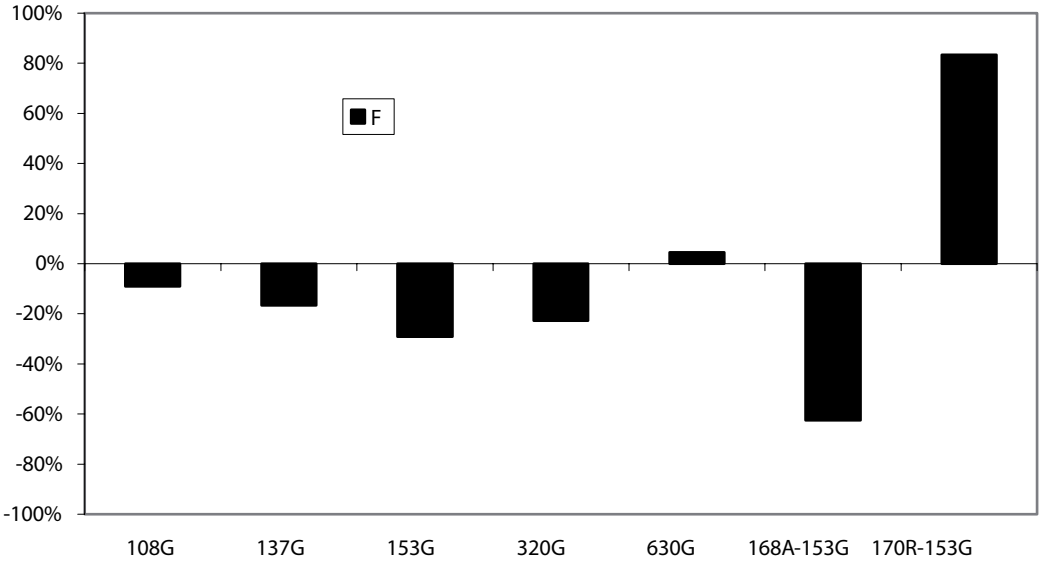

Figure 7-43. *Plot of normative changes of F between red-stained samples and reference samples.*

Rare Earth Elements (REE)

The difference in REE concentrations between reference samples and red-stained samples are generally very small (Figures 7-44, 7-45 and 7-46), which indicates that these elements are either fixed in minerals that are resistant to alteration or that the elements are redistributed within a very limited rock volume. The REE might be concentrated in the apatite, as suggested by /Landström et al. 2001/ and in titanite as suggested by /Gebel et al. 1999/.

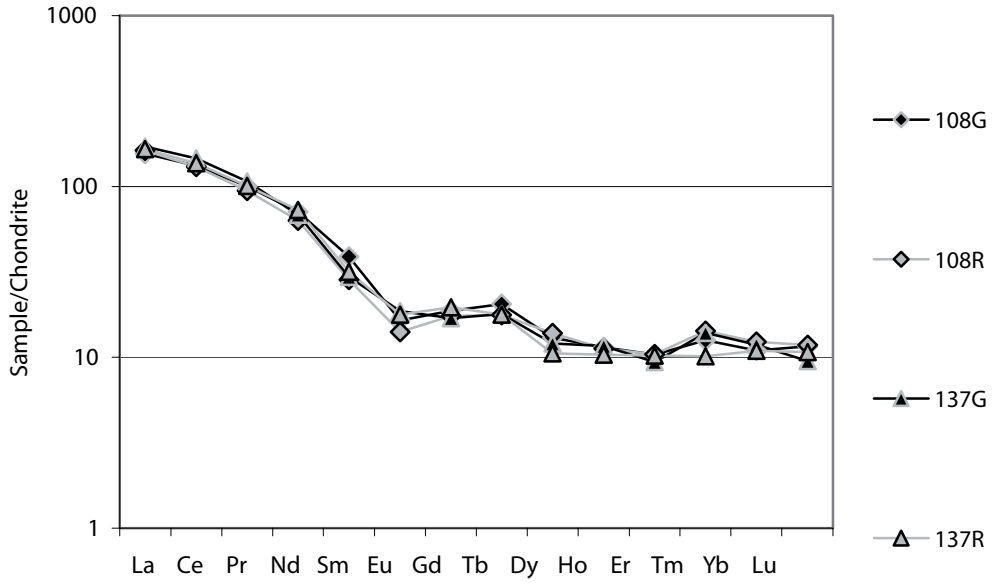

Figure 7-44. *Chondrite normalised REE-plot of samples 108 and 137, using chondrite values from /Evansen et al. 1978/.*

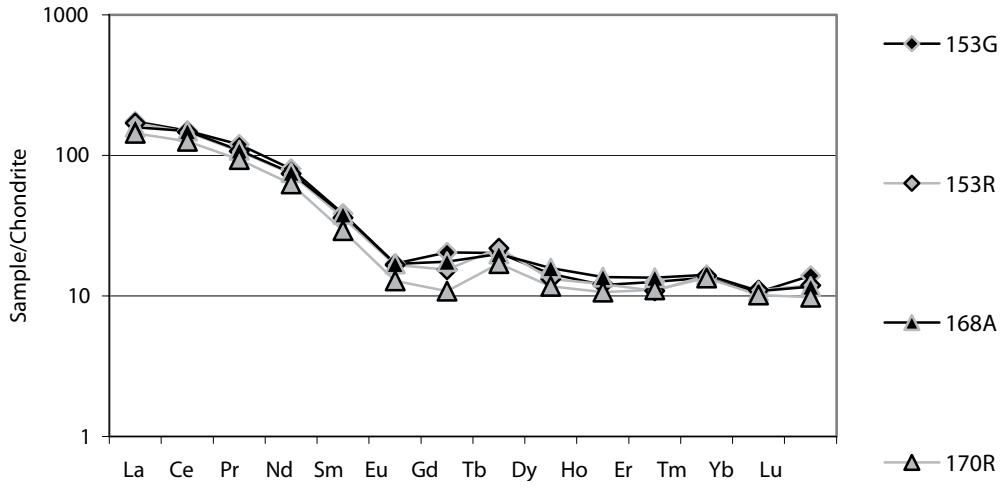

Figure 7-45. *Chondrite normalised REE-plot of 153, 168 and 170, using chondrite values from /Evansen et al. 1978/.*

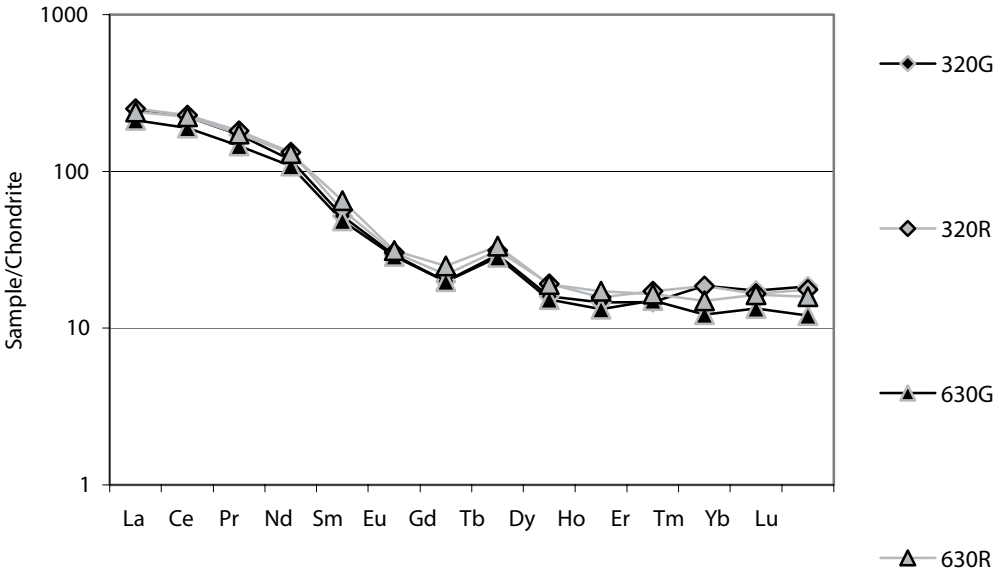

Figure 7-46. *Chondrite normalised REE-plot of samples 320 and 630, using chondrite values from /Evansen et al. 1978/.*

Both of these minerals are relatively resistant to alteration, and the REE-content in easily altered minerals such as biotite is low /Gebel et al. 1999/. The REE-contents are highest in samples 320 and 630, where the contents of titanite, hornblende, apatite and biotite are highest. Noteworthy is that this fairly unchanged behaviour also include the redox sensitive elements such as Ce and Eu /Bau 1991/, which generally have not been mobilised. The lack of major fractionation of Eu relative to other REE may further indicate that the hydrothermal event is of low-temperature origin. This is since Eu fractionation is associated to high-temperature hydrothermal alteration processes. This is since Eu fractionation is commonly assumed to be associated to high-temperature hydrothermal alteration processes e.g. /Sverjensky 1983/.

7.5 Mössbauer spectroscopy

Written in cooperation with Hans Annersten, Uppsala University.

Mössbauer spectroscopy analyses were carried out for all samples (see Section 6.4). The analyses give the total $Fe^{3+}/(Fe^{3+} + Fe^{2+})$ (=oxidation factor[total]) in the whole rock sample, in silicates and in oxides, respectively. The oxidation factor (total) is obtained by combining the oxidation factor (silicate) with oxidation (oxide). Oxidation factor (total) provides the most reliable results, since the resolution is better than for e.g. oxidation factor (oxide). All Mössbauer spectroscopy results are shown in Table 7-19. The results from Mössbauer analyses of sample 168A are discussed in Section 7.6.

Table 7-19. Mössbauer spectroscopy results.

Sample	Fe3+-bearing minerals	Oxidation factor (silicate)	Oxidation factor (oxide)	Oxidation factor (total)	Fe_{tot} (wt%)[a]	Fe^{2+}_{tot} (wt%)	Fe^{3+}_{tot} (wt%)
108R	mt,FeMg-s,epi	0.26	0.66	0.37	2.11	1.33	0.78
137R	mt,hem,FeMg-s,epi,tr gt	0.34	0.87	0.53	2.20	1.04	1.17
153R	mt,hem,FeMg-s,epi	0.28	0.83	0.44	2.46	1.37	1.08
170R	mt,hem,FeMg-s,epi	0.33	0.92	0.51	2.24	1.10	1.14
320R	mt,FeMg-s,epi	0.20	0.74	0.32	3.69	2.51	1.18
630R	hem,FeMg-s,epi	0.19	1.00	0.37	4.04	2.54	1.49
108G	mt, FeMg-s, epi	0.31	0.66	0.39	2.06	1.25	0.80
137G	mt,hem,FeMg-s,epi	0.38	0.77	0.49	2.29	1.17	1.12
153G	mt,hem,FeMg-s,epi	0.33	0.84	0.5	2.23	1.12	1.12
320G	mt,hem,FeMg-s,tr epi	0.31	0.75	0.39	3.66	2.23	1.43
630G	mt,FeMg-s	0.20	0.76	0.36	3.90	2.49	1.40
168A	hem,FeMg-s,epi,tr.mt	0.56	0.96	0.63	2.43	0.90	1.53

Abbreviations: FeMg-s = Fe-Mg silicates (mainly chlorite and occasionally biotite, amphibole and clinopyroxene), epi = epidote, mt = magnetite, hem = hematite, gt = goethite, tr = trace amounts. [a] = Fe_2O_3*0.6995.

7.5.1 Silicates

Most of the Fe^{3+} in the silicates is found in epidote and Fe-Mg silicates (mainly chlorite), although chlorite contains higher concentrations of Fe^{2+} than Fe^{3+}. The Mössbauer spectra for chlorite overlap with the spectra for other Fe-Mg silicates, e.g. biotite, amphibole and clinopyroxene and it is difficult to separate these minerals in the spectra. However, the thin Mössbauer-lines for Fe-Mg silicates suggest that the major part of the Fe-Mg-silicates is chlorite while other Fe-Mg silicates (biotite, amphibole and clinopyroxene) constitute a small part at most. The Fe^{3+}/Fe_{tot}-ratio of the silicates is similar or slightly lower in the red-stained samples than in the reference samples. The Fe^{3+}/Fe_{tot}-ratio of the silicates in the red-stained samples is about 19 to 34% (average 26.7%). The Fe^{3+}/Fe_{tot}-ratio of silicates in the reference samples is about 20 to 38% (average 30. 6%). The higher Fe^{3+}/Fe_{tot}-ratio in the reference samples is probably due to higher epidote contents, as verified by thin section investigations. /Tullborg 1995/ reports higher Fe^{3+}/Fe_{tot}-contents in wall rock chlorite than in wall rock biotite. Since the high amount of chlorite in the red-stained samples compared to the reference samples does not compensate for the higher epidote contents (although generally smaller than the Fe-Mg-silicate contents) regarding the Fe^{3+}/Fe_{tot}-ratio it is inferred that the amount of epidote in the sample influence the Fe^{3+}/Fe_{tot}-ratio to a very high degree.

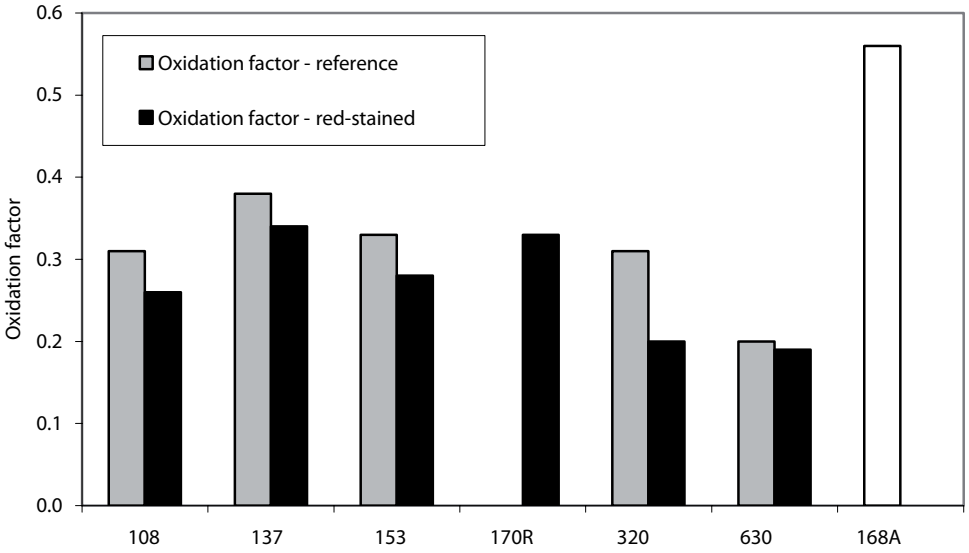

Figure 7-47. *Oxidation factor (silicate) obtained from Mössbauer spectroscopy. Sample 168A is altered but not red-stained.*

This is also strengthened by the fact that the highest Fe^{3+}/Fe_{tot}-ratios are generally found in the samples with the highest epidote contents. The higher epidote contents in the reference samples may be due to heterogeneities in the samples or that the reference rock is enriched in epidote to a higher degree than the red-stained samples during alteration or that primary epidote in the red-stained samples are altered during alteration.

7.5.2 Oxides

The most important Fe^{3+}-bearing oxides are magnetite (Fe^{3+}/Fe_{tot} = 2/3) and hematite (100% Fe^{3+}). Since magnetite has an oxidation factor of about 0.6667 and hematite has an oxidation factor of 1.0, the oxidation factor is increased with increasing hematite-content. The oxidation factor for oxides has poor accuracy for many samples since the oxide-content (in vol.%) in the samples often is close to the detection limit. That is for instance the reason why the magnetite content in 630R is left out although thin section investigations show that there is some magnetite in this sample. It is however evident that the average oxidation factor for oxides is higher in the red-stained samples (average 0.837) than in the reference samples (average 0.756), due to the generally higher hematite content in the red-stained samples (cf Table 8-1). However, thin section investigations show that magnetite is altered to hematite to some degree in most of the reference samples as well which results in small changes in the oxidation factor for oxides between some reference samples and related red-stained samples (Figure 7-48). For the same reason the oxidation factor is slightly higher in the reference samples 137G and 320G compared to red-stained samples 137R and 320R. Hematite does commonly not replace the entire magnetite, which also is evident from the characteristic incomplete pseudomorphic replacement of magnetite by hematite that is observed in a most of the red-stained samples. The oxidation factor (oxide) is increased by up to 24% in the red-stained samples compared to the reference samples and the average increase is about 8%.

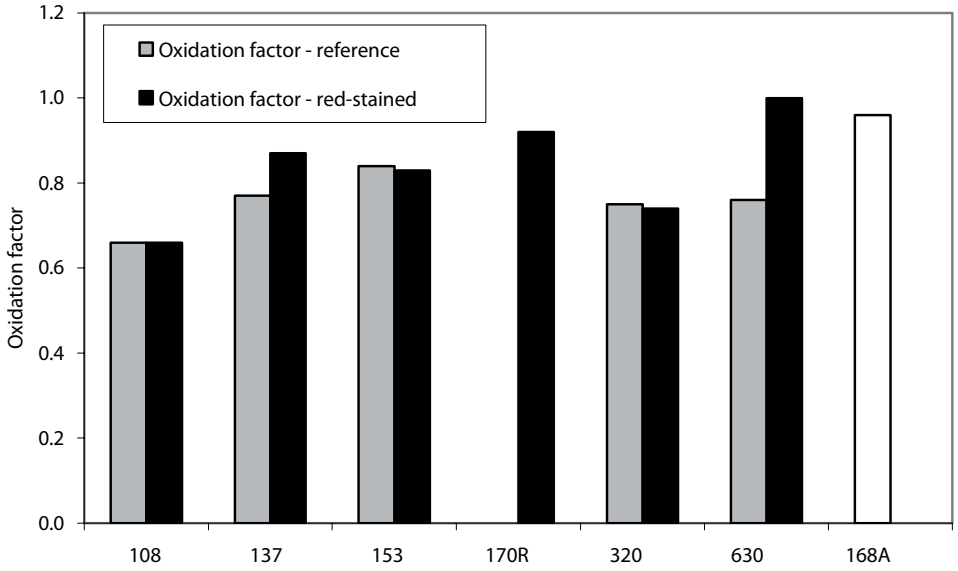

Figure 7-48. *Oxidation factor (oxide) obtained from Mössbauer spectroscopy. Sample 168A is altered but not red-stained.*

7.5.3 Total

As stated above the oxidation factor (total) is the most reliable measurement of the oxidation and it is obtained by combining oxidation factor (silicate) and oxidation factor (oxide), which are both described above. The total oxidation factor (Fe^{3+}/Fe_{tot}) is about 42–43% in average both for the reference samples and red-stained samples and the change in the Fe^{3+}/Fe_{tot}-ratio is in average very small (< 1%). Slightly higher (up to 4%) as well as slightly lower (up to 7%) Fe^{3+}/Fe_{tot}-ratios are found in the red-stained samples compared to the reference samples. The total Fe^{3+}/Fe_{tot} is lower in the red-stained samples than in the reference samples due to higher epidote contents in the reference samples, although the hematite contents are higher in the red-stained rock than in the reference rock. However, since the total oxide content is low in most of the samples and since magnetite is occasionally replaced by hematite in the reference rock, the Fe^{3+}/Fe_{tot}-ratios in oxides play a less significant role than in the silicates regarding the total change in Fe^{3+}/Fe_{tot}.

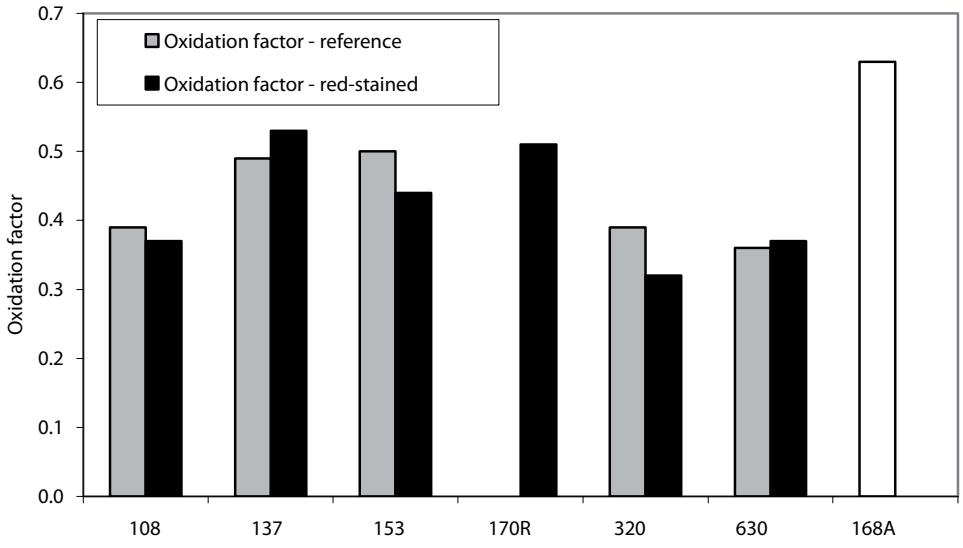

Figure 7-49. *Oxidation factor (total) obtained from Mössbauer spectroscopy. Sample 168A is altered but not red-stained.*

7.6. Features of the altered but not extensively red-stained rock sample; 168A

The sample 168A of grey, altered rock was included in this study. This sample has a quite high porosity (0.42%), due to a high degree of micro-fractures, as shown by microscope studies. The plagioclase crystals in this sample are extensively altered to fine-grained secondary minerals like albite, epidote, sericite, K-feldspar etc. The epidote content is rather high and biotite is fairly unaltered and the chlorite content is low. Most of the magnetite is completely or partially altered to hematite.

Compared to sample 153G, which is quite close to sample 168A and has similar chemistry (based on QAP and TAS-classification) and density, the concentrations of some elements are different. Al, Ca, Be, Ga and Sr are depleted in sample 168A compared to sample 153G mainly because of break down of plagioclase to secondary minerals, mainly albite and epidote. This break down also explains the enriched concentrations of Na in sample 168A. The increased content of secondary minerals in sample 168A is also shown by the higher LOI-values of this sample compared to sample 153G. The higher amount of K and Rb in sample 168A might also depend on higher contents of biotite in this sample compared to sample 153G, but also to formation of secondary K-feldspar and sericite in altered plagioclase crystals. SEM-EDS analyses of altered plagioclase crystals show that these crystals contain lower amounts of K and Fe and higher amounts of Na than the average red-stained plagioclase crystals in other samples, which might explain why the sample is not intensively red-stained. The concentrations of Mg and Mn are rather constant since no major chloritization of biotite is observed in sample 168A. Fe is however higher in sample 168A than in 153G, possibly because of a higher epidote content and Fe-rich minerals in micro-fractures.

Sample 168A is the sample with highest Fe^{3+}/Fe_{tot}-ratio, both regarding silicates (0.56) and in total (0.63). This is probably due to high amount of epidote, extensive hematitization of magnetite, and possibly due to Fe-rich minerals in micro-fractures. Since only small contents of chlorite is found in this sample it is inferred that epidote influences the total Fe^{3+}/Fe_{tot}-ratio to a very high degree. The Fe^{3+}/Fe_{tot}-ratio in oxides is higher in sample 168A (0.96) compared to sample 153G (0.84) due to a higher content of hematite. The fact that sample 168A shows higher a Fe^{3+}/Fe_{tot}-ratio than the red-stained samples infers that a high epidote content influence the Fe^{3+}/Fe_{tot}-ratio more than hematite formation does, especially in samples with low Fe-oxide contents.

7.7 Comparison to the Simpevarp study

In this section the similarities and differences between the major red-staining features from this study at Laxemar (KLX04) and the red-staining study at Simpevarp (KSH01A+B and KSH03A+B) /Drake and Tullborg 2006c/ are presented. These two studies were generally executed in the same way. Differences are that the red-staining study at Simpevarp featured a broader set of samples (24 compared to 12 of this study) and rock types. The samples from Simpevarp were made up of rocks mapped as “Fine-grained dioritoid”, “Quartz monzodiorite” and “Ävrö granite”, while the samples in the present study are all mapped as “Ävrö granite”. The rocks in the present study are thus generally more granitic, richer in quartz, K-feldspar, silicon and potassium with lower concentrations of e.g. ferromagnesian minerals and calcium. The reference samples in the present study are less altered than the reference samples in the Simpevarp study. This difference is mainly due to that the reference samples in the Simpevarp study were sampled closer to the red-stained rock than in the present study. The sample volumes are also larger in the present study. In the

study at Simpevarp the reproducibility of the changes in most of the elements were tested by reanalysing a couple of samples. In the Simpevarp study attempts were made to relate changes to so called “immobile elements”. Measurement of porosity and density was carried out in the present study in contrast to the study at Simpevarp.

The general features of the red-staining are similar in both of the studies. Some differences exist, although they depend on the nature of the samples, e.g. more altered reference rock samples in the Simpevarp study and partly more heterogeneous samples in the present study.

7.7.1 Mineralogy

The changes in mineralogy between the red-stained rock and the reference rock are about the same in both of the studies. The main features of the red-staining and hydrothermal alteration are alteration of plagioclase to secondary K-feldspar, albite, sericite, Fe-oxide, prehnite and epidote, chloritization of biotite and hematitization of magnetite. The red-staining varies widely between the samples, as a result of the secondary mineral assemblage in altered plagioclase crystals, where K-feldspar crystals with Fe-oxides in minute pores give the most intense red colour. Epidote and subordinately muscovite are more common as secondary minerals in this study. Biotite is commonly fairy well preserved in the reference rock in this study, in contrast to the study at Simpevarp where biotite was commonly completely or partially replaced by chlorite. This is however probably a matter of distance between the sampled reference rock and the red-stained rock. Although not commonly occurring, the biotite has been replaced by muscovite in a higher degree, and by prehnite to a lesser degree, in the present study than in the study at Simpevarp. Hematitization of magnetite is more wide-spread in the reference samples and not as extensive in the red-stained samples in the present study compared to the Simpevarp study. The samples at Simpevarp included more primary amphibole and less quartz and phenocrysts of K-feldspar than the present study. Pyroxene and ilmenite are lacking in the present study and secondary pyrite (formed after the oxidation event) is more common in the present study. Secondary prehnite and micro-fractures filled with Fe-oxide/Fe-oxydydroxides are less common in the present study, although they are quite common. The higher amount of secondary epidote and muscovite and the lower amounts of prehnite in the present study compared to the Simpevarp study might suggest that the temperatures of alteration were higher in the rock volume at Laxemar than at Simpevarp. A reason for this might be that the Laxemar area represents a rock block that was situated deeper in the crust at the time of alteration. Another reason for the somewhat different secondary mineralogy might be that the Laxemar area is situated closer to the adjacent granite intrusions at Götemar and Uthammar, assuming that the red-staining of the rocks in the area are related to these intrusions. These intrusions are thought to be dipping towards the site investigation area cf Figure 11-1 in /SKB 2005/.

7.7.2 Whole rock chemistry

The changes in concentrations are similar in the present study and the study at Simpevarp. The red-stained rock show general enrichment of K_2O, Na_2O, Rb, LOI and U, and depletion in CaO, Al_2O_3, Cr, Cs, Sr and Ga in both studies. These changes reflect breakdown of primary plagioclase, biotite, and magnetite and formation of secondary K-feldspar, albite, hematite and water-bearing minerals such as chlorite, sericite, epidote, muscovite and prehnite. The changes are however generally smaller in this study. This is mainly because of differences in the sampling procedure and differences between the sampled rock types,

of the different studies. The normative enrichment in e.g. K_2O is lower in the present study partly because the K_2O content is higher in the rock in general – a similar enrichment as in the Simpevarp study gives a smaller normative change. Further, the K-bearing biotite is commonly fresh in the reference rock, while it was generally partially or completely altered to chlorite in the reference rock at Simpevarp. The chloritization of biotite in the red-stained samples in the present study results in an enrichment of MgO, MnO and subordinately FeO in the red-stained rock, because chlorite contain higher concentrations of these elements than biotite. Such enrichment was not found in the Simpevarp study. REE:s were generally constant during alteration in both of the studies. TiO_2 (and Y) show more variation than in the present study, largely because of the heterogeneous distribution of titanite. Sulphur was generally depleted in the red-stained samples at Simpevarp, due to oxidation of dominantly pyrite. Enrichment of S in some of the samples in the present study is due to the formation of pyrite in micro-fractures after the major red-staining event.

7.7.3 Mössbauer spectroscopy

The results from the Mössbauer analyses of the study at Simpevarp and the present study show that the difference in the Fe^{3+}/Fe_{tot}-ratio of the red-stained samples compared to the reference samples is quite small. The Fe^{3+}/Fe_{tot}-ratio was however generally enriched in the red-stained samples at Simpevarp (average 4.25% enrichment), while the changes in the present study are much smaller < 1% with no obvious trend of enrichment of the Fe^{3+}/Fe_{tot}-ratio in the red-stained samples. This might depend on the high epidote contents of the reference samples compared to the red-stained samples of the present study and that the magnetite is altered to hematite to a higher degree in the reference samples than in the reference samples at Simpevarp. The average Fe^{3+}/Fe_{tot}-ratio is also lower in the samples of the present study (average about 42–43% in all samples, average about 46% in granitic/granodioritic samples and 34.5–37.5 in quartz monzodioritic samples) compared to the Ävrö granite samples in the Simpevarp study (average about 48% in reference samples and 56% in red-stained samples). The higher Fe^{3+}/Fe_{tot}-ratio in the Ävrö granite samples than in the samples at Simpevarp is mainly due to higher epidote contents in general. For comparison, the Fe^{3+}/Fe_{tot}-ratio of quartz monzodiorite samples was in average 36% for reference samples and 39% for red-stained samples in the study at Simpevarp. The Fe^{3+}/Fe_{tot}-ratio of fine-grained dioritoid samples was in average about 28–29% for both reference samples and red-stained samples in the study at Simpevarp.

The remaining Fe^{2+} content of the samples in the present study is in average 1.18–1.21 wt.% for granitic to granodioritic Ävrö granite and 2.3–2.53 wt.% for quartz monzodioritic Ävrö granite. The Ävrö granite samples at Simpevarp contained in average 1.53–1.72 wt.% Fe^{2+}, while quartz monzodiorite samples contained 3.72–3.92 wt.% Fe^{2+} and fine-grained dioritoid samples contained 3.65–3.79 wt.% Fe^{2+}.

8 Summary of the mineralogical and geochemical changes and related changes in redox capacity and porosity

The red-staining of the wall rock adjacent to fractures is caused by oxidation in association with hydrothermal alteration. The red-staining is caused by minute inclusions of Fe^{3+}-rich minerals, mainly hematite. These are present in secondary pores, mostly hosted in K-feldspar (adularia) and to lesser extent in albite replacing primary plagioclase. Accompanying this alteration is hematitization of magnetite, chloritization of biotite (and occasionally hornblende) and formation of secondary sericite, prehnite, grothite (titanite), epidote and muscovite. An increase in total porosity, intragranular porosity and micro-fractures, as well as a decrease in density is also evident. Minerals like quartz, primary K-feldspar and titanite were mainly unaffected. The red-staining of feldspar has obviously taken place at hydrothermal conditions and temperatures around 280–400°C. This is based on temperatures of chloritization, prehnite formation, epidote formation, feldspar composition (thermometry) and the low-temperature paragenesis in general, based on information from /Liou et al. 1983, Nekvasil and Burnham 1987, Frey et al. 1991, Deer et al. 1992, Slaby 1992, Eliasson 1993, Spear 1993, Lee and Parsons 1997, Bucher and Frey 2002, Wilamowski 2002, Benisek et al. 2004/. The chemistry of chlorite in the altered rock is similar to the chemistry of early formed chlorite in fracture fillings in the area /Drake and Tullborg 2004, 2005, 2006b/. Intense local red-staining caused by hematite and possibly also Fe-oxyhydroxide in micro-fractures is thought to be formed subsequently to the major red-staining. /Eliasson 1993/ proposed this red-staining to occur at temperatures of about 150–250°C.

The red-stained rock is enriched in e.g. K, Na, Mg, Rb, H_2O, and slightly enriched in Fe and Mn. This enrichment is associated to formation of secondary adularia, albite, chlorite, prehnite and sericite. Small enrichment of P and U is also noted in the red-stained rock and is thought to represent higher amounts of apatite and fine-grained U-rich minerals in the red-stained rock. The enrichment of S in some samples is attributed to formation of pyrite in the red-stained rock after the major red-staining event.

The red-stained rock is depleted in e.g. Ca, Sr, Cs, Al and Ga. This depletion is mainly associated to break down of primary plagioclase and alteration of biotite. The total contents of e.g. Ti, Si, Y, Sc, V and REE:s remained fairly constant or are only slightly changed.

Mössbauer spectroscopy reveals that Fe^{3+}/Fe_{tot}-contents are only slightly different in the red-stained rock compared to the reference rock, in contrast to what is found from studies at Simpevarp /Drake and Tullborg 2006c/. Average change is < 1%, and average Fe^{3+}/Fe_{tot}-contents are 42–43%, although enrichment of up to 4% and depletion of up to 7% of Fe^{3+}/Fe_{tot} are found in the red-stained samples. The unexpected small change in Fe^{3+}/Fe_{tot} is mainly dependant on the higher content of epidote in the reference rock, which might be due to heterogeneities of the rock, and to partial hematitization of magnetite in the reference rock. The Fe^{3+}/Fe_{tot}-ratios of oxides are however generally higher in the red-stained rock. The highest Fe^{3+}/Fe_{tot}-ratios are found in the samples with the highest amounts of epidote. The samples have quite varying Fe-contents with the highest concentrations in samples 320 and 630 (Fe_2O_3 = about 4.6–5.5 wt.%) and the lowest concentrations in samples 108, 137, 153 and 170R (Fe_2O_3 = about 3.7–3.9%). The average Fe^{2+}-content is slightly higher in the red-stained samples than in the reference samples. The Fe^{2+}-content is about twice as high in samples 320 and 630 as in samples 108, 137, 153 and 170R.

A schematic summary of how the Fe^{3+}/Fe_{tot}-ratios and related mineralogy have changed in the different rock types in the red-stained samples compared to the reference samples is shown in Table 8-1.

Some of the reference samples in this study were not completely unaltered and some chloritization of biotite, partial alteration of plagioclase and various degree of hematitization of magnetite are observed. These samples are however not strongly oxidized which shows that the hydrothermal alteration may reach further into the wall rock than the oxidation, in agreement with studies of /Landström et al. 2001/. A schematic illustration of the characteristic features of the red-staining is found in Figure 8-1.

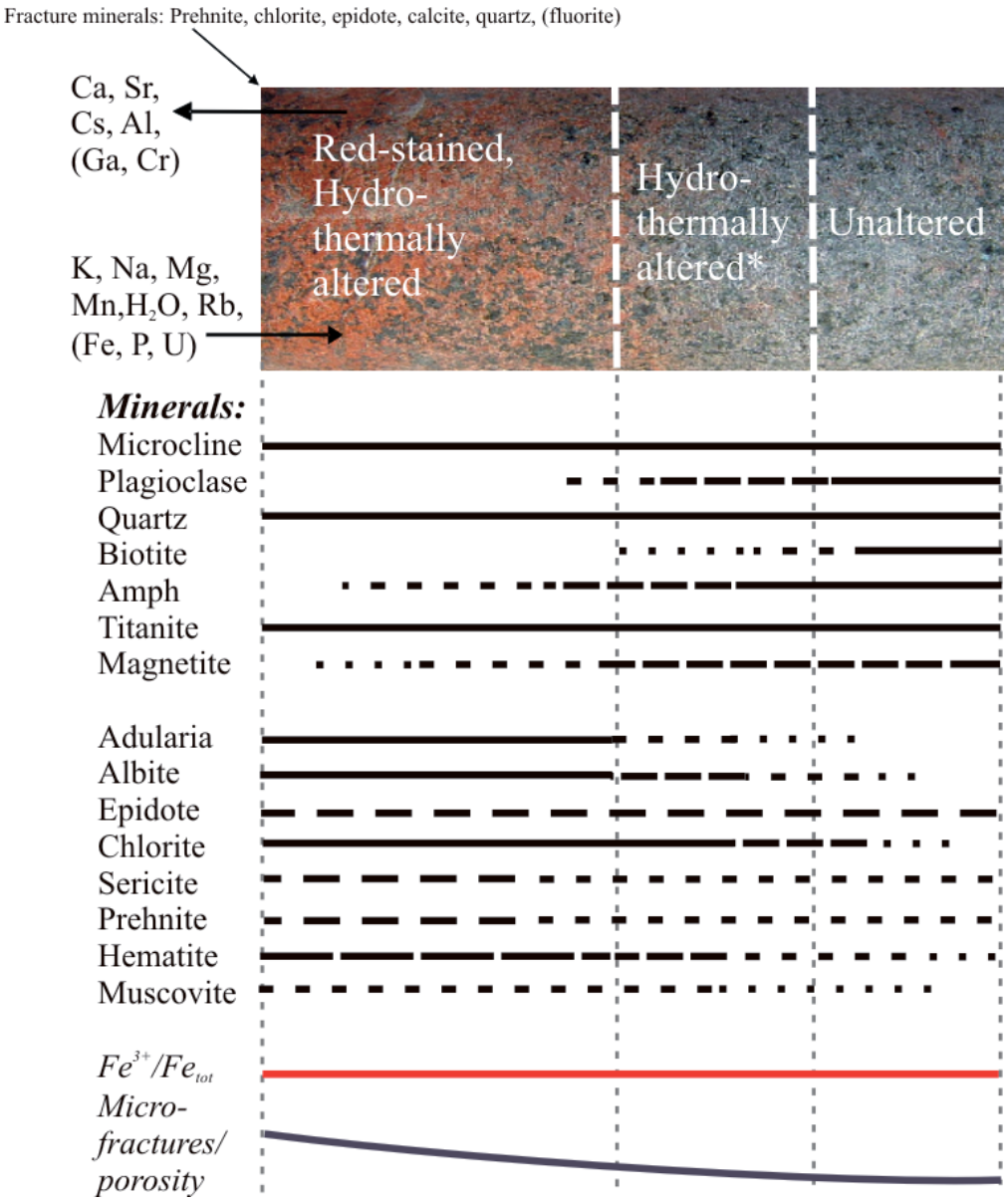

Figure 8-1. *Tentative sketch of the major features of the wall rock. Vertically stippled lines indicate which part that is red-stained due to oxidation/hydrothermal alteration, hydrothermally altered (but not red-stained(*)) and fairly unaltered, respectively. The fracture rim is at the left side of the sketch. Arrows indicate which element that is enriched or depleted in the red-stained rock compared to the reference rock. The horizontal lines (partly stippled), show where the major minerals occur in the different zones adjacent to the fracture. The red and black lines at the bottom illustrate the change in Fe^{3+}/Fe_{tot} and the amount of micro-fractures/porosity from the fracture surface into the wall rock.*

Table 8-1. Schematic summary of the changes in Fe^{3+}/Fe_{tot}-ratios and related mineralogy in the different rock types. Values in brackets are average values.

Sample	Silicates Biotite (vol.%)	Chlorite (vol.%)	Epidote (vol.%)	Fe^{3+}/Fe_{tot} silicate(%)	Oxides Oxides [a] (vol%)	Magnetite (vol%)[b]	Hematite (vol%) [b]	Mt+Hem (vol%) [b]	Fe^{3+}/Fe_{tot} oxide (%)	Total Fe^{3+}/Fe_{tot} total (%)	Fe_{tot} (wt%)[c]	Fe^{2+}_{tot} (wt.%)	Fe^{3+}_{tot} (wt%)
108G,137G,	1.2–9.8	1.1–3.7	2.7–4.3	31–38	0.9–1.7	0–100	0–15.8	0–90.9	66–84	39–50	2.06–2.29	1.12–1.25	0.8–1.12
153G	(6.9)	(2.1)	(3.2)	(34)	(1.2)	(33.3)	(8.3)	(58.4)	(75.7)	(46)	(2.19)	(1.18)	(1.01)
108R,137R,	0–3.1	3.8-8.9	1.5–3.8	26–34	0.4–1.7	0–100	0–76.9	0–83.3	66–92	37–53	2.11–2.45	1.04–1.37	0.78–1.14
153R,170R	(0.8)	(6.1)	(2.6)	(30.2)	(1.1)	(25)	(40.1)	(34.9)	(82)	(46.3)	(2.25)	(1.21)	(1.04)
320G,630G	9–12	0.6–1.3	0.6–1.5	20–31	1.7–1.8	44–65.4	0–3.8	30.8–55.6	75–76	36–39	3.66–3.90	2.23–2.49	1.40–1.43
	(10.5)	(1.0)	(1.0)	(25.5)	(1.7)	(54.9)	(1.9)	(43.2)	(75.5)	(37.5)	(3.78)	(2.36)	(1.41)
320R,630R	0	8–17.6	0.5-0.6	19–20	1.7–2.7	0–41.7	8.3–16.7	50–83.3	74–100	32–37	3.69–4.04	2.51–2.54	1.18–1.49
		(12.8)	(0.55)	(19.5)	(2.2)	(20.8)	(12.5)	(66.7)	(87)	(34.5)	(3.87)	(2.53)	(1.34)
Reference	3.1–12	0.6-3.7	0.6-4.3	19–38	0.9–1.8	0–100	0–15.8	0–90.9	66–84	36–50	2.06–3.90	1.12–2.23	0.8–1.43
All samples	(8.3)	(1.7)	(2.3)	(30.6)	(1.4)	(42)	(5.7)	(52.3)	(75.6)	(42.6)	(2.83)	(1.65)	(1.17)
Red-stained	0–3.1	3.8–17.6	0.5–3.8	20–34	0.4–2.7	0–100	0–76.9	0–83.3	66–100	32–53	2.11–4.04	1.04–2.54	0.78–1.49
All samples	(0.5)	(8.4)	(1.9)	(26.7)	(1.5)	(23.6)	(30.9)	(45.5)	(83.7)	(42.3)	(2.79)	(1.65)	(1.14)
168A	5.7	0.2	4.2	56	2.0	0	76.2	23.8	96	63	2.43	0.9	1.53

The samples are divided into samples with low Fe_2O_3 content (108, 137, 153, 170) and samples with higher Fe_2O_3 content (320, 630). Values for sample 168A is presented separately. Abbreviations: G = reference samples, R = red-stained samples, Mt+Hem = magnetite partially replaced by hematite. [a] = Magnetite and hematite, [b] =% of counted oxide vs total counts of magnetite, hematite and magnetite+hematite, [c] = Fe_2O_3 multiplied by 0.6995. Pyrite is commonly present in very small amounts in the samples (< 0.2 vol.%) and is thus not included in Table 8-1. However, both point-counting and whole rock chemical analyses show that pyrite and sulphur is enriched in samples 108R and 153R, due to formation of secondary pyrite (after the main oxidation and hydrothermal event). Depletion of S and pyrite is found in some samples, probably due to oxidation of primary pyrite.

9 Changes in properties of concern for a deep repository for spent radioactive fuel

The oxidation and hydrothermal alteration described in this study has resulted in changed properties of the rock, potentially influencing several parameters that need to be considered for the planning and modelling of a nuclear waste repository. These parameters are reducing capacity, porosity, sorption, thermal conductivity and rock strength. The possible effects caused by the alteration are discussed below. Since no detailed study of changing rock strength properties (rock mechanics) of altered, oxidized rock compared to unaltered rock has been carried this is not discussed here. However, the higher porosity in the red-stained rock may lead to lower rock strength.

9.1 Reducing capacity

At the planned depth of a repository (approx. 500 m) reduced groundwater is a prerequisite. In order to maintain the stability of the canister it is important that groundwaters do not contain dissolved O_2 during the life time of the repository. Oxygen will be introduced during the construction and operation of the repository. This oxygen will be consumed by the inorganic (mainly Fe^{2+}) and organic redox buffers. Experiments have previously been carried out on Äspö in order to prove this /Puigdomenech et al. 2001/. Another scenario which may introduce oxygenated water into the bedrock is glacial meltwater. The basic idea is that such meltwater can contain more dissolved O_2 than the present recharge and in addition, the organic buffer may be severely reduced below the ice. Furthermore high hydraulic heads beneath the inland ice sheet may force this oxygen-rich water to large depth in the bedrock. The extent and potential for O_2 intrusion to large depth, related to the glacial scenario is debated but nevertheless it is of importance to show that Fe^{2+} is available in the bedrock and along the fractures in order to provide enough reducing capacity. One of the tasks of the present study is to determine how much reducing capacity is left in the oxidised and hydrothermally altered red stained parts of the wall rock compared to fresh host rock. The results are summarised below:

1) The main Fe^{2+} -bearing minerals in the relatively fresh Ävrö granite in the Laxemar subarea are commonly biotite, chlorite and magnetite. In addition, the more quartz monzodioritic varieties of the Ävrö granite also contain amphibole (mainly hornblende). In the altered and red stained samples the most common Fe^{2+} mineral is chlorite.
2) The change in Fe^{3+}/Fe_{tot} ratio between the relatively fresh samples and the red-stained and altered samples is relatively small. Mean values are:
   a) 46% Fe^{3+}/Fe_{tot} changed to 46.3% in the red-stained samples of granitic to granodioritic Ävrö granite (samples 108, 137, 153 and 170),
   b) 37.5% Fe^{3+}/Fe_{tot} changed to 34.5% in the red-stained samples of quartz monzodioritic Ävrö granite (samples 320 and 630).
3) The available Fe^{2+} varies between 1.18 to 1.21 wt.% in fresh and red-stained. Ävrö granite of granitic/granodioritic composition, and 2.36 to 2.53 wt.% in fresh and red-stained Ävrö granite of quartz monzodioritic composition. Thus, the red-stained samples of the quartz monzodioritic Ävrö granite contain more Fe^{2+} than the Ävrö granite samples of granitic to granodioritic composition.

4) Pyrite has been documented in small amounts in most samples (< 0.2%). The sulphide content is however decreased in some of the red-stained samples because of oxidation of pyrite. In two of the red-stained samples formation of pyrite subsequent to the major red-staining has led to an increased S content in these samples.

The overall conclusion is that the reducing capacity is not significantly reduced in the oxidized wall rock, in contrast to what the red-staining might suggest. The red-staining is produced by mineralogical changes in combination with a modest oxidation and formation of minute hematite grains.

9.2 Porosity

The mineralogical changes related to hydrothermal alteration usually increase the porosity, but most of all changes the structure and distribution of the pores. This is also the case for the alteration/oxidation observed within the Simpevarp area. Diffusion and sorption are the two main retention mechanisms for radionuclides considered in the safety assessment modelling. Porosity is a key parameter for both;

1) Diffusion depends to a large extent on the amounts of connected pores and their shape.
2) Sorption is dependent on mineral composition but also on the surface area available, which in turn is related to the porosity.

Measurements of porosity in the present study show that it is generally increased in the red-stained rock. The results of the porosity measurements are:

- Red-stained samples: 0.22–1.14% (average 0.44%).
- Reference samples: 0.21–0.31% (average 0.29%).

These results are in accordance with studies of connected porosities carried out within the Oskarshamn site investigations on drill core samples from KSH01, KSH02 at Simpevarp and KLX02, KLX03, KLX04, KLX05 and KLX06 at Laxemar /Savukoski 2004, Savukoski and Carlsson 2004, Börjesson and Gustavsson 2005, Savukoski 2005ab/. These studies did not focus on comparisons of porosity differences between red-stained and fresh rock. However, some of the samples in these studies are clearly red-stained (oxidized) and comparisons of red-stained and fresh samples based on results from the above mentioned studies are evaluated briefly in this report. Sample descriptions from (Gustavsson pers. com) were also used. It should be noted that the samples measured for porosity in the above mentioned studies are thinner than the samples in the present study (about 1/2 the thickness). This might give higher porosity values than expected, especially for the heterogeneous and coarse-grained Ävrö granite cf e.g. /Tullborg and Larson 2005/. The results from the above mentioned studies are:

1. Ävrö granite:
   – Fresh: 0.2 to 0.6% (average = 0.34%, 13 samples, KLX03, KLX05)
   – Red-stained: 0.5 to 0.8% (average: 0.59%, 15 samples, KLX04)
2. Quartz monzodiorite:
   – Fresh: 0.1 to 0.4% (average = 0.23%, 15 samples, KSH01, KLX03, KLX05)
   – Red-stained: 0.2 to 0.4% (average = 0.3%, 5 samples, KSH01, KLX03)
3. Fine-grained diorite:
   – Fresh: 0.1 to 0.3% (average = 0.2%, 8 samples, KSH01, KLX05)
   –Red-stained: 0.2 to 0.4% (average = 0.3%, 2 samples, KSH01)

In the drill core KSH02 at Simpevarp it was shown that the porosity is higher in altered fine-grained dioritoid (porosity = 1 to 2.5%) compared to fresh fine-grained dioritoid (porosity = 0.2 to 1%) /Mattsson and Thunehed 2004/.

In studies at Äspö HRL it has been shown that the porosity is higher in altered, oxidized granitic rock adjacent to fractures (porosity = 0.15 to 0.83%, average 0.35%) compared to fresh granitic rock further away from the fractures (porosity = 0.13 to 0.20) /Eliasson 1993/.

Distribution of the pores and the textures of the connected pores can be studied using different impregnation techniques. Such studies have been carried out on altered and fresh rock samples from Äspö /Mazurek et al. 1995, Byegård et al. 1998, Johansson 2000/. These studies show that the distribution of pores is heterogeneous and that the orientation effects may be considerable. A higher porosity close to the fracture wall is shown in PMMA studies on Äspö /Kelokaski et al. 2001/, where the porosity in some wall rock samples is due to connected pores with preferred orientation. This porosity is increased in connection to micro-fractures which are more common in the altered wall rock. Results from impregnation studies also show that connected porosity in crystalline rock is mainly made up of micro-fractures and to some extent porous minerals (often secondary or altered minerals) /Mazurek et al. 1995, Johansson 2000/. Frequency, size and orientation of the micro-fractures are crucial for the connectivity of the pores. At Äspö, the connected porosity shows a distinct decrease from the partly gouge filled breccia centre of water conducting structures through the altered wall rock and further into unaltered fresh bedrock /Andersson et al. 2002/.

Introduction of new micro-fractures caused by drilling and disturbances of the samples due to stress release might however influence the porosity of the samples.

In this study, micro-porosity-features have been found to be more prominent in the red-stained samples than in the reference samples. The main porosity-affecting features of the red-stained rock compared to the reference rock are:

- Higher amount of micro-fractures through crystals (particularly in quartz and subordinately in K-feldspar phenocrysts) and along grain boundaries in the red-stained rock.
- Higher porosity of secondary and altered minerals, especially in plagioclase pseudomorphs, chlorite and prehnite.
- Grain expansion associated to chloritization of biotite, resulting in radial fractures.

These features are more common in the red-stained rock than in the reference samples.

9.3 Sorption

Sorption of radionuclides on the fracture walls combined with diffusion into the fracture coatings and further into micro-fractures in the wall rock is the main retardation factors for nuclide transport. Sorption capacity for each trace element is dependent on the water/mineral system present. Therefore are changes in wall rock mineralogy related to changes in the sorption capacity.

Laboratory and *in situ* experiments studying the sorption of different tracers have been carried out on altered and fresh Äspö diorite at the Äspö HRL /Byegård et al. 1998/. These batch experiments showed that the sorptivity of the tracers increases in the order $^{22}Na^{+}$ < $^{47}Ca^{2+}$ ≈ $^{85}Sr^{2+}$ < $^{86}Rb^{+}$ ≈ $^{133}Ba^{2+}$ < $^{137}Cs^{+}$ (both in laboratory and *in situ*). This study also

indicates that the sorption is stronger in the fresh Äspö diorite compared to the altered Äspö diorite. The lower sorptivity in the altered rock is supposed to be due to the alteration of biotite to chlorite, since biotite has much higher sorption capacity than chlorite, especially regarding Cs^+. Subsequent sorption studies on gouge and rim zone (altered wall rock) materials from the TRUE Block Scale site in the Äspö Hard Rock laboratory show more complex patterns. These indicate similar or slightly higher sorption coefficients in the rim zone material compared to the fresh host rock /Byegård and Tullborg in manuscript/. Concerning very altered and red stained sections of the bedrock, the fine grained hematite present in the altered feldspar grains may enhance the sorption of some tracers (e.g. U and Ra). Red-stained samples are included in the presently running laboratory program of the site investigations.

The effective sorption is related to available surfaces and therefore the net effect of the alteration can not only be described in terms of changed mineralogy. Within the ongoing site investigation programme batch sorption experiments on samples from fracture zones, altered wall rock and fresh host rock are carried out. BET surface measurements on this type of materials are compiled in the background report for transport modelling /Byegård et al. in manuscript/ and show significantly higher areas for the altered material than for the fresh host rock, i.e. a larger active surface as a result of alteration.

9.4 Thermal properties

The thermal properties of the rock influence the planning of a repository for spent nuclear fuel. Heat is produced by the spent fuel and preferable the buffer and the rock surrounding the canister should be kept at temperatures below 100°. The capability of the rock to transfer the heat from the deposition holes and further into the bedrock away form the repository is therefore an important parameter. Low thermal conductivity, low thermal diffusivity and high thermal capacity in rock surrounding the deposition holes will require a larger distance between the holes.

The thermal properties of the rock depend on e.g. mineralogy. For example, quartz has a high thermal conductivity compared to other minerals and therefore a rock with high quartz content (granitic to granodioritic) usually has a higher thermal conductivity than quartz monzodiorite.

Studies of thermal properties at the Äspö HRL showed that samples of altered Äspö diorite had higher thermal conductivity, higher thermal diffusivity and lower thermal capacity than fresh Äspö diorite ("Äspö diorite" is here synonymous to Ävrö granite of quartz monzodioritic composition) /Sundberg and Gabrielsson 1999/. The thermal conductivity is 2.70 W/m°C for the altered Äspö diorite and 2.32 W/m°C for the fresh Äspö diorite (based on mean calculated values and laboratory measurements). The difference in thermal properties between the altered rock and the fresh rock is mainly depending on the higher content of chlorite, which has replaced biotite, in the altered rock /Sundberg and Gabrielsson 1999/. Chlorite has considerably higher thermal conductivity (5.1 W/m°C) than biotite (2.0 W/m°C) /Horai and Simmons 1969, Horai 1971/. The higher thermal conductivity in the altered Äspö diorite compared to the fresh Äspö diorite may also depend on the replacement of plagioclase by albite in the altered rock /Sundberg and Gabrielsson 1999/. This is because the thermal conductivity of albite (2.1 W/m°C) is higher than that of plagioclase with an An-content of 25% (1.61 W/m°C) /Horai and Simmons 1969, Horai 1971/. The Äspö diorite samples investigated in the study at Äspö HRL are similar in chemistry and mineralogy to samples 320 and 630 in the present study at Laxemar.

The changes in thermal properties of the oxidized and hydrothermally altered rock adjacent to fractures compared to the fairly fresh reference samples in the present study can be estimated hypothetically by comparing mineralogical changes. The major changes in thermal properties are probably due to the replacement of biotite by chlorite and leads to increased thermal conductivity in the red-stained samples. The replacement of plagioclase by albite and K-feldspar (2.51 W/m°C, /Horai and Simmons 1969, Horai 1971/) also leads to higher thermal conductivity of the red-stained rock compared to the reference rock. However, biotite is already partially replaced by chlorite in some of the reference samples. This decreases the difference in thermal conductivity between the reference samples and the related red-stained samples. So far, the thermal conductivity measurements carried out within the site investigations program have not been interpreted based on sample specific mineralogical compositions and therefore the significance of the changes in thermal conductivity caused by the hydrothermal alteration can not be evaluated properly at this stage.

10 Acknowledgements

We would like to thank the staff at the SKB Simpevarp site investigations for their support. Analytica AB is thanked for whole rock chemical analyses. Prof. Hans Annersten, Uppsala University is thanked for carrying out Mössbauer spectroscopy. Swedish National Testing and Research Institute is thanked for carrying out measurements of density and porosity. Kjell Helge (Minoprep AB) is thanked for carrying out sample preparation. Prof. Sven Åke Larson, Göteborg University is thanked for giving useful comments, improving the manuscript. Thomas Eliasson, SGU, Björn Sandström, Göteborg University kindly provided some references. David Cornell, Göteborg University, is thanked for SEM-EDS instructions and method description. Fredrik Hartz, SKB, kindly helped us with the map for the area.

11 References

Andersson P, Byegård J, Dershowitz B, Doe T, Hermanson J, Meier P, Tullborg E-L, Winberg A, 2002. Final report of the TRUE Block Scale project, 1. Characterisation and model development. SKB TR-02-13. 224 pp. Svensk Kärnbränslehantering AB.

Bailey J C, 1971. Geochemistry of igneous rocks. Division of petrology, Geology Institute, Copenhagen University, Öster Voldgade 10, DK-1350 Copenhagen., 287 pp.

Bau M, **1991.** Rare-earth element mobility during hydrothermal and metamorphic fluid-rock interaction and the significance of the oxidation state of europium, Chemical Geology, Volume 93, p. 219–230.

Beane R E, Titley S R, **1981.** Porphyry copper deposits; Part II. Hydrothermal Alteration and Mineralization, Economic Geology, 75th Anniversary Volume, p. 235–269.

Benisek A, Kroll H, Cemic L, **2004.** New developments in two-feldspar thermometry, American Mineralogist, 89, p. 1,496–1,504.

Bucher K, Frey M, 2002. Petrogenesis of Metamorphic Rocks. Springer-Verlag. Berlin, Heidelberg, 341 pp.

Busenberg E, Clemency C V, **1976.** The dissolution kinetics of feldspars at 25 degrees C and 1 atm CO (sub 2) partial pressure, Geochimica et Cosmochimica Acta, 40, p. 41–49.

Byegård J, Tullborg E-L, in manuscript. Sorption experiments and leaching studies using fault gouge material and rim zone material from the Äspö Hard Rock Laboratory. SKB IPR-06-xx. Svensk Kärnbränslehantering AB.

Byegård J, Johansson H, Skålberg M, Tullborg E-L, 1998. The interaction of sorbing and non-sorbing tracers with different Äspö rock types, Sorption and diffusion experiments in the laboratory scale. SKB TR-98-18. 111 pp. Svensk Kärnbränslehantering AB.

Byegård J, Gustavsson E, Tullborg E L, Crawford J, in manuscript. Bedrock transport properties. Preliminary site description Laxemar subarea – version 1.2. SKB R-06-xx. Svensk Kärnbränslehantering AB.

Börjesson S, Gustavsson E, 2005. Laboratory data from the site investigation programme for the transport properties of the rock. Data delivery for data freeze Laxemar 2.1. Oskarshamn site investigation. P-05-106. 23 pp. Svensk Kärnbränslehantering AB.

De Albuquerque C A R, **1975.** Partition of trace elements of co-existing biotite, muscovite and potassium feldspar of granitic rocks, northern Portugal, Chemical Geology, 16, p. 89-108.

Debon F, Le Fort P, **1982.** A chemical-mineralogical classification of common plutonic rocks and associations, Transactions of the Royal Society of Edinburgh: Earth Sciences, 73, p. 135–149.

Deer W A, Howie R A, Zussman J, 1992. An introduction to the rock-forming minerals. Longman Scientific & Technical;Wiley. Harlow, Essex, England; New York, NY, 696 pp.

Drake H, Tullborg E-L, 2004. Fracture mineralogy and wall rock alteration, results from drill core KSH01A+B. SKB-P-04-250. 120 pp. Svensk Kärnbränslehantering AB.

Drake H, Tullborg E-L, 2005. Fracture mineralogy and wall rock alteration, results from drill cores KAS04, KA1755A and KLX02. SKB-P-05-174. 69 pp. Svensk Kärnbränslehantering AB.

Drake H, Tullborg E-L, 2006a. Fracture mineralogy of the Götemar granite, Results from drill cores KKR01, KKR02 and KKR03. SKB P-06-04. Svensk Kärnbränslehantering AB, submitted to SKB.

Drake H, Tullborg E-L, 2006b. Fracture mineralogy, Results from drill core KSH03A+B. SKB P-06-03. Svensk Kärnbränslehantering AB, Submitted to SKB.

Drake H, Tullborg E-L, 2006c. Mineralogical, chemical and redox features of red-staining adjacent to fractures, Results from drill cores KSH01A+B and KSH03A+B. SKB P-06-01. Svensk Kärnbränslehantering AB, Submitted to SKB.

Eliasson T, 1993. Mineralogy, geochemistry and petrophysics of red coloured granite adjacent to fractures. SKB TR-93-06. 68 pp. Svensk Kärnbränslehantering AB.

Ellis A J, Mahon W A J, 1977. Geochemistry and Geothermal System. Academic Press. New York, N.Y., 392 pp.

Ennis D J, Dunbar N W, Campbell A R, Chapin C E, **2000.** The effects of K-metasomatism on the mineralogy and geochemistry of silicic ignimbrites near Socorro, New Mexico, Chemical Geology, 167, p. 285–312.

Evansen N M, Hamilton P J, and O'Nions R K, **1978.** Rare Earth Abundances in Chondritic Meteorites, Geochimica et Cosmochimica Acta, 42, p. 1,199–1,212.

Ferry J M, **1979.** Reaction mechanisms, physical conditions, and mass transfer during hydrothermal alteration of mica and feldspar in granitic rocks from South-central Maine, USA, Contributions to Mineralogy and Petrology, 68, p. 125–139.

Frey M, de C C, Liou J G, 1991. A new petrogenetic grid for low-grade metabasites. In,1991, Sixth meeting of the European Union of Geosciences. 3; 1. p. 106. Blackwell Scientific Publications, Oxford, International

Gaal G, Gorbatschev R, 1987, An outline of the Precambrian evolution of the Baltic Shield. In,1987, Precambrian geolo.gy and evolution of the central Baltic Shield; 1st Symposium on the Baltic Shield. 35. p. 15–52. Elsevier, Amsterdam, International

Gebel A, Stosnach H, Mengel K, Schmidt K H, **1999.** Trace element analysis of granitoid minerals using Laser-Ablation ICP-MS. EUG10, Strasbourg, March 28–April 1, Journal of Conference Abstracts, 4(1), p. 795.

Helgeson H C, Murphy W M, Aagaard P, **1984,** Thermodynamic and kinetic constraints on reaction rates among minerals and aqueous solutions; II, Rate constants, effective surface area, and the hydrolysis of feldspar, Geochimica et Cosmochimica Acta, 48, p. 2405–2432.

Holness M B, **2003,** Growth and albitization of K-feldspar in crystalline rocks in the shallow crust: a tracer for fluid circulation during exhumation? Geofluids, 3, p. 89–102.

Horai K i, **1971,** Thermal conductivity of rock-forming minerals, Journal of Geophysical Research, 76, p. 1,278–1,308.

Horai K i, Simmons G, **1969.** Thermal conductivity of rock-forming minerals, Earth and Planetary Science Letters, 6, p. 359–368.

Hughes C J, **1973.** Spilites, keratophyres, and the igneous spectrum, Geological Magazine, 109, p. 513–527.

Johansson H, 2000. Retardation of tracers in crystalline rocks, PhD Thesis. Series 1582,Chalmers University of Technology, Göteborg, Sweden.

Kastner M, Siever R, **1979.** Low temperature feldspars in sedimentary rocks, American Journal of Science, 279, p. 435–479.

Kelokaski M, Oila E, Siitari-Kauppi M, 2001. Investigation of porosity and micro-fracturing in granitic fracture wall rock and fault breccia specimens using the PMMA technique, TRUE Block Scale project, Äspö Hard Rock Laboratory. 57 pp. Svensk Kärnbränslehantering AB.

Kerrich R, Fryer B J, **1979.** Archaean precious-metal hydrothermal systems, Dome Mine, Abitibi greenstone belt; II, REE and oxygen isotope relations, Canadian Journal of Earth Sciences = Journal Canadien des Sciences de la Terre, 16, p. 440–458.

Kornfält K A, Wikman H, 1987. Description of the map of solid rocks around Simpevarp. SKB PR-25-87-02. 45 pp. Svensk Kärnbränslehantering AB.

Kornfält K A, Persson P O, Wikman H, **1997.** Granitoids from the Äspo area, southeastern Sweden; geochemical and geochronological data, Gff, 119, p. 109–114.

Krauskopf K B, Bird D K, 1995. Introduction to Geochemistry, third edition. McGraw-Hill Book Co. Singapore. 647 pp.

Kresten P, Chyssler J, **1976.** The Götemar Massif in south-eastern Sweden; a reconnaissance survey, Geologiska Föreningen i Stockholm Förhandlingar, 98, Part 2, p. 155–161.

Lagache M, Weisbrod A, **1977.** The system: two alkali feldspars-KCl-NaCl-H (sub 2) O at moderate to high temperatures and low pressures, Contributions to Mineralogy and Petrology, 62, p. 77–101.

Landström O, Tullborg E-L, 1991. Results of mineralogical studies and trace element analyses (U, Th and REEs) of fracture coatings, groundwaters and rock samples. In: Tullborg E-L, Wallin B, and Landström O, (1991); Hydrogeochemical studies of fracture minerals from water conducting fractures and deep groundwaters at Äspö. SKB PR-25-90-01. pp. Svensk Kärnbränslehantering AB.

Landström O, Tullborg E-L, 1995. Interactions of trace elements with fracture filling minerals from the Äspö Hard Rock Laboratory. SKB TR-95-13. 71 pp. Svensk Kärnbränslehantering AB.

Landström O, Tullborg E-L, Eriksson G, Sandell Y, 2001. Effects of glacial/post-glacial weathering compared with hydrothermal alteration – implications for matrix diffusion. Results from drillcore studies in porphyritic quartz monzodiorite from Äspö SE Sweden. SKB R-01-37. 60 pp. Svensk Kärnbränslehantering AB.

Larson S Å, Berglund J, **1992.** A chronological subdivision of the Transscandinavian igneous belt three magmatic episodes? Geologiska Föreningen i Stockholm Förhandlingar, p. 459–461.

Larsson D, Gronvold K, Oskarsson N, Gunnlaugsson E, **2002.** Hydrothermal alteration of plagioclase and growth of secondary feldspar in the Hengill volcanic centre, SW Iceland, Journal of Volcanology and Geothermal Research, 114, p. 275–290.

Le Maitre R W, Ed. 1989. A Classification of Igneous Rocks and Glossery of Terms. Oxford, Blackwell. 193 pp.

Le Maitre R W, Ed. 2002. Igneous Rocks: A Classification and Glossary of Terms: Recommendations of the International Union of Geological Sciences Subcommission on the Systematics of Igneous Rocks. Cambridge University Press. 240 pp.

Lee M R, Parsons I, **1997.** Dislocation formation and albitization in alkali feldspars from the Shap Granite, American Mineralogist, 82, p. 557–570.

Lee M R, Parsons I, **1998.** Microtextural controls of diagenetic alteration of detrital alkali feldspars; a case study of the Shap Conglomerate (Lower Carboniferous), Northwest England, Journal of Sedimentary Research, Section A: Sedimentary Petrology and Processes, 68, p. 198–211.

Liou J G, Kim H S, Maruyama S, **1983.** Prehnite – epidote equilibria and their petrologic applications, Journal of Petrology, 24, p. 321–342.

Ludden J, Gelinas L, Trudel P, **1982.** Archean metavolcanics from the Rouyn-Noranda District, Abitibi greenstone belt, Quebec; 2, Mobility of trace elements and petrogenetic constraints, Canadian Journal of Earth Sciences = Journal Canadien des Sciences de la Terre, 19, p. 2,276–2,287.

Maddock R H, Hailwood E A, Rhodes E J, Muir Wood R, 1993. Direct fault dating trials at the Äspö Hard Rock Laboratory. SKB TR-93-24. 189 pp. Svensk Kärnbränslehantering AB.

Mattsson H, Thunehed H, 2004. Interpretation of geophysical borehole data and compilation of petrophysical data from KSH02 (80–1,000 m) and KAV01. Oskarshamn site investigation. SKB P-04-77. 70 pp. Svensk Kärnbränslehantering AB.

Mattsson H, Thunehed H, Keisu M, 2005. Intepretation of geophysical borehole measurements and compilation of petrophysical data from KLX01, KLX03, KLX04, HLX21, HLX22, HLX23, HLX24, HLX25, HLX26, HLX27 and HLX28. Oskarshamn site investigation. SKB P-05-34. 91 pp. Svensk Kärnbränslehantering AB.

Mazurek M, Bossart P, Eliasson T, 1995. Classification and characterization of water-conducting fractures at Äspö: Results of phase 1 investigations. SKB PR 25-95-03. 76 pp. Svensk Kärnbränslehantering AB.

Morad S, Bergan M, Knarud R, Nystuen J P, **1990.** Albitization of detrital plagioclase in Triassic reservoir sandstones from the Snorre Field, Norwegian North Sea, Journal of Sedimentary Petrology, 60, p. 411–425.

Nekvasil H, Burnham C W, 1987. The calculated individual effects of pressure and water content on phase equilibria in the granite system. In,1987, Magmatic processes; physico-chemical principles; a volume in honor of Hatten S Yoder, Jr. 1. p. 433–445. Geochemical Society, University Park, PA, United States

Nilsson K P, Bergman T, Eliasson T, 2004. Bedrock mapping 2004 – Laxemar subarea and regional model area. Outcrop data and description of rock types. Oskarshamn site investigation. SKB P-04-221. pp. Svensk Kärnbränslehantering AB.

O'Neil J R, **1977.** Stable isotopes in mineralogy, Physics and Chemistry of Minerals, 2, p. 105–123.

Orville P M, **1963.** Alkali ion exchange between vapor and feldspar phases, American Journal of Science, 261, p. 201–237.

Parneix J C, Beaufort D, Dudoignon P, Meunier A, **1985.** Biotite chloritization process in hydrothermally altered granites, Chemical Geology, 51, p. 89–101.

Petersson J, Eliasson T, **1997.** Mineral evolution and element mobility during episyenitization (dequartzification) and albitization in the postkinematic Bohus Granite, southwest Sweden, Lithos, 42, p. 123–146.

Puigdomenech I, Ambrosi J-P, Eisenlohr L, Lartigue J-E, Banwart S A, Bateman K, Milodowski A E, West J M, Griffault L, Gustafsson E, Hama K, Yoshida H, Kotelnikova S, Pedersen K, Michaud V, Trotignon L, Rivas Perez J, 2001. O_2 depletion in granitic media. The REX project. SKB TR-01-05. 86 pp. Svensk Kärnbränslehantering AB.

Putnis A, 2002. Mineral replacement reactions; from macroscopic observations to microscopic mechanisms. In,2002, Mineralogy for the new millennium. 66; 5. p. 689–708. Mineralogical Society, London, United Kingdom

Saigal G C, Morad S, Bjorlykke K, Egeberg P K, Aagaard P, **1988.** Diagenetic albitization of detrital K-feldspar in Jurassic, Lower Cretaceous, and Tertiary clastic reservoir rocks from offshore Norway; I, Textures and origin, Journal of Sedimentary Petrology, 58, p. 1,003–1,013.

Savukoski M, 2004. Drill hole KLX04A. Determining of porosity by water saturation and density by buoyancy technique. Oskarshamn site investigation. SKB P-04-268. 28 pp. Svensk Kärnbränslehantering AB.

Savukoski M, Carlsson L, 2004. Drill hole KSH01A. Determining of porosity by water saturation and density by buoyancy technique. Oskarshamn site investigation. SKB P-04-56. 30 pp. Svensk Kärnbränslehantering AB.

Savukoski M, 2005a. Drill hole KLX03A. Determination of porosity by water saturation and density by buoyancy technique. Oskarshamn site investigation. SKB P-05-94. 26 pp. Svensk Kärnbränslehantering AB.

Savukoski M, 2005b. Drill hole KLX05A. Determination of porosity by water saturation and density by buoyancy technique. Oskarshamn site investigation. SKB P-05-127. 28 pp. Svensk Kärnbränslehantering AB.

SKB, 2005. Preliminary site description, Simpevarp subarea – version 1.2. SKB R-05-08. 589 pp. Svensk Kärnbränlsehantering AB.

Slaby E, Lensch G, Mihm A, **1990.** Metasomatic aplites from Rauschermuehle and Kreimbach, Palatinate, West Germany, Neues Jahrbuch fuer Mineralogie, Monatshefte. 1990, p. 343–352.

Slaby E, **1992.** Changes in the structural state of secondary albite during progressive albitization, Neues Jahrbuch fuer Mineralogie, Monatshefte. 1992, p. 321–335.

Spear F S, **1993.** Metamorphic phase equilibria and pressure-temperature-time paths., Mineralogical Society of America Monograph Series, 1, p. 799.

Stanfors R, Rhen I, Tullborg E L, Wikberg P, 1999. Overview of geological and hydrogeological conditions of the Aspo Hard Rock Laboratory site. In,1999, Geochemistry of the Aspo Hard Rock Laboratory, Sweden. 14; 7. p. 819–834. Pergamon, Oxford-New York-Beijing, International

Stosnach H, Mengel K, 1998. An assessment of the distribution of trace elements in Äspö granitoids: Implication for the use of granites as geological barrier. HRL 98-02. pp.

Streckeisen A, **1976.** To each plutonic rock its proper name, Earth-Science Reviews, 12, p. 1–33.

Streckeisen A, **1978.** IUGS Subcommission on the Systematics of Igneous Rocks; classification and nomenclature of volcanic rocks, lamprophyres, carbonatites and melilitic rocks; recommendation and suggestions, Neues Jahrbuch fuer Mineralogie, Abhandlungen. 134, p. 1–14.

Sundberg J, Gabrielsson A, 1999. Laboratory and field measurements of thermal properties of the rocks in the prototype repository at Äspö HRL. SKB IPR-99-17. 67 pp. Svensk Kärnbränslehantering AB.

Sverjensky D A, 1983. Europium redox equilibria in aqueous solution, Earth and Planetary Science Letters, Volume 67, p. 70–78.

Taboada T, Garcia C, **1999.** Pseudomorphic transformation of plagioclases during the weathering of granitic rocks in Galicia (NW Spain), Catena, 35, p. 291–302.

Tullborg E-L, 1995. Section 4. Mineralogical/Geochemical Investigations in the Fracture Zone. In: Banwart S,1995, The Redox experiment in block scale. SKB PR 25-95-06. p. 81–101. Svensk Kärnbränslehantering AB.

Tullborg E-L, 1997. Recognition of low-temperature processes in the Fennoscandian Shield: Doctoral thesis, Earth Science Centre A17, Göteborg University, 35 pp.

Tullborg E-L, 2002. Matrix Fluid Chemistry Report, Borehole KF0051A01:4 – Results from chemical and SEM/EDS analyses and porosity/density measurements, Äspö Hard Rock Laboratory. SKB ITD-02-04. 18 pp. Svensk Kärnbränslehantering AB.

Tullborg E-L, Larson S Å, **2005.** Porosity in crystalline rocks – a matter of scale, Engineering geology, in press, p.

Tulloch A J, **1979.** Secondary Ca-Al silicates as low-grade alteration products of granitoid biotite, Contributions to Mineralogy and Petrology, 69, p. 105–117.

Wahlgren C-H, Ahl M, Sandahl K-A, Berglund J, Petersson J, Ekström M, Persson P-O, 2004. Bedrock mapping 2003 – Simpevarp subarea. Outcrop data, fracture data, modal and geochemical classification of rock types, bedrock map, radiometric dating. Oskarshamn site investigation. SKB P-04-102. 59 pp. Svensk Kärnbränlehantering AB.

Van Baalen M R, 1993. Titanium mobility in metamorphic systems; a review. In,1993, Geochemistry of accessory minerals; papers presented at the Third V M Goldschmidt conference. 110; 1–3. p. 233–249. Elsevier, Amsterdam, Netherlands

van der Weijden C H, van der Weijden R D, **1995.** Mobility of major, minor and some redox-sensitive trace elements and rare-earth elements during weathering of four granitoids in central Portugal, Chemical Geology, 125, p. 149–167.

van Gaans P F M, Vriend S P, Poorter R P E, 1995. Hydrothermal processes and shifting element association patterns in the W-Sn enriched granite of Regoufe, Portugal. In,1995, Geochemical exploration 1993. 55; 1-3. p. 203–222. Elsevier, Amsterdam-New York, International

Wilamowski A, **2002.** Chloritization and polytypism of biotite in the Lomnica granite, Karkonosze Massif, Sudetes, Poland: Stable isotope evidence, Chemical Geology, 182, p. 529–547.

Wollast R, Chou L, 1985. Kinetic study of the dissolution of albite with a continuous flow-through fluidized bed reactor. In,1985, The chemistry of weathering. Series C: Mathematical and Physical Sciences. 149. p. 75–96. D Reidel Publishing Company, Dordrecht-Boston, International

Åberg G, **1978.** A geochronological study of the Precambrian of southeastern Sweden., Geologiska Föreningens i Stockholm Förhandlingar, 100, p. 125–154.

Åberg G, **1988.** Middle Proterozoic anorogenic magmatism in Sweden and worldwide., Lithos, p. 279–289.

Åberg G, Löfvendahl R, Levi B, **1984.** The Götemar granite-isotopic and geochemical evidence for a complex history of an anorogenic granite, Geologiska Föreningen i Stockholm Förhandlingar, 106, p. 327–333.

Åhäll K-I, 2001. Åldersbestämning av svårdaterade bergarter i sydöstra Sverige. SKB R-01-60. 28 pp. Svensk Kärnbränslehantering AB.

Åhäll K I, Larson S Å, **2000.** Growth-related 1.85-1.55 Ga magmatism in the Baltic Shield; a review addressing the tectonic characteristics of Svecofennian, TIB 1-related, and Gothian events, GFF, 122, p. 193–206.

Appendix 1

Element changes and porosity changes for each sample

In this section the element changes of selected elements and the normative porosity changes is presented for each sample.

Sample – 108R/108G:

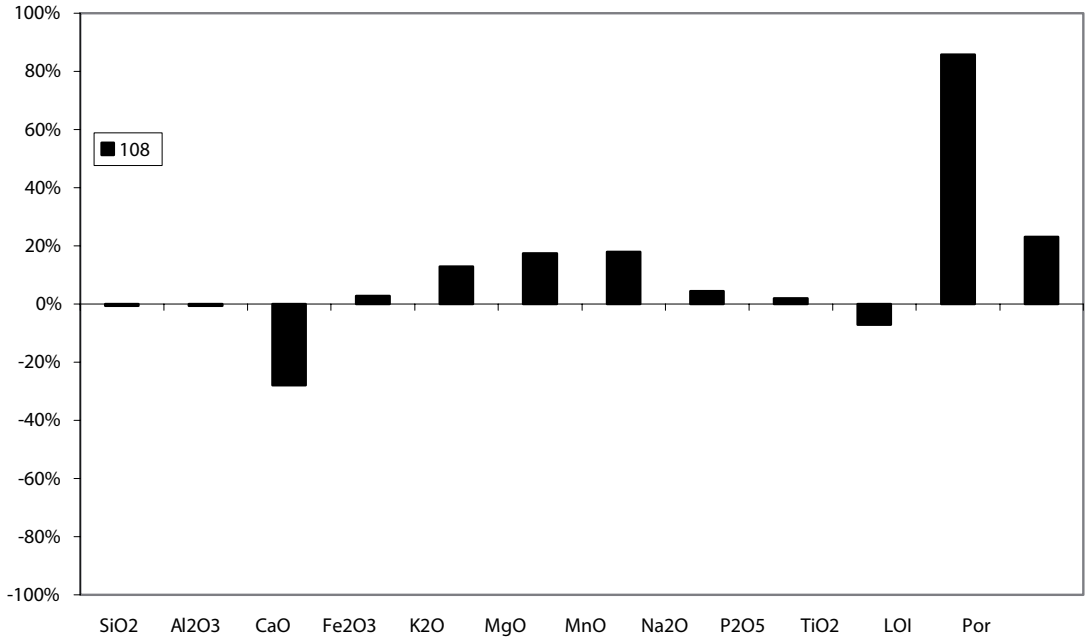

108: *Changes in major elements, minor elements, loss on ignition (LOI) and porosity (Por).*

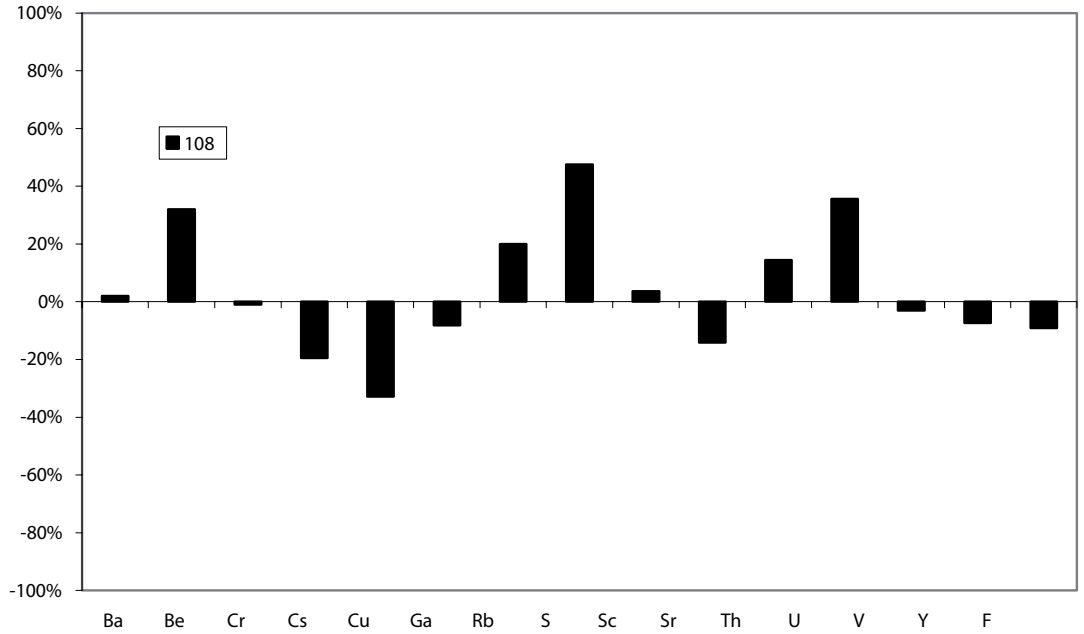

108: *Changes in selected trace elements.*

Sample 137R/137G:

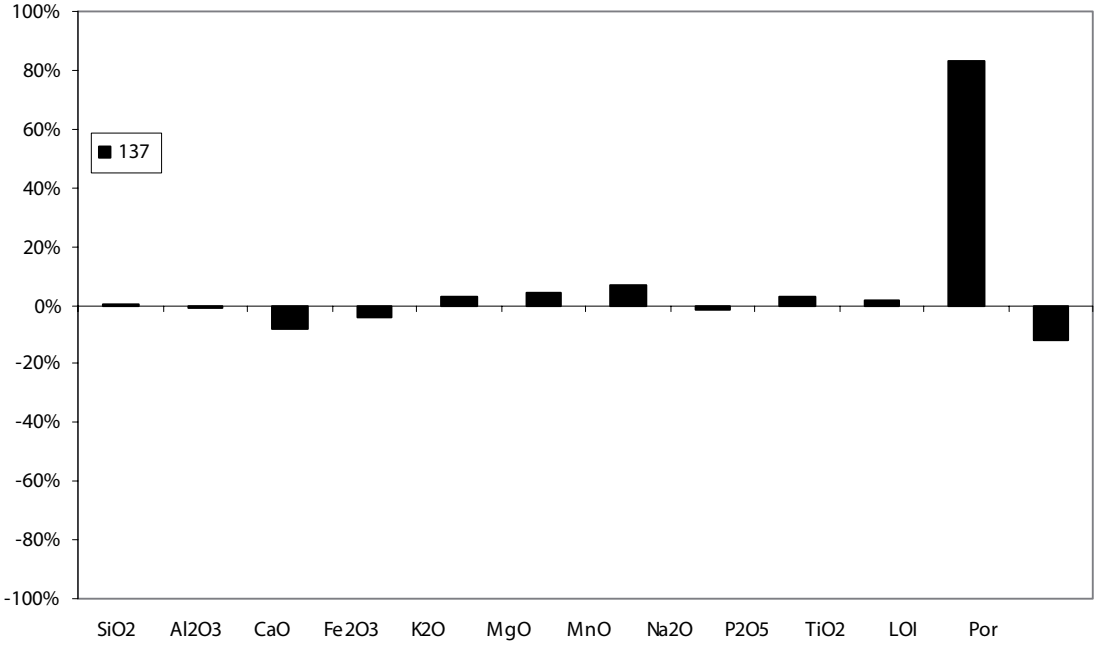

137: *Changes in major elements, minor elements, loss on ignition (LOI) and porosity (Por).*

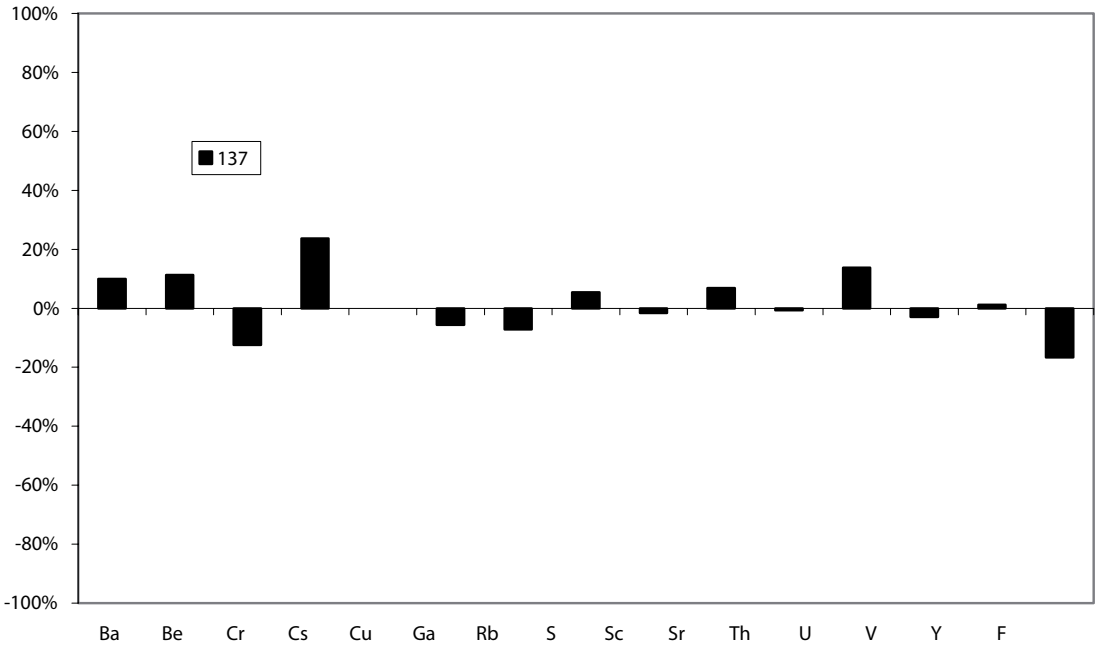

137: *Changes in selected trace elements.*

Sample – 153R/153G:

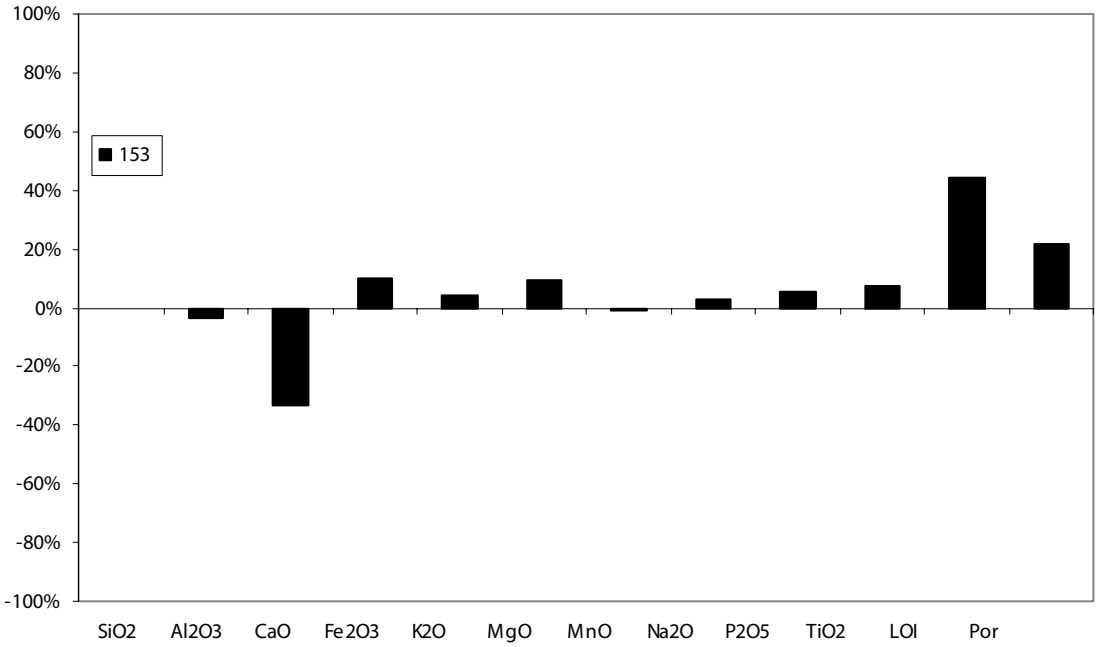

153: *Changes in major elements, minor elements, loss on ignition (LOI) and porosity (Por).*

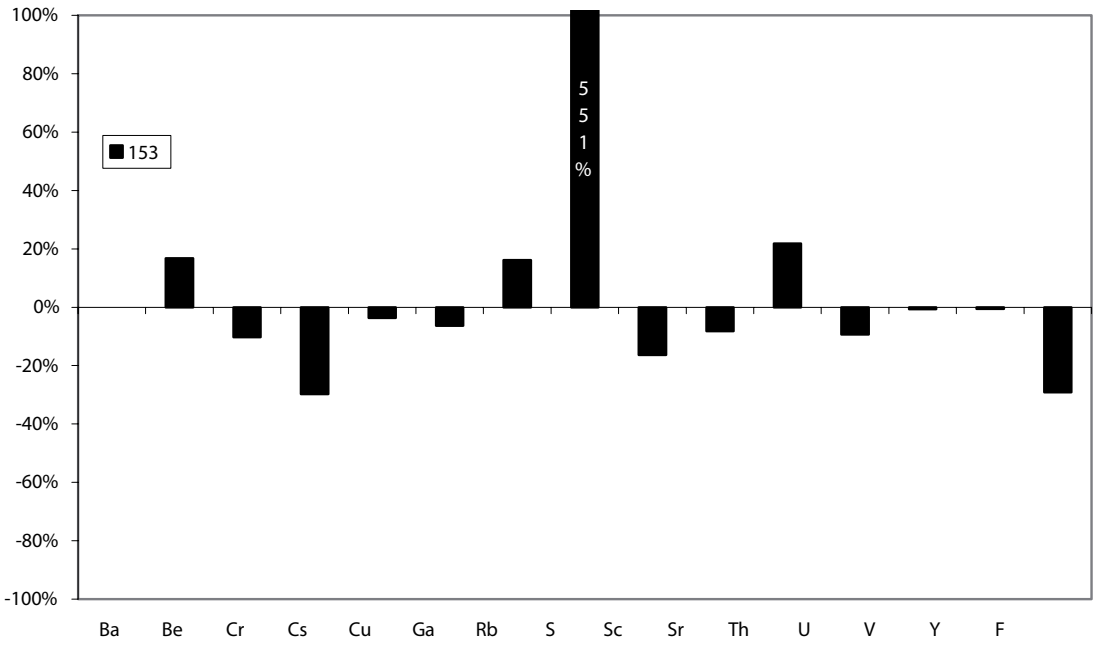

153: *Changes in selected trace elements.*

Sample – 168A/153G:

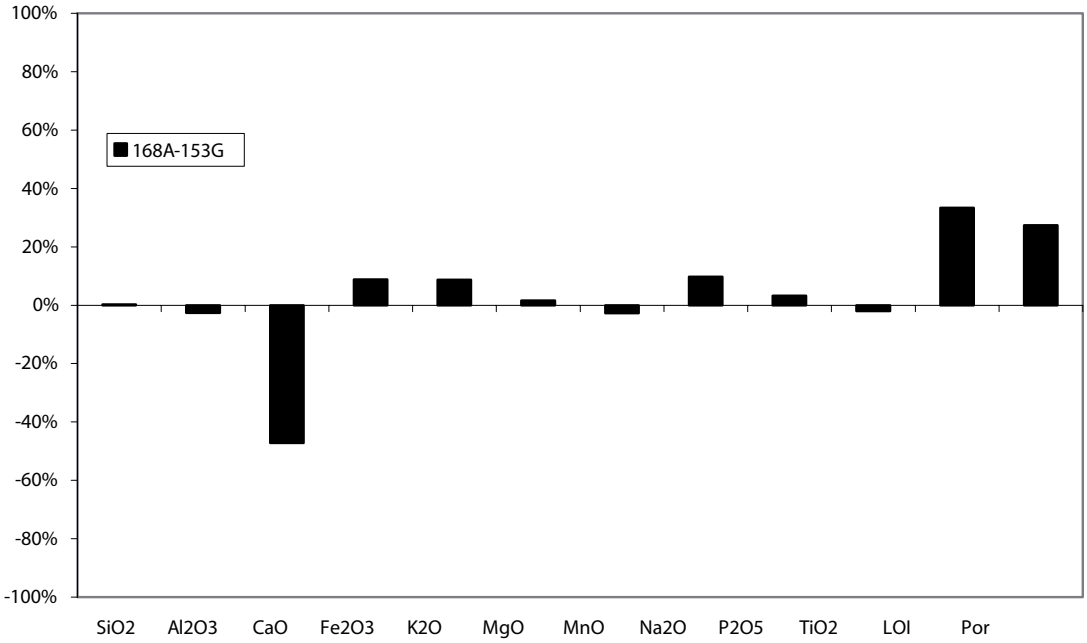

168A/153G: *Changes in major elements, minor elements, loss on ignition (LOI) and porosity (Por).*

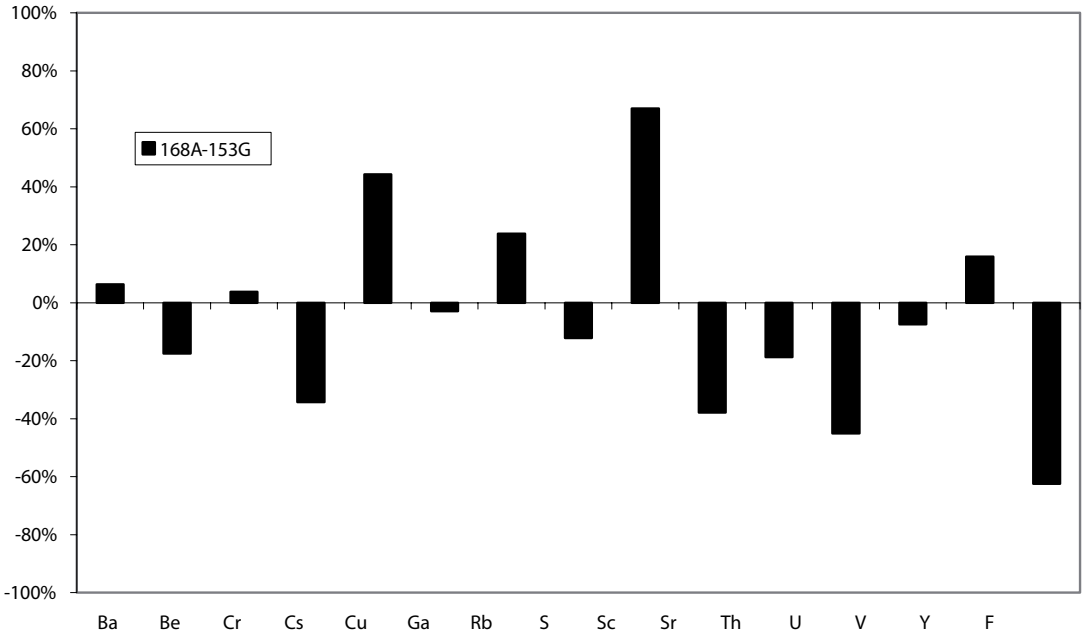

168A/153G: *Changes in selected trace elements.*

Sample 170R/153G:

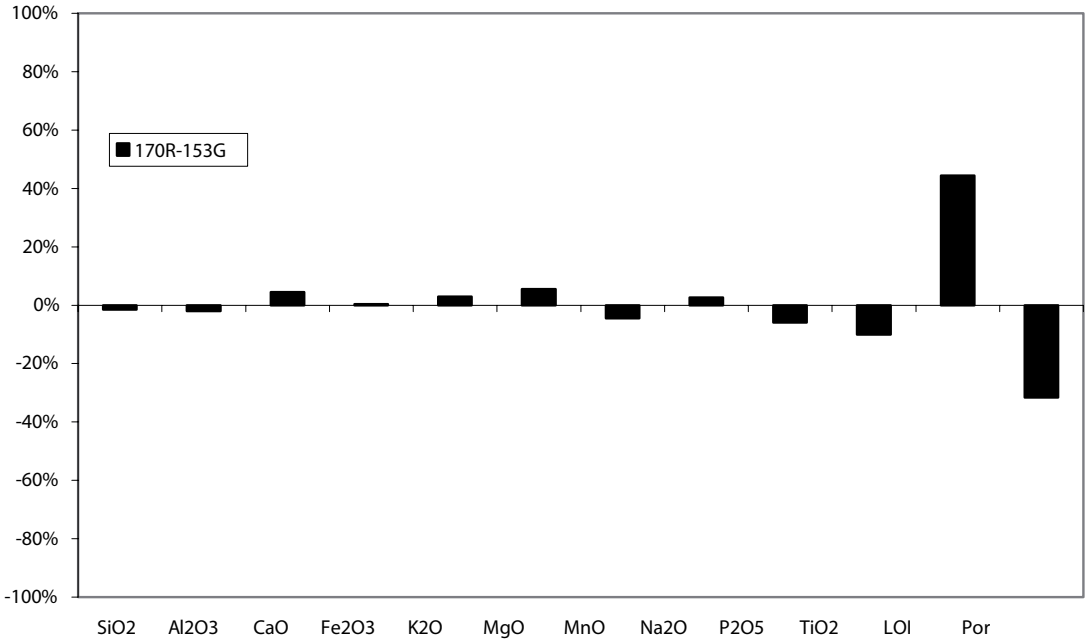

168A/153G: *Changes in major elements, minor elements, loss on ignition (LOI) and porosity (Por).*

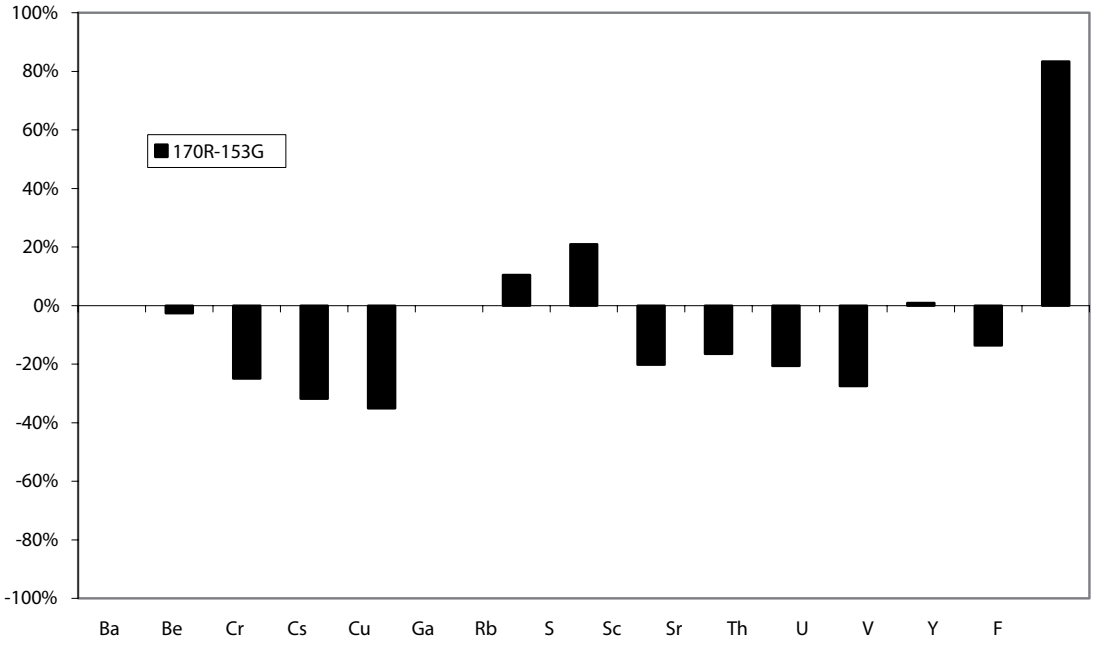

170R/153G: *Changes in selected trace elements.*

Sample 320R/320G:

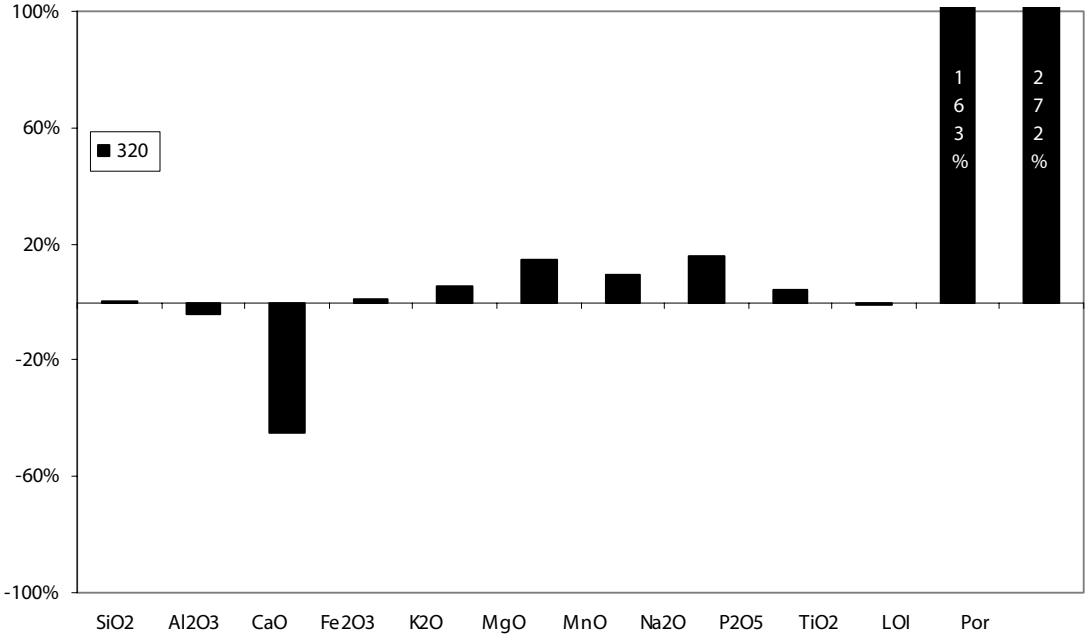

320: *Changes in major elements, minor elements, loss on ignition (LOI) and porosity (Por).*

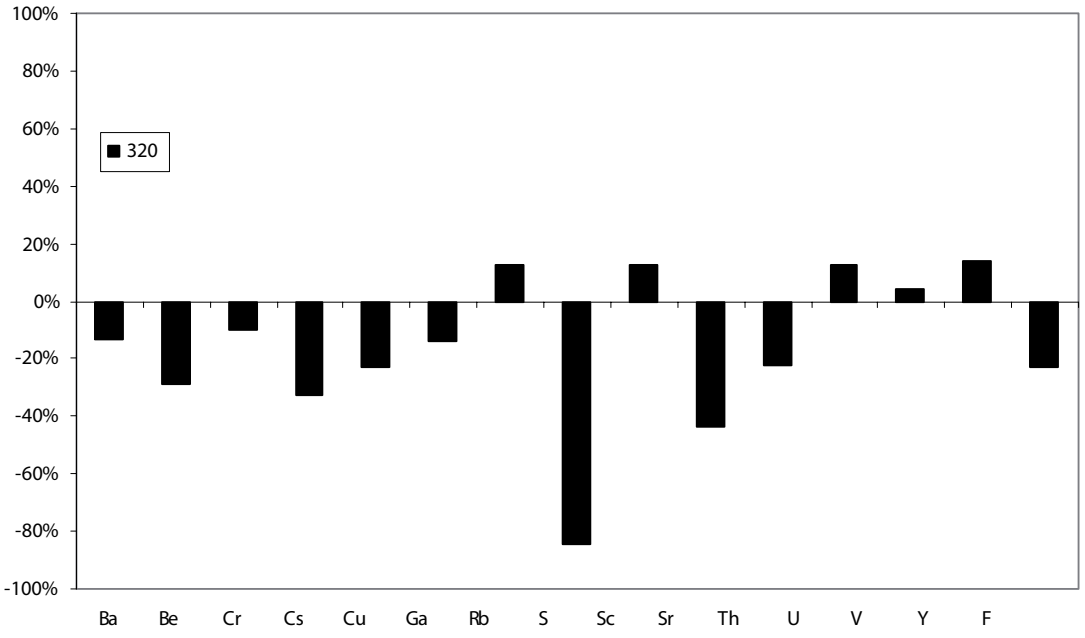

320: *Changes in selected trace elements.*

Sample 630R/630G:

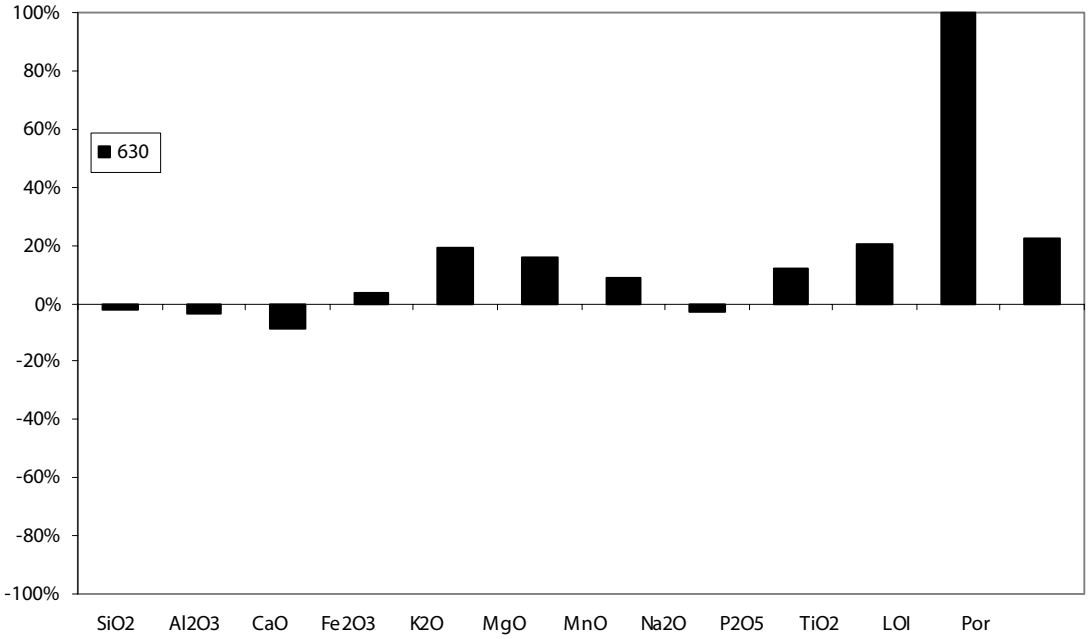

630: *Changes in major elements, minor elements, loss on ignition (LOI) and porosity (Por).*

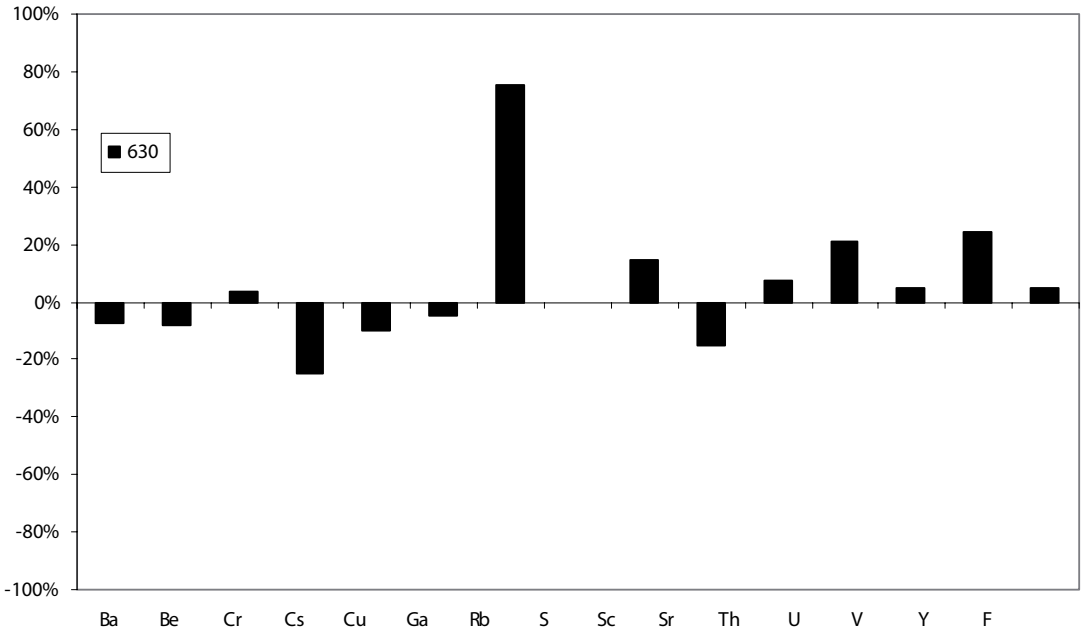

630: *Changes in selected trace elements.*

Appendix 2

SEM-EDS analyses

SEM-EDS analyses of K-feldspar, plagioclase, albite, entire plagioclase crystals (in reference samples; G), entire pseudomorphs after plagioclase (in red-stained samples; R +168A), biotite, chlorite, hornblende, epidote and titanite. *=below detection limit of SEM-EDS.

K-feldspar	Na_2O	Al_2O_3	SiO_2	K_2O	FeO	BaO	Total	Comments
108G-1	0.54	18.00	63.98	16.19	*	0.53	99.24	Microcline
108G-2	0.66	18.25	63.81	16.03	*	0.56	99.31	Perthite
108G-3	0.72	18.12	64.13	16.08	*	0.25	99.30	Microcline
108R-1	0.93	18.46	64.91	15.87	*	0.41	100.58	Perthite
108R-2	0.21	18.55	63.61	16.46	*	0.61	99.44	In albitized plagioclase
108R-3	0.19	18.49	64.64	16.68	*	0.59	100.59	In albitized plagioclase
108R-4	0.62	18.09	63.81	16.02	*	0.58	99.12	Microcline
108R-5	0.27	18.24	64.26	16.21	*	*	99.31	In albitized plagioclase
137G-1	0.61	18.24	63.97	16.16	*	0.27	99.25	Perthite
137R-1	0.48	18.12	64.50	16.31	*	*	99.41	Perthite
137R-2	0.61	18.28	64.14	16.10	*	0.66	99.79	Perthite
153G-1	0.49	18.18	64.53	16.38	*	*	99.58	Perthite
153R-1	0.59	19.62	62.62	15.13	0.21	1.07	99.24	In albitized plagioclase
153R-2	0.59	18.11	64.03	16.14	*	0.43	99.30	Perthite
168A-1	0.38	18.32	64.56	16.35	*	0.40	100.01	Perthite
170R-1	0.21	20.48	62.92	16.09	*	0.00	99.70	In albitized plagioclase
170R-2	0.35	18.87	64.34	16.67	*	*	100.23	In albitized plagioclase
320G-1	1.19	18.68	64.77	14.99	*	0.82	100.45	Perthite
320R-1	0.66	18.69	64.34	15.67	*	1.17	100.53	Perthite
320R-2	0.49	18.20	64.23	16.08	*	0.82	99.82	Microcline
320R-3	0.00	18.23	64.38	16.85	*	0.44	99.90	In albitized plagioclase
320R-4	0.00	18.35	65.10	16.92	*	0.19	100.56	In albitized plagioclase
630G-1	0.65	18.19	63.58	15.72	*	1.02	99.16	Microcline
630G-2	0.99	18.47	63.68	15.23	*	1.46	99.83	Perthite
630R-1	1.26	18.36	64.00	14.87	*	1.06	99.55	Microcline
630R-2	*	19.37	63.44	16.01	*	0.75	99.57	In albitized plagioclase
630R-3	1.34	18.27	63.88	14.90	*	1.58	99.97	Perthite
630R-4	*	18.76	63.72	16.14	0.29	1.05	99.96	In albitized plagioclase

Plagioclase	Na_2O	Al_2O_3	SiO_2	K_2O	CaO	FeO	Total
108G-1	8.52	23.67	62.38	0.00	5.41	*	99.98
108G-2	7.89	24.45	60.79	0.22	6.42	*	99.77
137G-1	8.43	23.86	61.37	*	5.50	*	99.16
137G-2	8.33	23.45	62.19	0.78	5.00	*	99.75
153G-1	8.59	23.56	62.41	0.12	5.31	*	99.99
153G-2	8.80	23.68	62.80	*	4.97	0.20	100.45
320G-1	8.33	24.56	61.52	0.18	6.08	*	100.67
320G-2	8.07	24.47	60.61	0.26	6.34	*	99.75
630G-1	8.22	23.97	61.75	0.39	5.55	0.27	100.15
630G-2	8.26	24.07	61.41	0.16	5.76	*	99.66
630G-3	8.50	24.53	61.89	0.00	5.84	*	100.76

Albite	Na_2O	Al_2O_3	SiO_2	K_2O	CaO	FeO	Total
108R-1	11.15	19.42	68.14	*	0.29	*	99.00
137R-1	11.36	19.55	68.20	*	0.35	*	99.46
153R-1	11.45	19.99	67.83	0.31	0.38	*	99.96
168A-1	11.41	19.46	68.53	*	*	*	99.40
168A-2	11.47	19.87	68.92	0.23	0.19	*	100.68
320R-1	11.53	19.42	69.11	*	*	*	100.06
320R-2	11.51	19.43	68.19	*	0.17	*	99.30
630R-1	11.24	19.78	68.21	0.13	0.36	*	99.72
630R-2	11.13	19.61	67.25	0.18	0.45	0.53	99.15

Entire plagioclase crystals (reference rock)	Na_2O	MgO	Al_2O_3	SiO_2	K_2O	CaO	FeO	Total
108G-1	7.96	*	24.18	60.45	0.46	5.92	0.24	99.21
108G-2	8.10	*	23.93	60.97	1.36	4.64	0.73	99.73
108G-3	8.11	*	24.28	61.87	0.38	6.21	0.00	100.85
108G-4	8.24	*	23.63	61.18	0.35	5.46	0.26	99.12
108G-5	8.31	*	23.82	61.41	0.62	5.08	0.39	99.63
137G-1	7.93	0.17	24.02	61.41	0.93	5.00	0.37	99.83
137G-2	7.97	0.28	23.67	60.31	1.04	5.07	0.95	99.29
137G-3	7.77	*	24.25	59.99	0.98	5.52	0.51	99.02
137G-4	7.57	*	25.03	60.81	0.79	6.17	0.52	100.89
137G-5	8.29	*	23.27	62.22	0.56	5.10	0.19	99.63
153G-1	8.31	0.24	22.58	65.01	1.19	3.26	0.33	100.92
153G-2	8.55	0.36	22.96	62.97	1.62	2.34	0.42	99.22
153G-3	8.77	*	22.81	63.45	0.91	3.37	0.00	99.31
153G-4	8.72	*	23.50	63.34	1.18	3.19	0.00	99.93
320G-1	8.11	*	23.65	61.60	1.32	4.72	0.42	99.82
320G-2	7.97	*	23.42	61.78	2.30	3.46	0.38	99.31

Entire plagioclase crystals (reference rock)	Na_2O	MgO	Al_2O_3	SiO_2	K_2O	CaO	FeO	Total
320G-3	7.66	*	23.45	61.67	1.08	5.26	0.41	99.53
320G-4	8.08	*	24.06	61.32	0.83	5.20	0.28	99.77
320G-5	8.00	*	24.31	61.47	0.72	5.50	0.28	100.28
630G-1	7.58	*	24.33	60.62	1.70	4.58	0.35	99.16
630G-2	7.82	*	24.19	60.76	1.84	4.38	0.28	99.27
630G-3	8.11	*	23.39	62.36	0.92	5.20	0.31	100.29
630G-4	7.13	0.32	24.58	60.32	2.30	4.61	0.64	99.9

Entire pseudomorph after plagioclase (red-stained rock)	Na_2O	MgO	Al_2O_3	SiO_2	K_2O	CaO	FeO	Total
108R-1	6.71	0.26	22.19	63.89	6.24	0.55	0.99	100.83
108R-2	8.25	*	21.22	65.89	4.31	0.46	0.55	100.68
108R-3	8.39	0.33	20.78	65.60	3.65	0.54	0.73	100.02
108R-4	8.06	0.35	20.75	65.13	4.29	0.39	1.00	99.97
108R-5	8.80	*	21.24	65.33	3.35	0.47	0.54	99.73
137R-1	8.74	*	24.17	64.24	2.39	0.97	0.39	100.90
137R-2	8.73	*	23.98	63.27	1.12	1.61	0.39	99.10
137R-3	8.47	0.29	23.15	63.48	2.53	1.60	1.13	100.65
137R-4	9.01	0.20	22.63	63.14	1.36	2.27	0.50	99.11
153R-1	8.10	0.34	22.95	63.21	3.60	0.97	0.76	99.93
153R-2	8.48	0.14	22.85	63.86	2.67	0.95	0.23	99.18
153R-3	8.71	*	23.01	62.82	2.51	0.97	0.41	98.43
153R-4	8.76	*	23.23	63.49	2.65	1.01	0.86	100.00
170R-1	6.46	0.46	22.22	61.97	4.85	2.49	0.87	99.32
170R-2	8.66	0.43	22.35	63.25	1.97	2.12	0.41	99.19
170R-3	8.86	0.29	22.35	64.46	1.63	2.53	0.55	100.67
170R-4	8.47	*	22.24	63.93	3.08	2.10	0.55	100.37
320R-1	8.55	*	20.11	65.86	3.96	0.37	0.75	99.60
320R-2	7.73	0.40	20.06	64.10	4.78	0.68	1.25	99.00
320R-3	8.15	*	20.65	64.80	4.58	0.45	0.84	99.47
320R-4	9.78	*	20.75	66.27	1.61	0.51	0.43	99.35
320R-5	10.42	*	20.14	66.89	1.26	0.58	0.89	100.18
320R-6	7.99	0.26	21.08	64.29	4.57	0.58	1.09	99.86
630R-1	5.20	*	20.06	65.16	7.37	1.39	0.71	99.89
630R-2	5.80	*	21.09	63.30	6.98	1.41	0.72	99.30
630R-3	7.93	*	22.19	64.57	4.16	1.33	0.35	100.53
630R-4	6.69	0.21	22.09	63.91	6.09	1.23	0.79	101.01
630R-5	8.21	0.26	21.61	64.71	3.74	1.15	0.68	100.36
630R-6	8.14	*	22.50	64.12	3.83	1.35	0.60	100.54
168A-1	9.67	*	21.34	64.92	2.16	0.48	0.42	98.99
168A-2	7.95	0.30	22.58	62.98	2.97	1.54	0.69	99.01
168A-3	9.00	0.29	21.88	63.67	2.44	0.57	0.54	98.39
168A-4	9.69	*	20.37	67.51	1.50	0.36	0.24	99.67

Biotite	MgO	Al_2O_3	SiO_2	K_2O	TiO_2	MnO	FeO	Total
108G	12.87	14.48	38.08	10.05	1.77	0.45	19.45	97.15
108G	12.65	14.41	37.61	9.96	1.89	0.45	19.26	96.23
108G	12.64	14.19	37.22	9.52	1.89	0.41	18.95	94.82
137G-1	13.69	14.73	37.08	8.55	1.56	0.38	18.85	94.84
137G-2	12.76	15.13	38.03	10.24	1.88	0.44	18.71	97.19
137R	13.37	15.18	37.12	9.10	1.61	0.54	17.14	94.06
320G-1	13.86	14.53	38.57	10.21	1.58	0.43	18.05	97.23
320G-2	13.73	14.51	37.75	9.00	1.55	0.60	19.71	96.85
630G-1	12.77	14.66	37.32	9.90	1.93	0.48	18.21	95.27
630G-2	13.59	14.02	37.44	9.63	1.75	0.49	18.59	95.51

Chlorite	MgO	Al_2O_3	SiO_2	K_2O	CaO	TiO_2	MnO	FeO	Total
108G	15.97	19.01	26.44	*	*	*	0.74	25.02	87.18
108R-1	16.86	16.87	28.33	*	*	*	0.69	23.62	86.37
108R-2	16.77	17.02	28.40	*	*	*	0.59	24.83	87.61
137G	19.33	16.29	29.41	*	0.16	*	0.79	22.55	88.53
137R	18.00	16.69	29.11	0.32	*	*	0.79	23.13	88.04
153G	17.51	16.50	29.59	0.37	0.13	0.31	0.76	22.54	87.71
153R	17.08	17.30	29.02	*	0.15	*	0.61	23.50	87.66
168A-1	18.65	17.44	29.76	*	*	*	0.70	20.68	87.23
168A-2	18.39	17.28	29.98	*	*	*	0.62	21.64	87.91
168A-3	18.79	17.77	29.72	*	0.16	*	0.73	20.95	88.12
170R-1	17.39	16.77	29.81	*	*	*	0.73	23.96	88.66
170R-2	18.03	16.48	28.81	*	*	*	0.66	23.20	87.18
170R-3	18.40	15.83	29.00	*	*	*	0.69	22.74	86.66
320R-1	18.23	16.94	29.57	*	*	*	1.02	23.22	88.98
320R-2	18.41	16.35	29.83	*	*	*	0.59	23.68	88.86
320R-3	18.13	17.08	29.63	*	*	*	0.63	22.87	88.34
630R-1	17.63	16.40	28.53	*	*	*	0.57	24.19	87.32
630R-2	18.07	16.12	28.73	*	*	*	0.56	23.88	87.36
630R-3	17.86	15.98	28.92	*	*	*	0.67	24.31	87.74

Hornblende	Na_2O	MgO	Al_2O_3	SiO_2	K_2O	CaO	TiO_2	MnO	FeO	Total
320G-1	1.15	12.33	7.18	46.54	0.95	12.17	0.94	0.55	16.70	98.51
320G-2	1.24	11.00	7.74	45.57	1.01	11.95	1.14	0.63	18.33	98.61
630G-1	1.06	12.41	6.55	47.31	0.59	12.39	0.71	0.64	16.06	97.72
630G-2	1.19	11.77	7.09	45.98	0.87	12.04	1.09	0.64	16.62	97.29
630G-3	1.35	11.76	7.59	45.23	0.95	12.03	1.03	0.70	16.81	97.45
630R-1	1.13	12.24	6.83	46.42	0.77	11.79	1.02	0.49	16.62	97.31
630R-2	1.33	11.60	7.80	45.16	0.98	11.80	1.09	0.54	17.26	97.56

Epidote	Al_2O_3	SiO_2	CaO	MnO	FeO	Total	Comments
108G-1	22.37	37.55	23.33	0.31	12.63	96.19	
108G-2	22.68	38.24	23.48	0.31	13.20	97.91	
108R	22.45	36.98	22.77	0.46	12.48	95.14	
137G	21.23	37.20	22.92	0.49	13.79	95.63	
137R	22.24	37.41	22.70	0.76	13.38	96.49	
153G	21.63	36.83	22.60	0.44	13.70	95.20	
153R-1	22.57	37.50	23.03	0.35	12.22	95.67	
153R-2	22.21	37.38	23.16	0.54	13.40	96.69	
168A-1	21.62	37.00	22.95	0.34	13.72	95.63	
168A-2	23.99	37.71	23.56	*	11.83	97.09	In plagioclase
168A-3	24.01	37.88	23.17	0.88	11.83	97.77	In plagioclase
170R	22.35	37.31	23.21	0.49	12.64	96.00	
320G	22.16	37.79	23.62	*	13.33	96.90	
630R	19.09	36.59	22.36	*	17.18	95.22	

Titanite	MgO	Al_2O_3	SiO_2	CaO	TiO_2	FeO	V_2O_5	Ce_2O_3	Nd_2O_3	Sc_2O_3	F	Total
108G-core	*	1.24	28.73	25.66	35.91	1.85	*	1.50	0.91	*	*	95.80
108G-core	*	1.29	28.82	25.47	35.53	2.00	*	1.50	0.91	*	*	95.52
108G-rim	*	1.35	29.05	26.1	35.18	1.66	*	1.21	0.62	0.66	*	95.83
108G-rim	*	1.54	29.01	26.71	35.16	1.66	*	*	*	0.23	*	94.31
108G-rim	*	1.23	28.97	25.31	35.14	1.73	*	1.5	0.91	*	*	94.79
108R-grothite	0.37	7.31	29.48	25.58	24.41	2.73	0.60	*	*	0.23	4.00	94.71
153G-core	*	1.49	29.29	26.13	35.88	1.91	*	1.55	*	0.20	*	96.45
153G-rim	*	1.46	30.11	27.45	36.73	1.45	0.48	0.80	*	0.20	*	98.68
320G-core	*	1.20	29.00	26.36	37.02	1.59	*	1.38	*	*	*	96.55
320G-rim	*	1.41	29.31	26.86	37.07	1.82	*	*	*	0.29	*	96.76
320R-grothite	1.04	6.27	30.37	25.99	26.74	3.05	0.65	*	*	*	3.76	97.87
630R-grothite	2.71	8.75	29.80	24.03	23.29	5.13	*	*	*	*	3.62	97.33